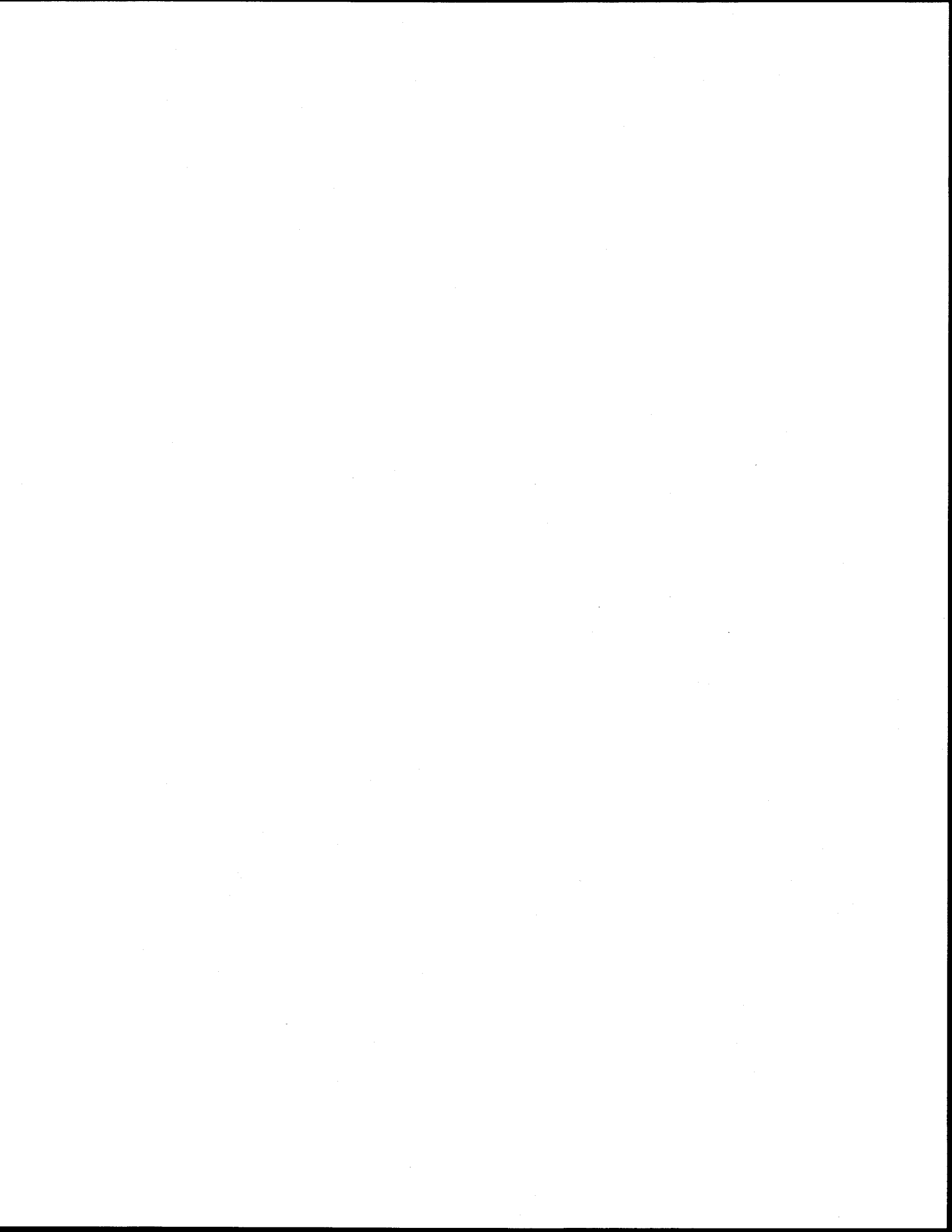


**COMPUTATION OF THE
TOPOGRAPHIC INDEX ON 16
WATERSHEDS IN QUEBEC**

Report N° R-800f

April 25, 2005



Computation of the Topographic Index on 16 Watersheds in Quebec

Final report

Agriculture and Agri-Food Canada

Prepared by :

Alain N. Rousseau
Achraf Hentati
Sébastien Tremblay
Renaud Quilbé
Jean-Pierre Villeneuve

Centre Eau, Terre et Environnement
Institut national de la recherche scientifique (INRS-ETE)
490, rue de la Couronne, Québec (QC), G1K 9A9

Report N° R800-f

April 25, 2005

© Alain N. Rousseau, 2005

ISBN : 2-89146-151-7

TABLE OF CONTENTS

LIST OF FIGURES	V
LIST OF TABLES	XI
LIST OF ACRONYMS	XIII
1 INTRODUCTION.....	1
2 REVIEW OF SOME COMPUTATIONAL ALGORITHMS	3
2.1 TOPOGRAPHIC INDEX (<i>TI</i>).....	3
2.1.1 Definition.....	3
2.1.2 Computation of the topographic index.....	5
2.2 PRESENTATION OF THE FLOW DIRECTION ALGORITHMS	6
2.2.1 Definition.....	6
2.2.2 Single Flow Direction algorithm (SFD)	6
2.2.3 Biflow Direction algorithm (BFD)	7
2.2.4 Multiple Flow Direction algorithm (MFD)	11
2.3 DISCUSSION.....	11
2.4 CONCLUSION	14
3 APPLICATION OF THE ALGORITHMS ON 16 WATERSHEDS	15
3.1 TECHNICAL PROCEDURE	15
3.1.1 Preparation of the DEM	15
3.1.2 Calculation of <i>TI</i> using the D8 algorithm (O'Callaghan and Mark, 1984).....	16
3.1.3 Calculation of <i>TI</i> using the D8-LTD algorithm (Orlandini <i>et al.</i> , 2003).....	17

3.1.4	Calculation of TI using the D8-LAD algorithm (Tarboton <i>et al.</i> , 1997).....	17
3.2	RESULTS AND DISCUSSIONS.....	18
3.3	RECOMMENDATIONS	24
4	CONCLUSION.....	25
5	REFERENCES	27
	APPENDIX A RESULTS OF TI DISTRIBUTION ON THE 16	
	WATERSHEDS	29

LIST OF FIGURES

Figure 2.1 :	Saturation excess overland flow.....	3
Figure 2.2 :	Influence of local slope and contributing area on the water balance of a catchment “block”. The inflow rate is proportional to the contributing area A (a) and the outflow rate is controlled by the local slope (b) [Hornberger <i>et al.</i> , 1998].....	4
Figure 2.3 :	High values of <i>TI</i> are in valleys and low values are at tops of hillslopes [Tarboton, 2003].	5
Figure 2.4 :	The upslope contributing area and the contour length	6
Figure 2.5 :	Eight flow direction method (D8).....	7
Figure 2.6 :	Flow directions defined as steepest downward slope on planar triangular facets on a block centered grid [Tarboton, 1997].....	8
Figure 2.7 :	Definition of variable for the calculation of slope on a single triangular facet [Tarboton, 1997].....	8
Figure 2.8 :	The elementary computational used in the D8-LAD and the D8-LTD methods [Orlandini <i>et al.</i> , 2003]	10
Figure 2.9 :	Weights attributed to flow directions in the MFD of Quinn <i>et al.</i> , [1991].	11
Figure 2.10 :	The “burning” process.....	13
Figure 3.1 :	Comparison of <i>TI</i> distributions obtained by the D8 method on the Beaurivage watershed (100 m grid resolution) without the ‘burning’ process (left) and with the ‘burning’ process (right).	21
Figure 3.2 :	<i>TI</i> distributions obtained by the D8 method on the Beaurivage watershed for the two grid resolutions (19.12 m and 100 m).	22
Figure 3.3 :	The resolution effect (19 m and 100 m) on <i>TI</i> distributions obtained by the D8 method on the Beaurivage watershed.	23

Figure A.1 : Hypsometric curve and <i>TI</i> distributions on Acadie river watershed obtained by the 3 flow direction algorithms.....	30
Figure A.2 : Hypsometric curve and <i>TI</i> distributions on Achigan river watershed obtained by the 3 flow direction algorithms.....	30
Figure A.3 : Hypsometric curve and <i>TI</i> distributions on Des Anglais river watershed obtained by the 3 flow direction algorithms.....	30
Figure A.4 : Hypsometric curve and <i>TI</i> distributions on Bayonne river watershed obtained by the 3 flow direction algorithms.....	31
Figure A.5 : Hypsometric curve and <i>TI</i> distributions on Beaurivage river watershed obtained by the 3 flow direction algorithms.....	31
Figure A.6 : Hypsometric curve and <i>TI</i> distributions on Boyer river watershed obtained by the 3 flow direction algorithms.....	31
Figure A.7 : Hypsometric curve and <i>TI</i> distributions on Chibouet river watershed obtained by the 3 flow direction algorithms.....	32
Figure A.8 : Hypsometric curve and <i>TI</i> distributions on Coaticook river watershed obtained by the 3 flow direction algorithms.....	32
Figure A.9 : Hypsometric curve and <i>TI</i> distributions on Des Hurons river watershed obtained by the 3 flow direction algorithms.....	32
Figure A.10 : Hypsometric curve and <i>TI</i> distributions on Du Chêne river watershed obtained by the 3 flow direction algorithms.....	33
Figure A.11 : Hypsometric curve and <i>TI</i> distributions on Etchemin river watershed obtained by the 3 flow direction algorithms.....	33
Figure A.12 : Hypsometric curve and <i>TI</i> distributions on Mascouche river watershed obtained by the 3 flow direction algorithms.....	33
Figure A.13 : Hypsometric curve and <i>TI</i> distributions on Nicolet river watershed obtained by the 3 flow direction algorithms.....	34
Figure A.14 : Hypsometric curve and <i>TI</i> distributions on Noire river watershed obtained by the 3 flow direction algorithms.....	34

Figure A.15 : Hypsometric curve and <i>TI</i> distributions on Saint-Esprit river watershed obtained by the 3 flow direction algorithms.	34
Figure A.16 : Hypsometric curve and <i>TI</i> distributions on Yamaska river watershed obtained by the 3 flow direction algorithms.	35
Figure A.17 : <i>TI</i> results for the Acadie river watershed using the D8 algorithm (Arc Hydro tool)	36
Figure A.18 : <i>TI</i> results for the Achigan river watershed using the D8 algorithm (Arc Hydro tool)	37
Figure A.19 : <i>TI</i> results for the Anglais river watershed using the D8 algorithm (Arc Hydro tool)	38
Figure A.20 : <i>TI</i> results for the Bayonne river watershed using the D8 algorithm (Arc Hydro tool)	39
Figure A.21 : <i>TI</i> results for the Beaurivage river watershed using the D8 algorithm (Arc Hydro tool)	40
Figure A.22 : <i>TI</i> results for the Boyer river watershed using the D8 algorithm (Arc Hydro tool)	41
Figure A.23 : <i>TI</i> results for the Chibouet river watershed using the D8 algorithm (Arc Hydro tool)	42
Figure A.24 : <i>TI</i> results for the Coaticook river watershed using the D8 algorithm (Arc Hydro tool)	43
Figure A.25 : <i>TI</i> results for the Des Hurons river watershed using the D8 algorithm (Arc Hydro tool)	44
Figure A.26 : <i>TI</i> results for the Du Chêne river watershed using the D8 algorithm (Arc Hydro tool)	45
Figure A.27 : <i>TI</i> results for the Etchemin river watershed using the D8 algorithm (Arc Hydro tool)	46
Figure A.28 : <i>TI</i> results for the Mascouche river watershed using the D8 algorithm (Arc Hydro tool)	47

Figure A.29 : <i>TI</i> results for the Nicolet river watershed using the D8 algorithm (Arc Hydro tool).....	48
Figure A.30 : <i>TI</i> results for the Noire river watershed using the D8 algorithm (Arc Hydro tool)	49
Figure A.31 : <i>TI</i> results for the Saint-Esprit river watershed using the D8 algorithm (Arc Hydro tool).....	50
Figure A.32 : <i>TI</i> results for the Yamaska river watershed using the D8 algorithm (Arc Hydro tool).....	51
Figure A.33 : <i>TI</i> results for the Acadie river watershed using the D8-LTD algorithm.....	52
Figure A.34 : <i>TI</i> results for the Achigan river watershed using the D8-LTD algorithm	53
Figure A.35 : <i>TI</i> results for the Des Anglais river watershed using the D8-LTD algorithm.....	54
Figure A.36 : <i>TI</i> results for the Bayonne river watershed using the D8-LTD algorithm	55
Figure A.37 : <i>TI</i> results for the Beaurivage river watershed using the D8-LTD algorithm.....	56
Figure A.38 : <i>TI</i> results for the Boyer river watershed using the D8-LTD algorithm	57
Figure A.39 : <i>TI</i> results for the Chibouet river watershed using the D8-LTD algorithm.....	58
Figure A.40 : <i>TI</i> results for the Coaticook river watershed using the D8-LTD algorithm.....	59
Figure A.41 : <i>TI</i> results for the Du Chêne river watershed using the D8-LTD algorithm.....	60
Figure A.42 : <i>TI</i> results for the Etchemin river watershed using the D8-LTD algorithm.....	61
Figure A.43 : <i>TI</i> results for the Des Hurons river watershed using the D8-LTD algorithm.....	62
Figure A.44 : <i>TI</i> results for the Mascouche river watershed using the D8-LTD algorithm.....	63
Figure A.45 : <i>TI</i> results for the Nicolet river watershed using the D8-LTD algorithm.....	64
Figure A.46 : <i>TI</i> results for the Noire river watershed using the D8-LTD algorithm.....	65
Figure A.47 : <i>TI</i> results for the Saint-Esprit river watershed using the D8-LTD algorithm.....	66

Figure A.48 : <i>TI</i> results for the Yamaska river watershed using the D8-LTD algorithm.....	67
Figure A.49 : <i>TI</i> results for the Acadie river watershed using the D8-LAD algorithm (TauDEM).....	68
Figure A.50 : <i>TI</i> results for the Achigan river watershed using the D8-LAD algorithm (TauDEM).....	69
Figure A.51 : <i>TI</i> results for the Des Anglais river watershed using the D8-LAD algorithm (TauDEM).....	70
Figure A.52 : <i>TI</i> results for the Bayonne river watershed using the D8-LAD algorithm (TauDEM).....	71
Figure A.53 : <i>TI</i> results for the Beaurivage river watershed using the D8-LAD algorithm (TauDEM).....	72
Figure A.54 : <i>TI</i> results for the Boyer river watershed using the D8-LAD algorithm (TauDEM).....	73
Figure A.55 : <i>TI</i> results for the Chibouet river watershed using the D8-LAD algorithm (TauDEM).....	74
Figure A.56 : <i>TI</i> results for the Coaticook river watershed using the D8-LAD algorithm (TauDEM).....	75
Figure A.57 : <i>TI</i> results for the Des Hurons river watershed using the D8-LAD algorithm (TauDEM)	76
Figure A.58 : <i>TI</i> results for the Du Chêne river watershed using the D8-LAD algorithm (TauDEM).....	77
Figure A.59 : <i>TI</i> results for the Etchemin river watershed using the D8-LAD algorithm (TauDEM).....	78
Figure A.60 : <i>TI</i> results for the Mascouche river watershed using the D8-LAD algorithm (TauDEM).....	79
Figure A.61 : <i>TI</i> results for the Nicolet river watershed using the D8-LAD algorithm (TauDEM).....	80

Figure A.62 : <i>TI</i> results for the Noire river watershed using the D8-LAD algorithm (TauDEM).....	81
Figure A.63 : <i>TI</i> results for the Saint-Esprit river watershed using the D8-LAD algorithm (TauDEM).....	82
Figure A.64 : <i>TI</i> results for the Yamaska river watershed using the D8-LAD algorithm (TauDEM).....	83

LIST OF TABLES

Tableau 3.1 : Statistics from the <i>TI</i> distributions on the 16 watersheds with the 3 flow direction algorithms.	19
---	----



LIST OF ACRONYMS

AAFC	Agriculture and Agri-Food Canada
BFD	Biflow direction algorithm
CDED	Canadian Digital Elevation Data
D8	Eight flow direction
DEM	Digital Elevation Model
DEMON	Digital Elevation Model Networks
DTA	Digital Terrain Analysis
GIS	Geographic Information System
IROWC	Indicators of Risk of Water Contamination
LAD	Least Angular Deviation
LTD	Least Transversal Deviation
MFD	Multiple flow direction algorithm
NAHARP	National Agri-Environmental Health Analysis and Reporting Program
NTDB	National Topographic Data Base
SFD	Single Flow Direction algorithm
TAUDEM	Terrain Analysis Using Digital Elevation Model
TFD	Tracking flow direction
TI	Topographic Index



1 INTRODUCTION

Under the National Agri-Environmental Health Analysis and Reporting Program (NAHARP) and since 2001, Agriculture and Agri-Food Canada (AAFC) has been developing Indicators of Risk of Water Contamination (IROWCs) for nitrogen, phosphorus, pesticides and coliforms. According to AAFC, the applications of IROWCs and their ensuing relations to economic and environmental models will improve and facilitate the decision making process needed to assess environmental policies in agriculture before they are put in place [Cessna and Junkins, 2003]. The possibility of a common hydrology component for the four IROWCs has been pointed out and is currently under investigation [Van Bochove *et al.*, 2004].

The hydrology component should take into account the different processes governing runoff production (saturation excess runoff and hortonian runoff). For areas with gentle slope and shallow soils on an impermeable bedrock or an impervious soil layer, topography plays a key role in surface runoff production, especially under temperate and humid climate conditions where saturation excess runoff dominates. For these areas, and under these specific conditions, the surface runoff process can be predicted with an index of hydrological similarity based on topographic considerations, the Topographic Index (*TI*) introduced by Beven and Kirkby [1979]. Following this concept, all topographic units or spatial elements of a watershed with an identical index value develop, in principle, the same conditions for saturation, surface and subsurface flow/runoff. In the context of a soil rich in nutrients, pesticides or pathogens, and prone to saturation excess runoff, the knowledge of the spatial distribution of *TI* values can be used to delineate watershed areas with a risk of pollutant loss to surface waters; that is the “hydrologically” active/connected areas.

A preliminary study focussing on the integration of *TI* concept in the hydrological component of IROWCs was recently completed [Rousseau *et al.*, 2004]. The results of this study were used to identify the conditions of application of the *TI* concept and more specifically the period of the year and the regions of Canada where it would be relevant. One of the advantages of determining the distribution of *TI* values is that it can be calculated directly using a Digital Elevation Model (DEM) within a geographic information system (GIS) environment. Several tests have shown that this approach is the simplest and the one giving the best results. However, it needs a flow direction algorithm to determine the way surface water flows downslope from one DEM pixel to another. Several different algorithms exist and have to be compared to select the most suitable one.

In this context, the goal of this study is to further investigate this approach and to apply the calculation procedure to several watersheds in Quebec. The scope of this report is to:

- (i) review existing methods and algorithms for calculating distribution of *TI* values and flow direction (Chapter 2);
- (ii) apply and compare three flow direction algorithms by calculating *TI* distribution on 16 agricultural watersheds in Quebec (Chapter 3); and
- (iii) propose further research avenues for the calculation and use of the *TI* concept within the hydrological component of IROWCs.

Note that the development of the integration procedure of the *TI* concept within the hydrological component of IROWCs is beyond the scope of this study.

2 REVIEW OF SOME COMPUTATIONAL FLOW DIRECTION ALGORITHMS

The determination of TI is very sensitive to the method or algorithm used to derive the flow direction matrix [Wilson and Gallant, 2000]. This chapter presents the basic concepts of the TI as well as a review of some flow directions algorithms.

2.1 TOPOGRAPHIC INDEX (TI)

2.1.1 Definition

The topographic index represents the propensity of a point within a watershed to generate saturation excess overland flow (see Figure 2.1). This kind of hydrological process is due to a topographic control of surface and subsurface flows [Hornberger *et al.*, 1998].

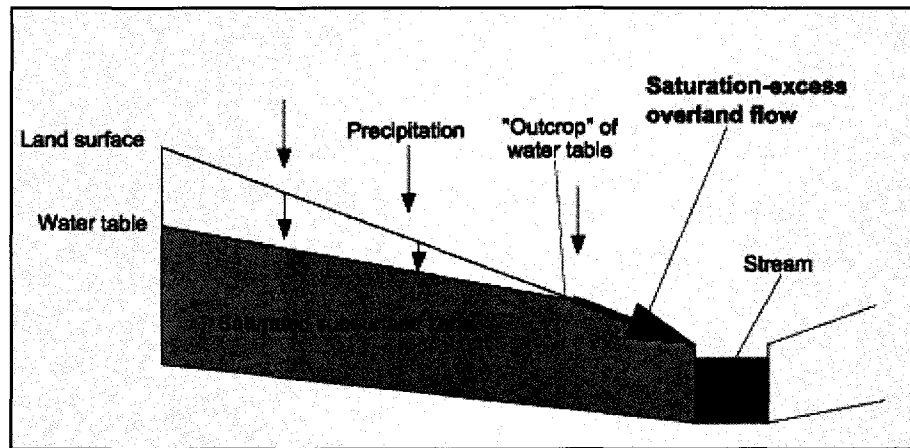


Figure 2.1: Saturation excess overland flow.

TI was first defined by Beven and Kirkby [1979] as follows:

$$TI = \ln\left(\frac{a}{\tan \beta}\right) \quad (2.1)$$

Where:

TI is the topographic index of a point/pixel within a watershed;

a is the upslope area per unit contour length draining through the point [L];

β is the local topographic slope angle acting at point.

The TI concept is closely linked to water balance (see Figure 2.2): a small and planar or divergent contributing area associated with a steep slope will imply a low inflow rate and a high outflow rate, hence a decline in water table (upper left case in Figure 2.2). Meanwhile, a large and convergent contributing area associated with a long and gentle slope will induce a high inflow rate and a low outflow rate (lower right case in Figure 2.2), hence a rise of water table and eventually occurrence of saturation excess runoff.

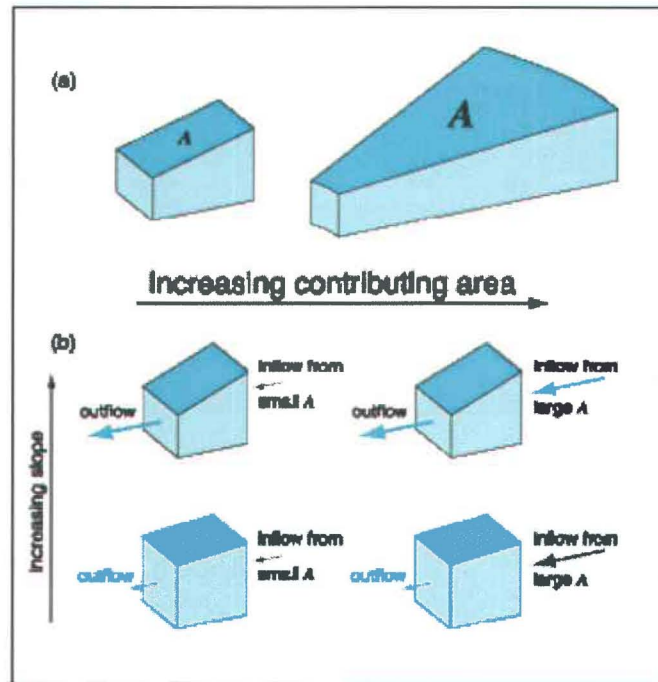


Figure 2.2 : Influence of local slope and contributing area on the water balance of a catchment “block”. The inflow rate is proportional to the contributing area A (a) and the outflow rate is controlled by the local slope (b) [Hornberger *et al.*, 1998].

Therefore, areas having identical TI values or having a TI value within a specific range are assumed to have a similar hydrological behavior. High values indicate areas characterized by large areas contributing to excess saturation runoff and relatively flat slopes, typically at the base of hillslopes, in valleys and riparian zones. Low TI values are found at the top of hillslopes, where there is relatively little upslope contributing areas and steep slopes (see figure 2.3).

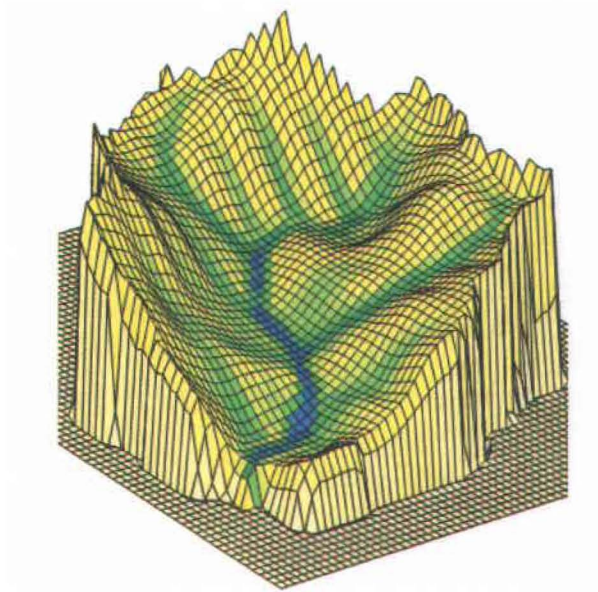


Figure 2.3 : High values of TI are in valleys and low values are at tops of hillslopes [Tarboton, 2003].

Under some conditions, the TI concept has shown good results within the classification of contributing areas to saturation excess runoff. Following that concept, several hydrological models such as TOPMODEL [Quinn *et al.*, 1991; 1995] were developed based on the theory of hydrological similarity within a watershed.

2.1.2 Computation of the topographic index

In its first version, the computation of TI was based on a manual analysis of local slope angle, upslope contributing area and cumulative area. Then, a computerized technique to derive the TI distribution was proposed by Beven and Kirkby [1979]. This technique is based on the division of the watershed into small local slope elements on the basis of dominant flow directions derived from field observations [Beven and Kirkby, 1997]. The TI values are calculated on the downslope edge of a local slope element.

At the present time, Digital Terrain Analysis (DTA) methods, also known as flow direction algorithms, are based on digital elevation model (DEM). DTA is used for the determination of the upslope area A and the specific upslope area a (the upslope area per unit contour length, L) which are needed for computation of TI values and delineation of the channel network (see Figure 2.4). The local topographic slope angle β is calculated using a slope algorithm. The TI algorithm is actually a combination of two algorithms, one that is used to calculate flow

directions, and another to calculate slopes [Pan *et al.*, 2004]. Particularly, *TI* values closely depend on the choice of a the flow direction algorithm.

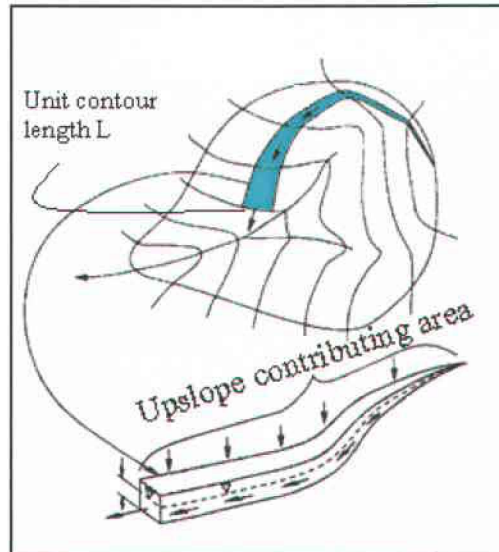


Figure 2.4: The upslope contributing area and the contour length.

2.2 PRESENTATION OF SOME FLOW DIRECTION ALGORITHMS

2.2.1 Definition

In a digital grid structure, each individual grid cell has at most eight adjacent cells. Therefore, water in a given cell can flow to one or more of its eight adjacent cells according to the slopes of the drainage paths. This is the general concept of all flow direction algorithms. There are several types of flow direction algorithms: Single Flow Direction (SFD) algorithm, Biflow Direction (BFD) algorithm, and Multiple Flow direction (MFD).

2.2.2 Single Flow Direction algorithm (SFD)

The SFD algorithm, also known as the D8 algorithm, is the earliest and the simplest method for specifying flow directions. It was introduced by O'Callaghan and Mark (1984). It calculates flow direction as the steepest downslope direction which is determined by the maximum downward gradient (see Figure 2.5).

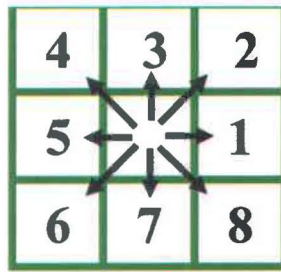


Figure 2.5 : Eight flow direction method (D8).

The steepest slope downward is the direction from the central cell to the neighboring cell (adjacent or diagonal) generating the largest downhill elevation gradient. Therefore, the drainage direction from each DEM cell is restricted to eight possibilities, separated by a $\frac{\pi}{4}$ angle when square cells are used. If the flow direction is along the diagonal, the slope is calculated as follows:

$$s = \frac{e_c - e_{dn}}{\sqrt{2} \cdot \Delta l} \quad (2.2)$$

Where:

s is the slope;

e_c and e_{dn} are respectively the central and diagonal cell elevations;

Δl is the grid cell size.

Along the cardinal direction, the slope is calculated simply as the elevation difference divided by the grid cell size [Maidment, 2002].

2.2.3 Biflow Direction algorithm (BFD)

The BFD algorithm allows flow in two directions. It constitutes a compromise between the D8 and the MFD methods.

2.2.3.1 Eight flow directions, Least Angular Deviation (D8-LAD)

Tarboton [1997] proposed the biflow direction algorithm, also known as D_{∞} . The block-centered 3×3 window cell is divided now into eight triangular facets. The flow direction is determined in the direction of the steepest downward slope within the eight facets. The flow is apportioned from the central pixel between two downslope pixels. In fact, the flow along each facet edge is inversely proportional to the angle between the steepest downward direction and the edge (see Figure 2.6).

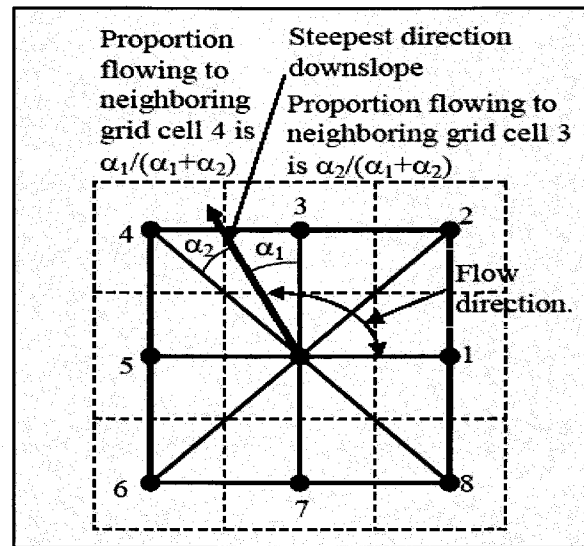


Figure 2.6: Flow directions defined as steepest downward slope on planar triangular facets on a block centered grid [Tarboton, 1997]

The implementation of this procedure is clearer by considering a single triangular facet (see Figure 2.7). The elevations e_i ($i = 0,1,2$) and the distances d_i ($i = 1,2$) are the three-dimensional geometry of each triangular facet.

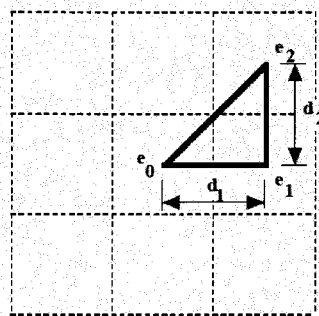


Figure 2.7: Definition of variable for the calculation of slope on a single triangular facet [Tarboton, 1997].

The elevations are arranged such that e_0 is in the central pixel, e_1 is in the side pixel and e_2 is in the diagonal pixel.

The downward slope can be represented by the vector (s_1, s_2) where:

$$s_1 = \frac{e_0 - e_1}{d_1} \quad (2.3)$$

$$s_2 = \frac{e_1 - e_2}{d_2} \quad (2.4)$$

The direction r and the magnitude of the maximum slope s are:

$$r = \arctan\left(\frac{s_2}{s_1}\right) \quad (2.5)$$

$$s = \sqrt{s_1^2 + s_2^2} \quad (2.6)$$

If r is not in the range $\left[0, \arctan\left(\frac{d_2}{d_1}\right)\right]$ of the facet at the center point, then r needs to be set as the direction along the appropriate edge and s assigned as the slope along that edge.

$$\text{If } r < 0, \text{ then } r = 0 \text{ and } s = s_1 \quad (2.7)$$

$$\text{If } r > 0, \text{ then } r = \arctan\left(\frac{d_2}{d_1}\right) \quad (2.8)$$

and

$$s = \frac{e_0 - e_2}{\sqrt{d_1^2 + d_2^2}} \quad (2.9)$$

Possible drainage directions from a given DEM cell are identified by the use of a pointer p which indicates the local cell number of the draining cell. In fact, a pointer p_1 is associated with a cardinal directions and a pointer p_2 denotes diagonal directions of the facet containing the theoretical drainage direction. α_1 and α_2 are the angular deviations (see Figure 2.5) produced when approximating the theoretical drainage direction by the cardinal and diagonal directions. Where:

$$\alpha_1 = r \quad (2.10)$$

and

$$\alpha_2 = \arctan\left(\frac{d_2}{d_1}\right) - r \quad (2.11)$$

The LAD criterion determines that the direction identified by p_1 is selected if $\alpha_1 \leq \alpha_2$, whereas the direction identified by p_2 is selected if $\alpha_2 > \alpha_1$.

2.2.3.2 Eight flow directions, Least Transversal Deviation (D8-LTD)

Orlandini *et al.* [2003] proposed an alternative strategy to the D8-LAD by introducing the criterion of the least transversal deviation (LTD). The transversal deviation is defined as the linear distance between the center of the draining cell and the path along the theoretical drainage direction that originates at the center of the drained cell (see Figure 2.8). The transversal deviation between the cardinal direction and the theoretical drainage direction is δ_1 , whereas δ_2 is the transversal deviation when approximating the theoretical drainage direction by the diagonal deviation. The formulation of δ_1 and δ_2 is as follows:

$$\delta_1 = d_1 \sin \alpha_1 \quad (2.12)$$

$$\delta_2 = \sqrt{d_1^2 + d_2^2} \cdot \sin \alpha_2 \quad (2.13)$$

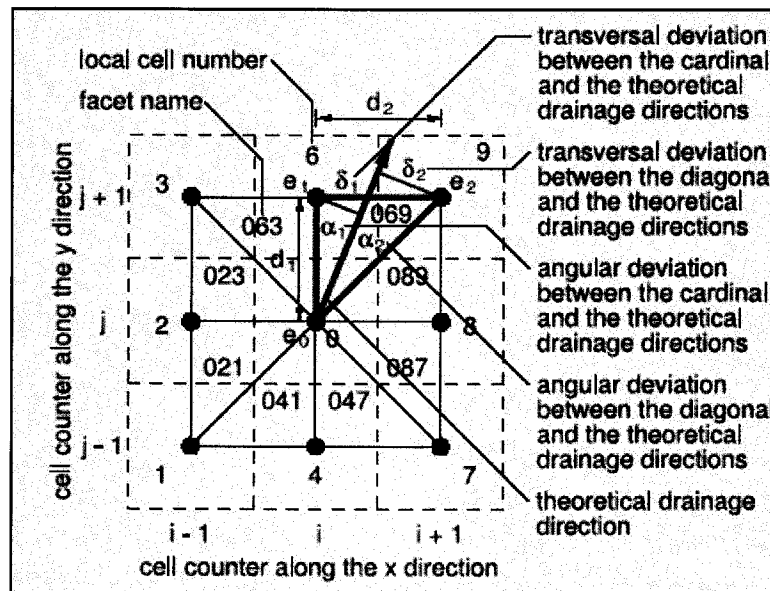


Figure 2.8 : The elementary computational used in the D8-LAD and the D8-LTD methods [Orlandini *et al.*, 2003]

The LTD criterion determines that the direction identified by p_1 is selected if $\delta_1 \leq \delta_2$, whereas the direction identified by p_2 is selected if $\delta_1 > \delta_2$.

2.2.4 Multiple Flow Direction algorithm (MFD)

MFD algorithms are a generalization of BFD as they allow flow in more than one or two directions, in order to improve representation of the flow convergence or divergence. In the MFD described by Quinn *et al.* [1991], each flow direction is weighted by the downward elevation gradient multiplied by the contour length (0.5 weighting for cardinal directions and 0.35 for a diagonal weighting) (see Figure 2.9).

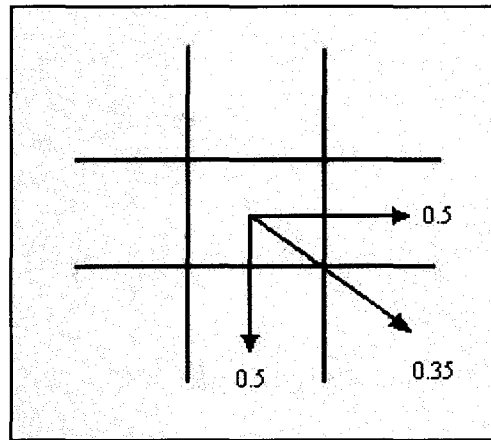


Figure 2.9: Weights attributed to flow directions in the MFD of Quinn *et al.*, [1991].

2.3 DISCUSSION

Several studies have shown that the popular D8 algorithm has some drawbacks. The major ones are:

- (i) it cannot predict flow divergence because the flow from one central cell is restricted only to a single downslope neighbouring cell; and
- (ii) it tends to delineate flow in parallel lines along preferred directions that are multiples of $\frac{\pi}{4}$; and
- (iii) It doesn't deal with flat areas and pits (local depressions in the DEM).

Many authors have attempted to bypass these problems. Fairfield and Leymarie [1991] introduced a stochastic version of the D8 method, known as the Rho8 (Random eight node) algorithm. It reduces problems associated with parallel flow lines but still can not model flow dispersion [Mendicino and Sole, 1997; Wilson and Gallant, 2000].

MFD algorithms allow flow to be distributed to multiple downslope neighbouring cells. These methods give better results as compared to the standard D8 but have a problem of high dispersion [Tarboton, 1997; Beaujouan *et al.*, 2000; Turcotte *et al.*, 2001]. However, it is noteworthy that the MFD algorithm of Quinn *et al.*, [1991] provides a way to consider that flow on hillslopes should be divergent while flow along valley bottoms should be convergent [Quinn *et al.*, 1995; Saulnier *et al.*, 1997].

Costa-Cabral and Burges [1994] proposed a set of procedures know as DEMON (Digital Elevation Model Networks). DEMON is deterministic and precisely resolves flow directions and hence reduces flow dispersion. Nevertheless, it does not cope with certain elevations combination which can lead to inconsistent or counter intuitive flow directions [Tarboton, 1997]. The method of Tarboton [1997; Kim and Lee, 2004] avoids this inconsistency introduced by DEMON.

Tarboton [1997] and Orlandini *et al.* [2003] have proposed the D8-LAD (or D^∞) and the D8-LTD, respectively. These two methods constitute a compromise between the simplicity of the D8 approach and the MFD formulations. These algorithms were developed to mitigate the effects of grid artifacts (pits, flat areas) produced by D8 algorithms and to avoid high dispersion and significant computational costs [Orlandini *et al.*, 2003]. Furthermore, the use of non-dispersive methods such as D8-LAD and D8-LTD provides more accuracy in the delineation of the drainage network both over hillslope areas and along valleys than the classical D8 method. The D8-LTD gives better results than the D8-LAD which still maintains a certain degree of dispersion [Orlandini *et al.*, 2003]. In the same way, Turcotte *et al.* [2001] reported that the MFD algorithms of Fairfield and Leymarie [1991], Quinn *et al.* [1991], Costa-Cabral and Burges [1994] and Tarboton [1997] reflect more accurately drainage flow directions than the D8 algorithm.

However, all these algorithms have troubles to define flow directions in flat areas [Garbrecht and Martz, 1997] which often make the computation of *TI* difficult. This has for consequence to eliminate the exact match between modelled flow directions and actual river network location. To bypass this problem, Turcotte *et al.* [2001] have developed a new method using a digital river and lake network (DRLN) as input in addition to the DEM in order to correct the modelled flow directions. Turcotte *et al.* [2001] made use of ancillary stream data to impose or “burn” the DRLN vector data to improve the accuracy of flow direction matrices in flat areas and in the riparian zone. “Burning” streams refers to the process of decreasing elevation of

grid cells representing watercourses to enforce the known drainage patterns on the flow direction matrix (see Figure 2.10).

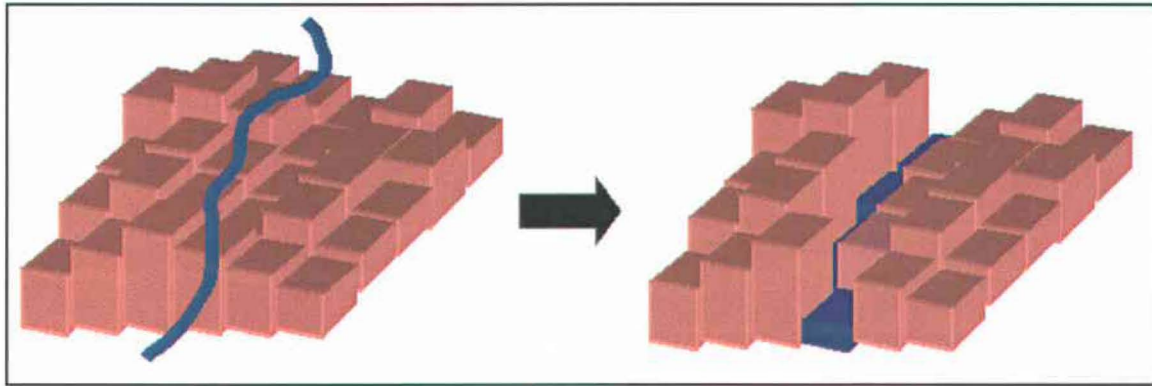


Figure 2.10 : The “burning” process.

Moreover, several algorithms have been proposed to improve the definition of flat areas by flow direction algorithms. In the recent study of Pan *et al.* (2004), two algorithms of slope calculation in flat areas were used:

- (i) the first one was proposed by Wolock and McCabe [1995] (W-M method); and
- (ii) the second one is called the tracking flow direction (TFD) introduced by [Pan *et al.*, 2004].

The W-M method assigns a value of $0.5 \frac{VR}{HR}$ (where VR and HR are the vertical and horizontal resolutions of a DEM, respectively) to zero-slope values of flat areas. The TFD method is more accurate than the W-M method because it can give smaller slope values than $0.5 \frac{VR}{HR}$ to replace zero-slope values [Pan *et al.*, 2004] and hence, maintains more consistency between flow direction and slope in flat areas. A combination of a MFD algorithm and TFD method is recommended by Pan *et al.* [2004] when the vertical resolution of a DEM is low.

2.4 CONCLUSION

By comparing a set of flow directions algorithms published in the literature, it seems that the D8-LTD [Orlandini *et al.*, 2003] is the most suited one for the determination of the drainage network. However, the use of an initial reconditioning of a DEM by the “burning” procedure and the elimination of pits is strongly recommended before the implementation of the flow direction algorithm. It is now necessary to apply and compare different algorithms on several watersheds to practically confirm this assumption. In addition to the D8-LTD algorithm, two other algorithms will be tested: the D8-LAD algorithm of Tarboton *et al.* [1997] and the D8 algorithm of O’Callaghan and Mark [1984] which is integrated in the ArcGIS software (ESRI).

3 APPLICATION OF THE ALGORITHMS ON 16 WATERSHEDS

The three flow direction algorithms selected from the literature review of Chapter 2 were applied on 16 watersheds in Quebec. This chapter presents the technical procedure for the application of each algorithm, the results obtained and recommendations for future work.

The 16 watersheds selected by AAFC are: Acadie, De l'Achigan, Des Anglais, Bayonne, Beaurivage, Boyer, Du Chêne, Chibouet, Coaticook, Etchemin, Des Hurons, Mascouche, Nicolet Sud-Ouest, Noire, Saint-Esprit, Yamaska Sud-Est.

3.1 TECHNICAL PROCEDURE

The computation of the *TI* distribution on a watershed is performed with ArcView 8. It follows five steps:

- (1) Preparation of the DEM;
- (2) DEM pre-processing by a "burning" procedure and a sink removal algorithm;
- (3) Computation of the slope by applying a slope algorithm on the original DEM;
- (4) Implementation of the flow direction algorithm on the reconditioned DEM;
- (5) Determination of the flow accumulation; and
- (6) Calculation of the *TI* values.

Steps 1, 2 and 6 are common to all the methods used, while the technical procedure followed for steps 3 through 5 is specific to each of the three flow direction algorithms.

Finally, the mean, median, standard-deviation and skewness of *TI* distributions are calculated using a C++ program we developed. These criteria allow us to evaluate the three algorithms used in this study. Consequently, we will be able to choose the most suited flow direction algorithm for the *TI* computation within the 16 agricultural watersheds.

3.1.1 Preparation of the DEM

- A preliminary step is to create, from the vector layer containing the 16 watersheds, a layer containing only the watershed of interest.

- Then, the 1:50 000 data sheets of the Canadian Digital Elevation Data (CDED) covering this watershed are identified and downloaded from the Geobase website (www.geobase.ca/geobase/Geobase). Note that DEMs are originally in USGS format and they have to be imported as Grid Format (ESRI).
- Once imported in ArcView, the DEMs are compiled into a DEM mosaic covering the watershed. If the mosaic contains pixels with 0 values, it has to be reclassified to change 0 into “No Data”.
- The next step is to create the layer that will be used as a mask, by converting the initial vector layer into a “grid” type layer.
- The coordinates system of the DEM mosaic and the mask are converted and projected into UTM NAD83 Z19 by creating two new layers.
- The DEM of the watershed is created using the mask.
- The hydrological network is also imported from the National Topographic Data Base (NTDB) in SHAPE format at the 1:50 000 scale. It will be used for the burning process.

3.1.2 Calculation of *TI* using the D8 algorithm [O’Callaghan and Mark, 1984]

This is the simplest of the three procedures since it is already incorporated in ArcView as “Arc Hydro” tool.

- The slope is first calculated (using the “Slope” option)
- The hydrological network is burnt with the “DEM reconditioning” option.
- The “Fill sinks” option is activated
- The flow direction matrix is generated (“Flow direction” tool) as well as the flow accumulation matrix.
- Slope and flow accumulation matrices are used to generate the *TI* values after defining the *TI* equation in the “Raster Calculator” window as follows :

$$TI = \ln \left(\frac{[flow_acc] + 1}{\frac{[slp]}{100} + 1} \right) \quad (3.1)$$

Where, $[flow_acc]$ is the flow accumulation matrix and $[slp]$ is the slope matrix (in percentage).

3.1.3 Calculation of TI using the D8-LTD algorithm [Orlandini *et al.*, 2003]

This method uses the D8-LTD computer program which runs independently from ArcView. It requires the burning of the DEM using the Arc Hydro Tool option (see Section 3.1.2).

- Before computing this algorithm, we need to check that the DEM has only one lowest elevation value, as it will be used to determine the outlet of the watershed. If it is not the case, the DEM has to be modified.
- Then the DEM is exported in ASCII format by using the script “GridToASCII”.
- The DEM (ASCII format) has to be modified to be compatible with the D8-LTD computer program: matrix must contain real values; commas must be replaced by points; “No Data” must be replaced by 0.0; headers must be removed.
- The input file “hap.in” is updated following the DEM proprieties (x, y cell sizes, number of lines and columns)
- The program is run. The slope and accumulation matrices are generated. Then, they have to be imported into ArcView to calculate TI of each individual pixel.
- The imported files are converted to be compatible with ArcView, that is: creation of headers, replacement of 0.0 by “No Data”, replacement of points by commas.
- The TI matrix is generated using Arc Hydro tool, following the same steps as those for the D8 algorithm (Section 3.1.2).

3.1.4 Calculation of TI using the D8-LAD algorithm [Tarboton *et al.*, 1997]

Similar to the Arc Hydro method, this algorithm uses TauDEM (Terrain Analysis Using Digital Elevation Models) which is a set of tools that can be integrated within the ArcView environment as extendable component (toolbar plug in). It can be downloaded from the Utah State University website (<http://hydrology.neng.usu.edu/taudem/>). The calculation requires burning of the DEM using the Arc Hydro Tool option (see Section 3.1.2).

- The sinks are filled using the “Fill Pits” tool of TauDEM.
- The flow direction algorithm is performed using the “Dinf Flow Direction” tool.
- The flow accumulation matrix is generated with the “Dinf Contributing Area” tool.
- Finally, the TI matrix is generated using Arc Hydro tool, following the same steps as for the D8 algorithm (Section 3.1.2).

3.2 RESULTS AND DISCUSSIONS

A total of 48 *TI* distribution maps were generated; results from the application three flow direction algorithms (D8, D8-LAD and D8-LTD) on 16 watersheds. These maps are presented in Appendix A. By a simple visual comparison, we can see that D8-LAD and D8-LTD algorithms give a better representation of *TI* than D8 which generates more parallel lines (see for example the Beaurivage watershed on Figures A.22, A.37 and A.53). This is not surprising since we noticed in chapter 2 that this is known to be a major drawback of the D8 algorithm.

Statistics were used to compare the *TI* distributions. Mean, median, standard deviation and skewness were calculated for each *TI* distribution (see Table 3.1). In all cases, the median value is lower than the mean, which means that the *TI* distribution is skewed to the right. Concerning the comparison of algorithms, the D8 and D8-LTD algorithms give similar mean and median values of *TI* (between 1.4 and 1.8 for the mean, and between 1 and 1.4 for the median) while the D8-LAD algorithm gives higher values (around 4.4 and 4.0 for the mean and the median respectively). In all likelihood, this is due to the numerous “Nodata” values generated by this algorithm which imply a reduction in the number of treated pixels (see Table 3.1). Tarboton [2004] explained that “Nodata” values are due to an edge contamination which can be introduced when the DEM is clipped along a watershed outline. These higher mean and median values for D8-LAD are also due to the fact that D8 and D8-LTD generate negative values while for D8-LAD, *TI* values are always higher than 2.9.

As introduced in Table 3.1, for each algorithm all statistical values are very homogeneous for all the 16 watersheds. In order to test the relationship between the *TI* distributions and the topography of the 16 watersheds, hypsometric curves were drawn and compared to the *TI* distributions obtained with the three algorithms (Figures A.1 to A.18). We can see that hypsometric curves vary among the 16 watersheds, some of them being very flat (Acadie, Des Anglais, Du Chêne, Chibouet, Mascouche,) while others display uniform distributions of elevations (Achigan, Des Hurons, Coaticook, Beaurivage, Yamaska). Meanwhile, the *TI* distribution remains homogeneous among the 16 watersheds for D8-LAD and D8-LTD algorithms. However, the *TI* distributions obtained with the D8 algorithm change from one class of watershed to another, with a shift between the two first classes of values ($[0;2[$ and $[-2;0[$). For instance, for the flat Mascouche watershed, 10% and 52% of *TI* values are in the $[0;2[$ and $[-2;0[$ classes respectively (see Figure A.12). On the other hand, for the Etchemin river watershed, which is characterized by a large variability of altitudes, these values are 29% and 40% (see Figure A.11). This suggests that the *TI* distribution calculated with the D8 algorithm is more sensitive to watershed topography than when using the two other algorithms.

Table 3.1: Statistics from the *TI* distributions on the 16 watersheds with the three flow direction algorithms.

	Algorithms	Number of pixels	Maximum	Minimum	Mean	Median	Standard Deviation	Skewness
Acadie	D8	1435361	13,95	-0,46	1,77	1,39	1,72	0,66
	D8-LAD	1388995	13,46	3,04	4,47	4,11	1,61	0,67
	D8-LTD	1435361	14,18	-0,59	1,56	1,10	1,84	0,75
Achigan	D8	1736236	14,27	-0,70	1,53	1,10	1,79	0,72
	D8-LAD	1680758	14,03	2,98	4,39	4,06	1,56	0,63
	D8-LTD	1736236	14,37	-0,81	1,44	0,99	1,86	0,73
Anglais	D8	1315658	14,04	-0,35	1,61	1,32	1,77	0,49
	D8-LAD	1275048	14,91	3,04	4,42	4,09	1,58	0,63
	D8-LTD	1315658	14,09	-0,58	1,50	1,05	1,84	0,73
Bayonne	D8	1015629	13,80	-0,64	1,50	1,07	1,81	0,71
	D8-LAD	970749	13,98	2,99	4,36	3,98	1,57	0,73
	D8-LTD	1015629	13,83	-0,90	1,43	0,96	1,87	0,75
Beaurivage	D8	1974409	14,44	-0,52	1,65	1,35	1,78	0,51
	D8-LAD	1916701	15,08	2,99	4,46	4,07	1,63	0,72
	D8-LTD	1974409	14,50	-0,69	1,51	1,05	1,87	0,74
Boyer	D8	589493	13,18	-0,42	1,60	1,10	1,79	0,84
	D8-LAD	559786	13,08	3,02	4,42	3,70	1,61	1,34
	D8-LTD	589493	13,29	-0,59	1,53	1,05	1,90	0,76
Chibouet	D8	303086	12,30	-0,38	1,60	1,36	1,69	0,43
	D8-LAD	285389	12,76	3,03	4,32	3,71	1,47	1,24
	D8-LTD	303086	12,62	-0,46	1,50	1,10	1,83	0,66
Coaticook	D8	2286652	14,05	-0,69	1,53	1,05	1,82	0,79
	D8-LAD	2217994	13,62	3,00	4,54	4,08	1,64	0,84
	D8-LTD	2286652	14,64	-0,85	1,55	1,05	1,87	0,80
Des Hurons	D8	835178	13,59	-0,69	1,69	1,39	1,71	0,53
	D8-LAD	803312	13,74	2,99	4,42	4,07	1,58	0,66
	D8-LTD	835178	13,64	-0,81	1,49	1,05	1,82	0,73
Du Chêne	D8	2169346	14,55	-0,52	1,74	1,39	1,79	0,59
	D8-LAD	2114044	13,83	2,99	4,41	4,07	1,60	0,64
	D8-LTD	2169346	14,59	-0,79	1,53	1,05	1,88	0,77
Etchemin	D8	3926981	15,15	-0,60	1,56	1,08	1,81	0,80
	D8-LAD	3815941	15,27	3,00	4,51	4,08	1,62	0,80
	D8-LTD	3926981	15,18	-0,92	1,50	1,05	1,87	0,72
Mascouche	D8	1114436	13,78	-0,38	1,75	1,39	1,73	0,62
	D8-LAD	1082506	13,89	3,00	4,41	4,07	1,61	0,63
	D8-LTD	1114436	13,92	-0,53	1,53	1,05	1,85	0,78
Nicolet	D8	4446620	15,27	-0,61	1,61	1,13	1,79	0,80
	D8-LAD	4331152	15,14	3,01	4,46	4,08	1,62	0,70
	D8-LTD	4446620	15,31	-0,76	1,51	1,05	1,86	0,74
Noire	D8	4236437	15,20	-0,70	1,63	1,30	1,80	0,55
	D8-LAD	4140950	15,30	3,00	4,47	4,08	1,65	0,71
	D8-LTD	4236437	15,26	-0,85	1,53	1,05	1,86	0,77
Saint-Esprit	D8	598467	13,18	-0,60	1,55	1,10	1,79	0,75
	D8-LAD	566761	13,07	2,99	4,34	4,00	1,51	0,68
	D8-LTD	598467	13,30	-0,74	1,45	1,00	1,88	0,72
Yamaska	D8	1116561	13,88	-0,63	1,53	1,07	1,81	0,76
	D8-LAD	1060162	13,36	3,00	4,44	4,07	1,54	0,72
	D8-LTD	1116561	13,93	-0,92	1,49	1,05	1,86	0,71

The above observations suggest that all studied watersheds display similar topographic and *TI* distribution features. These watersheds are characterized by contributing areas of varying sizes with a propensity to excess saturation runoff that are located in lowlands, typically at the base of hillslopes, in valleys and riparian zones. Lower *TI* values were found at the top of hillslopes, where there is relatively little upslope contributing areas and steep slopes. In other words, the *TI* distributions reveal that all these watersheds are somewhat hydrologically similar.

The influence of the 'burning' process on *TI* distribution values is shown on Figure 3.1. It is clear that when the DEM is burnt, the flow direction algorithm gives a modelled river network that corresponds to the actual one. Consequently, the results of the computed *TI* values will be more accurate.

The influence of DEM grid resolution on *TI* distributions was also studied. Two grid scales were compared: 19.12 m and 100 m. The results show that the use of a larger grid size is preferable because it allows an efficient 'burning' for wide rivers and hence better results for the delineation of the river network. We see on Figure 3.3 that the 'burning' process used on 19.12 m resolution DEM generates ridge lines for large rivers (in this case the Beaurivage river) and that this problem is bypassed when using the 100 m resolution DEM. However, there is a limit in the decrease of the grid resolution. Indeed, a large grid resolution also induces a loss of information and, when combined to a low vertical resolution, creates flat surfaces.

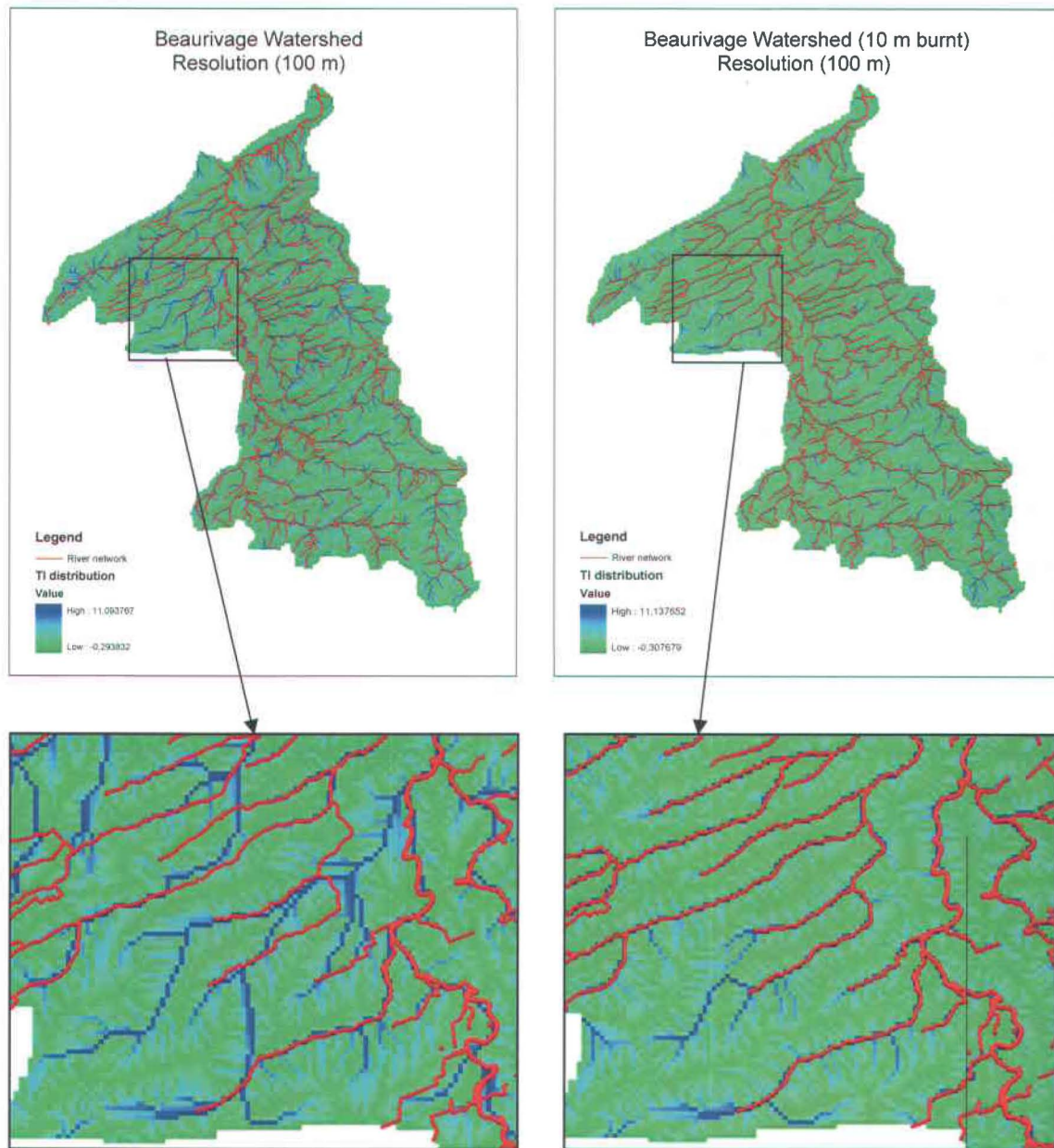


Figure 3.1: Comparison of *TI* distributions obtained by the D8 method on the Beaurivage watershed (100 m grid resolution) without the 'burning' process (left) and with the 'burning' process (right).

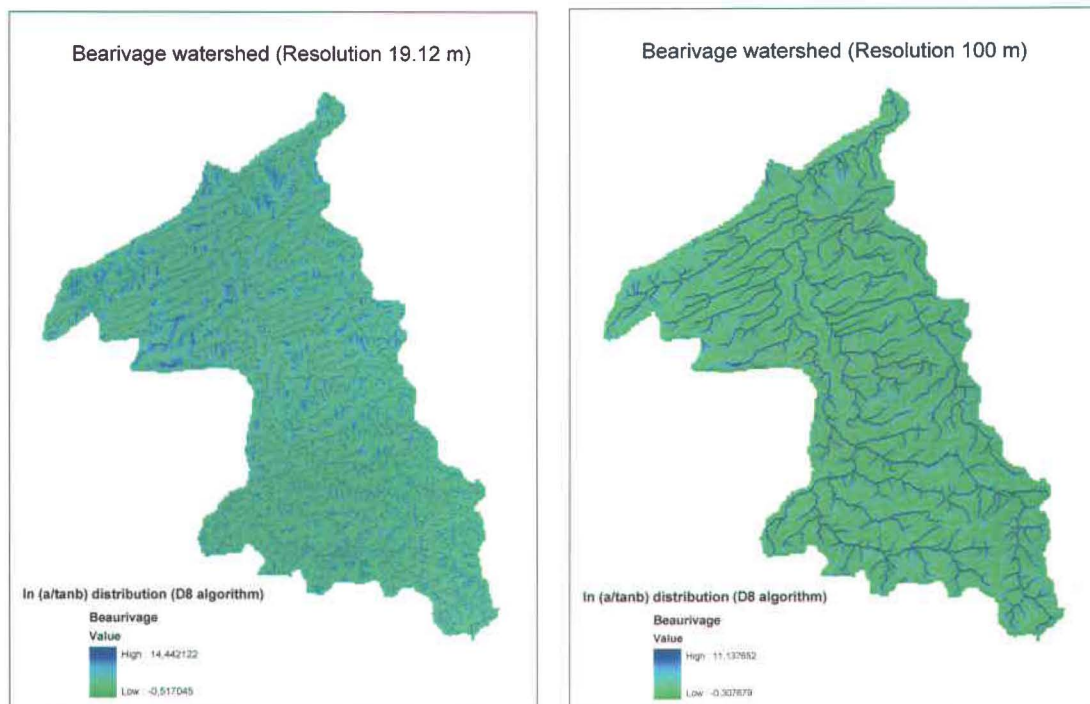


Figure 3.2 : *TI* distributions obtained by the D8 method on the Beaurivage watershed for the two grid resolutions (19.12 m and 100 m).

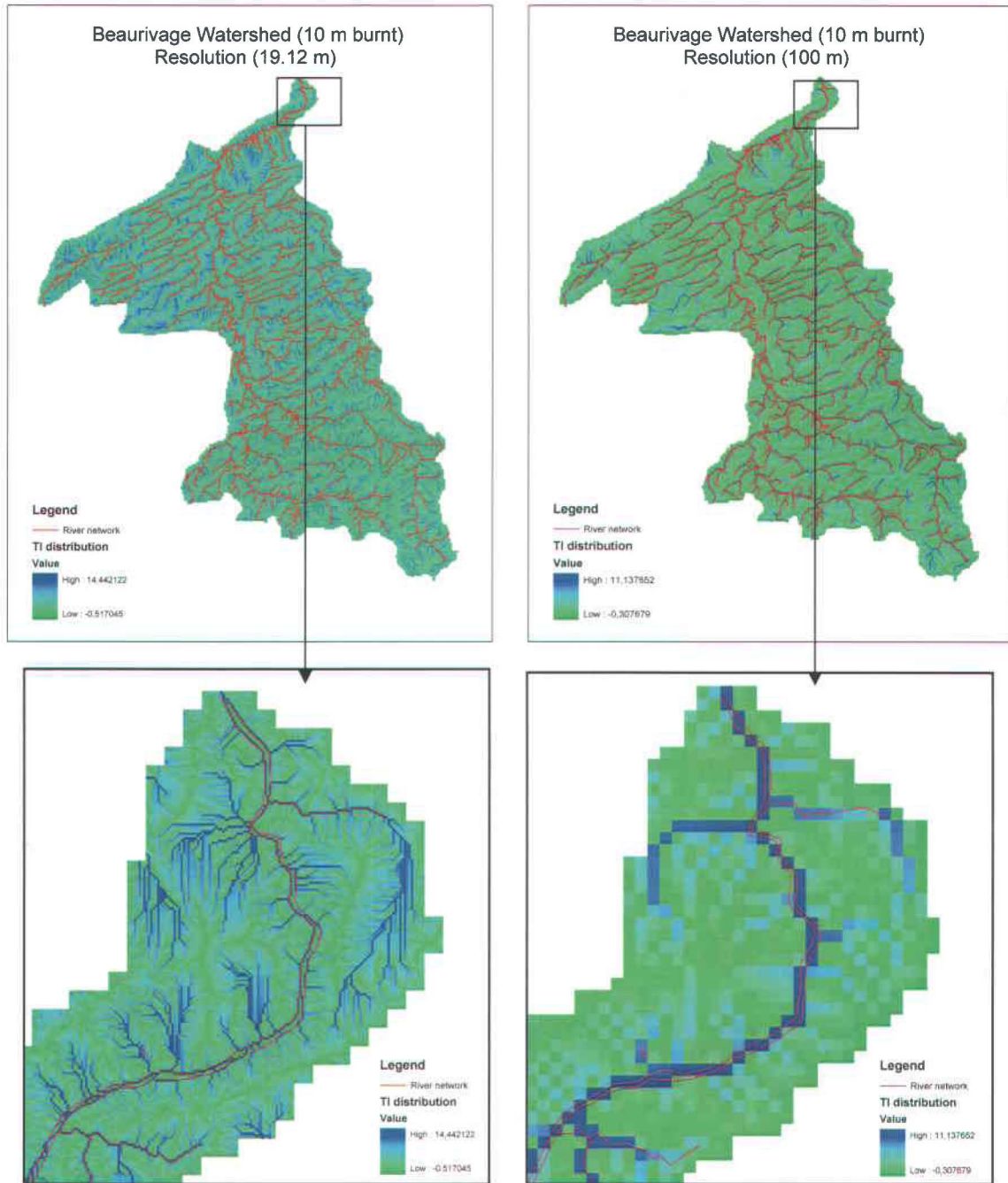


Figure 3.3 : The resolution effect (19 m and 100 m) on *TI* distributions obtained by the D8 method on the Beaurivage watershed.

3.3 RECOMMENDATIONS

The results obtained in this application on several watersheds confirm what has been reported in the literature review introduced in Chapter 2: the limitations of the D8 method (generation of parallel lines) and the “Nodata” generated by the D8-LAD algorithm lead us to recommend the use of the D8-LTD to compute the TI distribution. However, the results of these applications also showed that the D8 algorithm seems to be the most suited for discrimination of watersheds. Therefore, it would be interesting to test and compare these methods on watersheds with a larger range of topographic characteristics.

Regarding the problem of wide rivers delineation, the results obtained lead us to recommend the use of the ‘burning’ process before computing the flow direction algorithm on a 100-m grid resolution DEM.

However, flat surfaces and lakes still represent an obstacle for the computation of flow directions with the three algorithms. To solve this problem, algorithms of slope calculation in flat areas should be tested, such as the W-M and the TFD methods introduced in Section 2.3. The approach developed by Turcotte *et al.* (2001) that was subsequently integrated in PHYSITEL could also be a solution that should be investigated.

4 CONCLUSION

The objective of this study was to investigate several Topographic Index (*TI*) calculation procedures/algorithms to select the most suited one for integration in the hydrological component of IROWC. The algorithms compute *TI* values on a pixel by pixel basis using a GIS and require a DEM of the watershed and a vector-based river and lake networks as input data for calculating slope, flow direction and accumulation. Based on a literature review, several flow direction algorithms were described and compared. Three of them (D8, D8-LAD and D8-LTD) were selected and applied on 16 watersheds in Quebec in order to investigate their applicability under Quebec conditions. The results were used to select the most suited algorithm.

A procedure was developed, integrating the preparation of the DEM and a burning process that bypasses the problem of mismatching between modelled flow directions and the actual river and lake networks. Good results were obtained in all cases, showing that these algorithms can be easily applied on any watershed to generate *TI* distributions and their corresponding statistical parameters. The results showed that the D8 algorithm generates parallel flow lines in several areas while the D8-LAD algorithm generates "Nodata" values. This confirmed that the D8 and the D8-LAD are not well suited for *TI* computations and leads us to recommend the use of D8-LTD. We also recommend the use of a 100-m grid resolution DEM.

From a surface hydrology point of view, all studied watersheds displayed similar topographic and *TI* distribution features. These watersheds are characterized by contributing areas of varying sizes with a propensity to excess saturation runoff that are located in lowlands, typically at the base of hillslopes, in valleys and riparian zones. Lower *TI* values were found at the top of hillslopes, where there is relatively little upslope contributing areas and steep slopes. The *TI* distributions revealed that all watersheds are somewhat hydrologically similar.

From a computational point of view, there are still difficulties for computing flow directions for flat surfaces and lakes, and existing methods should be investigated to obtain better results. Algorithms and frameworks that provide a means to better define slopes and flow directions in flat areas of watersheds include W-M, TFD and PHYSITEL. Moreover, it would be interesting to test the procedure on more discriminating watersheds than those used in this study to verify the applicability of flow direction algorithms and *TI* computation under a larger range of topographic conditions.



5 REFERENCES

Beaujouan V., P. Arousseau, P. Durand, H. Squidant and L. Ruiz, 2000. Comparaison de méthodes de définitions des chemins hydrauliques pour la modélisation à l'échelle du bassin versant. *Géomatique*, **10**: 39-60.

Beven K.J. and M.J. Kirkby, 1979. A physically-based, variable contributing area model of basin hydrology. *Hydrological Sciences Bulletin*, **24**: 43-69.

Cessna A.J. and B. Junkins, 2003. Linking Agri-Environmental Water Quality Indicators (AEWQIs) to Policy: the Canadian Experience. Trilateral Cooperation to Promote the Protection of Water Quality through Sustainable Agriculture, Banff, Alberta, October 7 – 10, 2003.

Costa-Cabral M.C. and S. Burges, 1994. Digital elevation model networks (DEMON): A model of flow over hillslopes for computation of contributing and dispersal areas. *Water Resources Research*, **30**(6): 1681-1692.

Fairfield J. and P. Leymarie, 1991. Drainage networks from grid elevation models. *Water Resources Research*, **27**(5): 709-717.

Garbrecht J. and L.W. Martz, 1997. The assignment of drainage direction over flat surfaces in raster digital elevation models. *Journal of Hydrology*, **193**: 204-213.

Hornberger G.M., J. P. Raffensperger, P.L. Wiberg, and K.N. Eshleman 1998. Elements of Physical Hydrology. Science & Applied Mathematics Earth and Space Sciences. John Hopkins University Press. 312 pages.

Kim S. and H. Lee, 2004. A digital elevation analysis: a spatially distributed flow apportioning algorithm. *Hydrological Processes*, **18**: 1777-1794.

Maidment D.R. (editor), 2002. Arc Hydro GIS for Water Resources. ESRI. 203 pages.

Mendicino G. and A. Sole, 1997. The information content theory for the estimation of the topographic index distribution used in TOPMODEL. *Hydrological Processes*, **11**: 1099-1114.

O'Callaghan J.F. and D.M. Mark, 1984. The extraction of drainage networks from digital elevation data. *Comput. Vis. Graph. Image Process*, **27**: 323-344.

Orlandini S., G. Moretti and M. Franchini, 2003. Path-based methods for the determination of non dispersive drainage directions in grid-based digital elevation models. *Water Resources Research*, **39**(6), 1144.

Pan F., C.D. Peters-Lidard, M.J. Sale and A.W. King, 2004. A comparison of geographical information system-based algorithms for computing the TOPMODEL topographic index. *Water Resources Research*, **40**, W06303.

Quinn P.F., K.J. Beven and R. Lamb, 1995. The $\ln(a/\tan\beta)$ index: How to use it within the TOPMODEL framework. *Hydrological Processes*, **9**: 161-182.

Quinn P. and K. Beven, P. Chevalier and O. Planchon, 1991. The prediction of hillslope flow paths for distributed hydrological modelling using digital terrain models. *Hydrological Processes*, **5**: 59-79.

Rousseau, A.N., R. Quilbé, B. Lacasse and J.-P. Villeneuve, 2004. Integration of a Topographic Index in the Hydrology Component of the Indicator of Water Contamination by Phosphorus. Rapport n° R-727. INRS-ETE, Sainte-Foy (Qc), Canada.

Saulnier G.M., K. Beven and C. Obled, 1997. Digital elevation analysis for distributed hydrological modeling: Reducing scale dependence in effective hydraulic conductivity values. *Water Resources Research*, **33**(9): 2097-2101.

Tarboton D.G., 2004. Terrain Analysis Using Digital Elevation Models.
<http://hydrology.neng.usu.edu/taudem/>

Tarboton D.G., 2003. Terrain Analysis Using Digital Elevation Models in Hydrology. 23rd ESRI International Users Conference, San Diego, California, July 7-11.
<http://www.engineering.usu.edu/cee/faculty/dtarb/>

Tarboton D.G., 1997. A new method for determination of flow directions and upslope areas in grid digital elevation models. *Water Resources Research*, **33**(2): 309-319.

Turcotte R., J.-P. Fortin, A.N. Rousseau, S. Massicotte, J.-P. Villeneuve, 2001. Determination of the drainage structure of a watershed using a digital elevation model and a digital river and lake network. *Journal of Hydrology*, **240**: 225-242.

Van Bochove É., G. Thériault, F. Dechmi, A.N. Rousseau, R. Quilbé, M.-L. Leclerc and N. Goussard, 2004. Indicator of risk of water contamination by phosphorus from Canadian agricultural land. *Proceedings of the 8th International Conference on Diffuse/Nonpoint Pollutants of the International Water Association (IWA)*, 24-28 Octobre 2004, Kyoto, Japon.

Wilson P.J. and C.J. Gallant (editors), 2000. Terrain analysis: principles and applications. John Wiley & sons, Ltd, New York. 303 pages.

Wolock D.M. and G.J. McCabe Jr., 1995. Comparison of single and multiple flow direction algorithms for computing topographic parameters in TOPMODEL. *Water Resources Research*, **31**(50): 1315-1324.

APPENDIX A. COMPUTED TI DISTRIBUTIONS FOR THE 16 WATERSHEDS

This Appendix presents the results of the TI calculation for each of the 16 watersheds using the three flow direction algorithms: D8 [O'Callaghan and Mark, 1984], D8-LTD [Orlandini *et al.*, 2003] and D^∞ [Tarboton *et al.*, 1997].

Figures A.1 through A.16 present the statistical distributions of TI values for each watershed using the D8 method (Arc Hydro tool), the D8-LAD (TauDEM) and the D8-LTD. Hypsometric curves of the watersheds are also presented in the same figures. Figures A.17 to A.64 introduce the spatial distributions of TI values within the watersheds resulting from the application of the three methods.

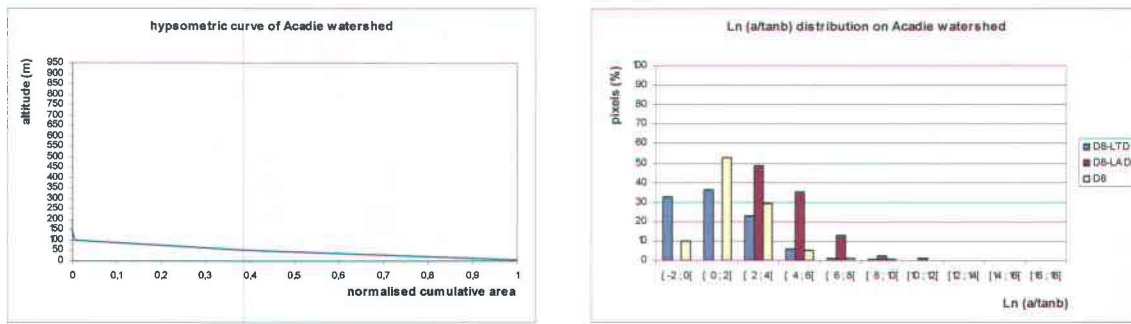


Figure A.1 : Hypsometric curve and *TI* distributions on Acadie river watershed obtained by the 3 flow direction algorithms.

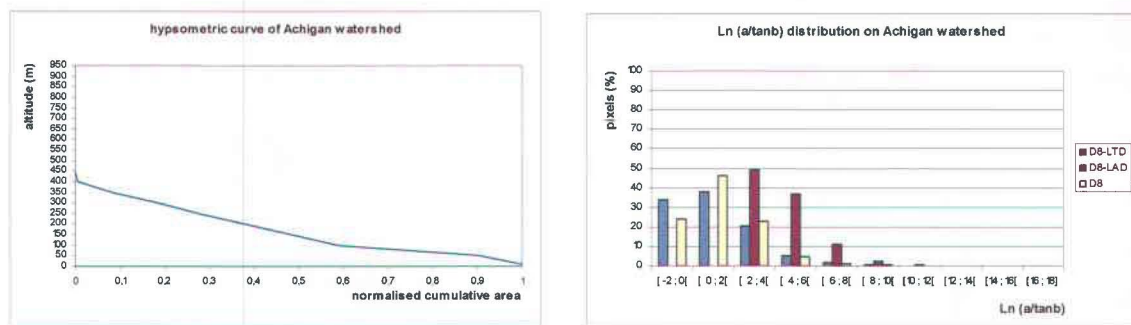


Figure A.2 : Hypsometric curve and *TI* distributions on Achigan river watershed obtained by the 3 flow direction algorithms.

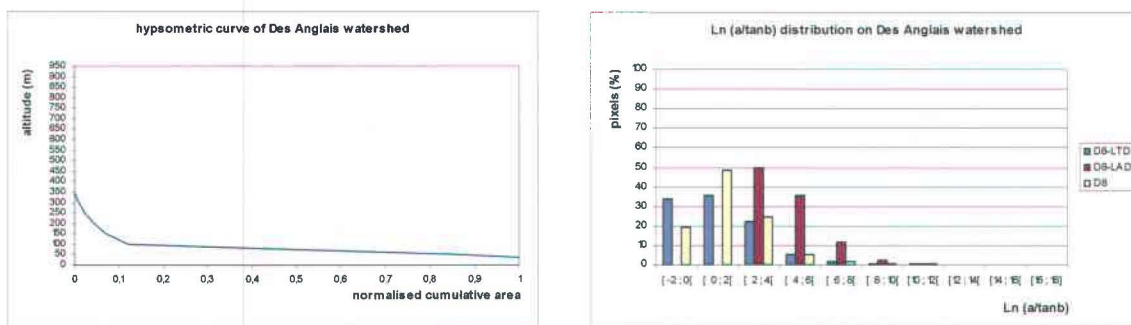


Figure A.3 : Hypsometric curve and *TI* distributions on Des Anglaises river watershed obtained by the 3 flow direction algorithms.

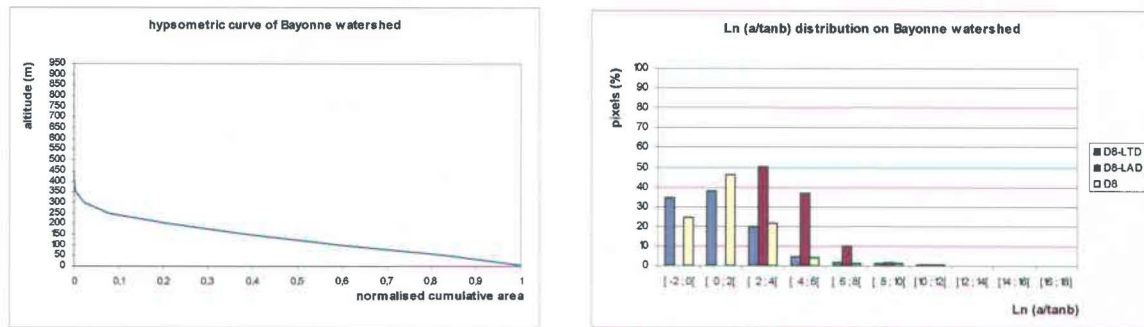


Figure A.4 : Hypsometric curve and TI distributions on Bayonne river watershed obtained by the 3 flow direction algorithms.

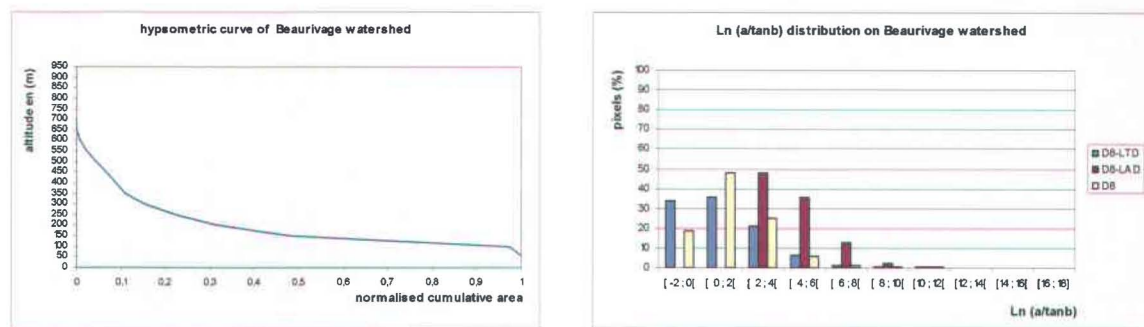


Figure A.5 : Hypsometric curve and TI distributions on Beaurivage river watershed obtained by the 3 flow direction algorithms.

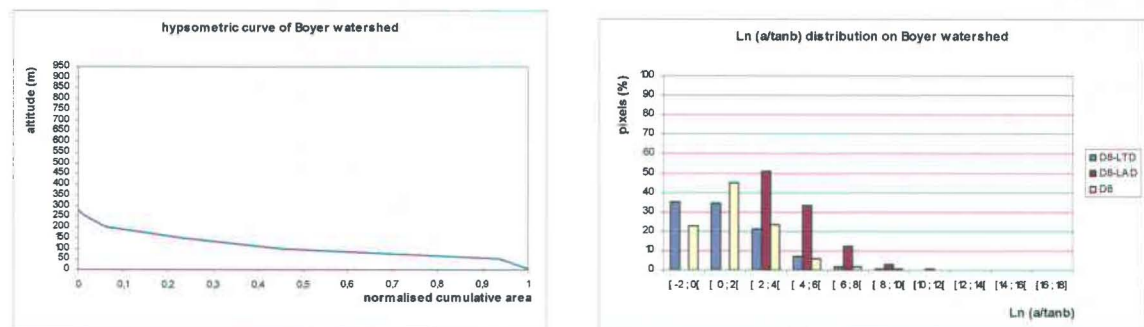


Figure A.6 : Hypsometric curve and TI distributions on Boyer river watershed obtained by the 3 flow direction algorithms.

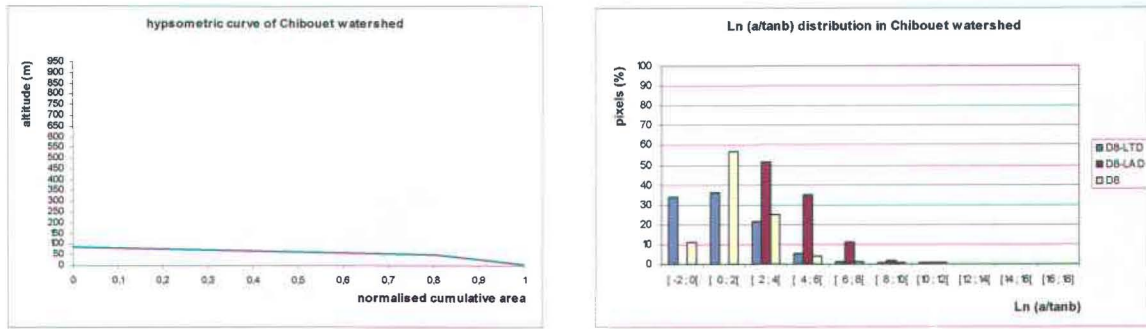


Figure A.7 : Hypsometric curve and *TI* distributions on Chibouet river watershed obtained by the 3 flow direction algorithms.

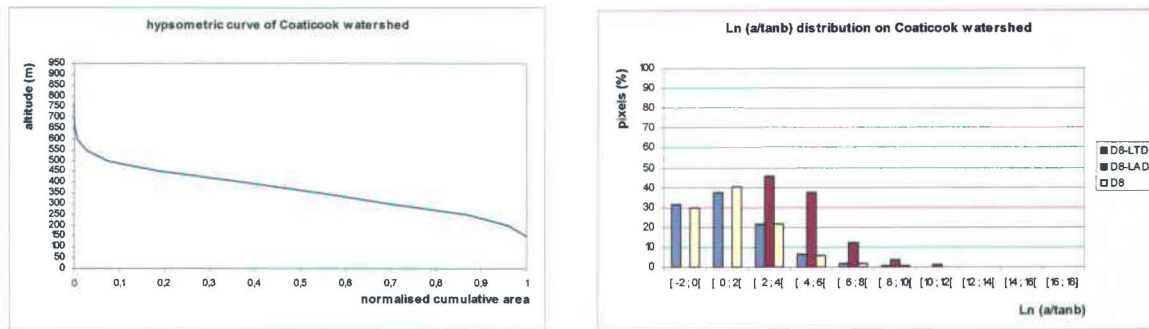


Figure A.8 : Hypsometric curve and *TI* distributions on Coaticook river watershed obtained by the 3 flow direction algorithms.

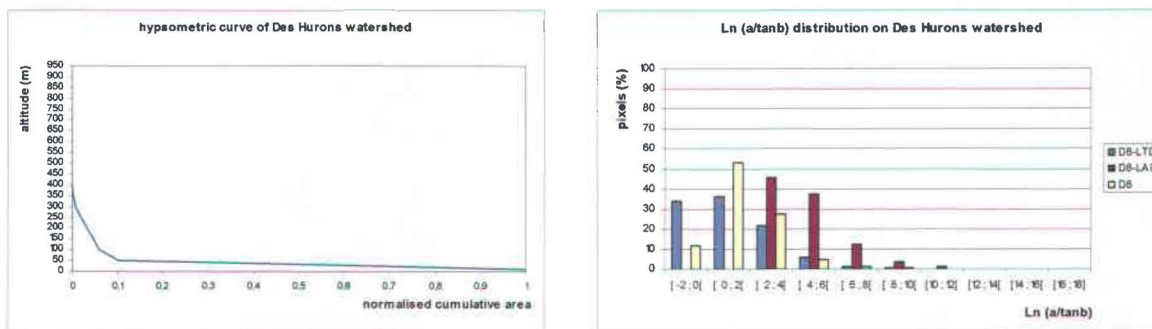


Figure A.9 : Hypsometric curve and *TI* distributions on Des Hurons river watershed obtained by the 3 flow direction algorithms.

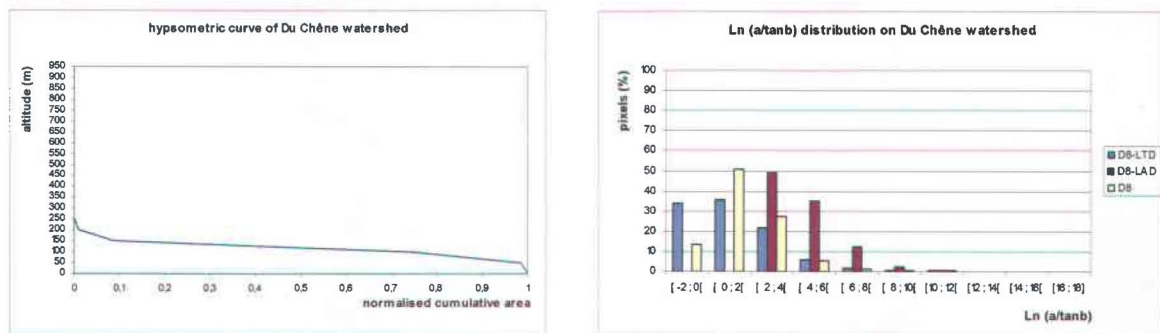


Figure A.10 : Hypsometric curve and *TI* distributions on Du Chêne river watershed obtained by the 3 flow direction algorithms.

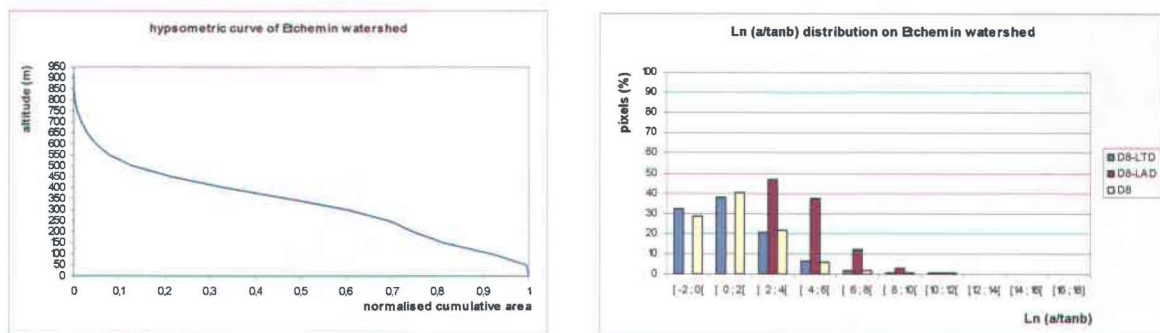


Figure A.11 : Hypsometric curve and *TI* distributions on Etchemin river watershed obtained by the 3 flow direction algorithms.

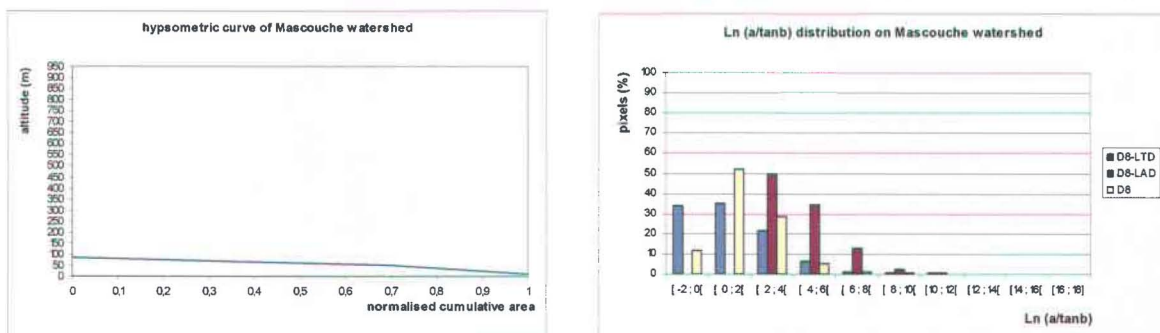


Figure A.12 : Hypsometric curve and *TI* distributions on Mascouche river watershed obtained by the 3 flow direction algorithms.

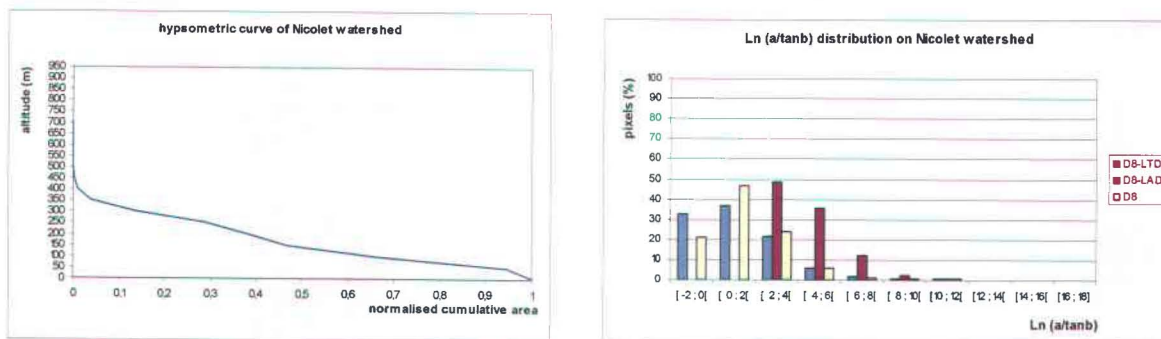


Figure A.13 : Hypsometric curve and *TI* distributions on Nicolet river watershed obtained by the 3 flow direction algorithms.

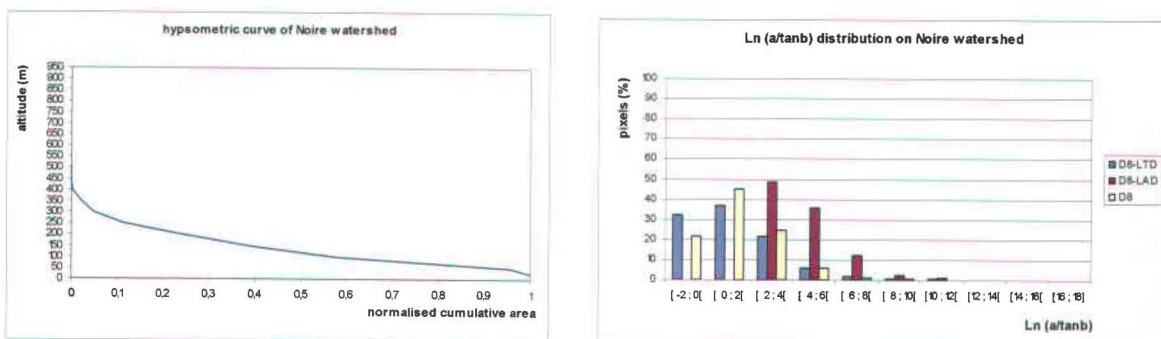


Figure A.14 : Hypsometric curve and *TI* distributions on Noire river watershed obtained by the 3 flow direction algorithms.

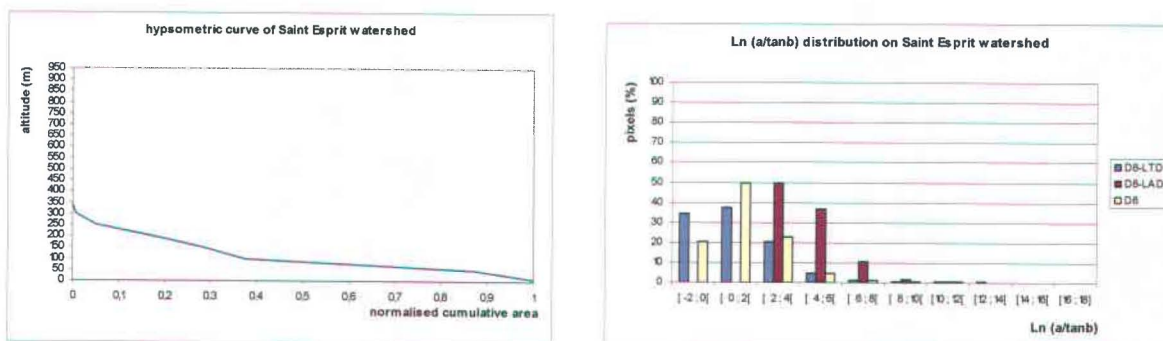


Figure A.15 : Hypsometric curve and *TI* distributions on Saint-Esprit river watershed obtained by the 3 flow direction algorithms.

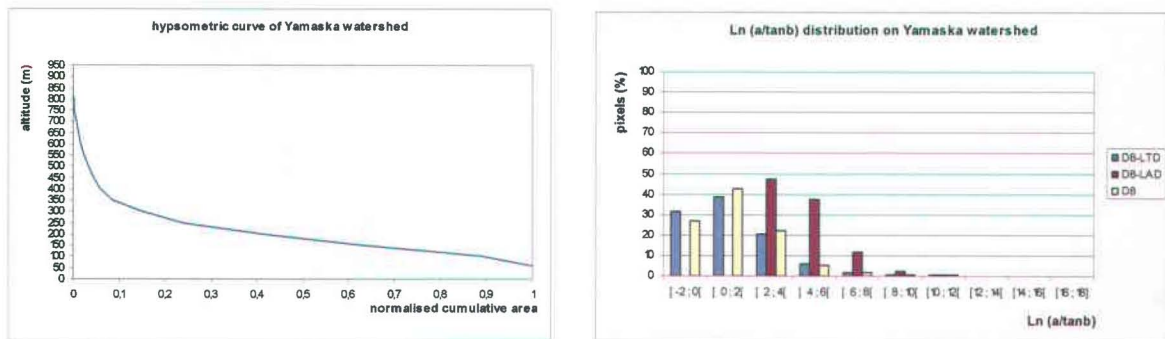


Figure A.16 : Hypsometric curve and *TI* distributions on Yamaska river watershed obtained by the 3 flow direction algorithms.

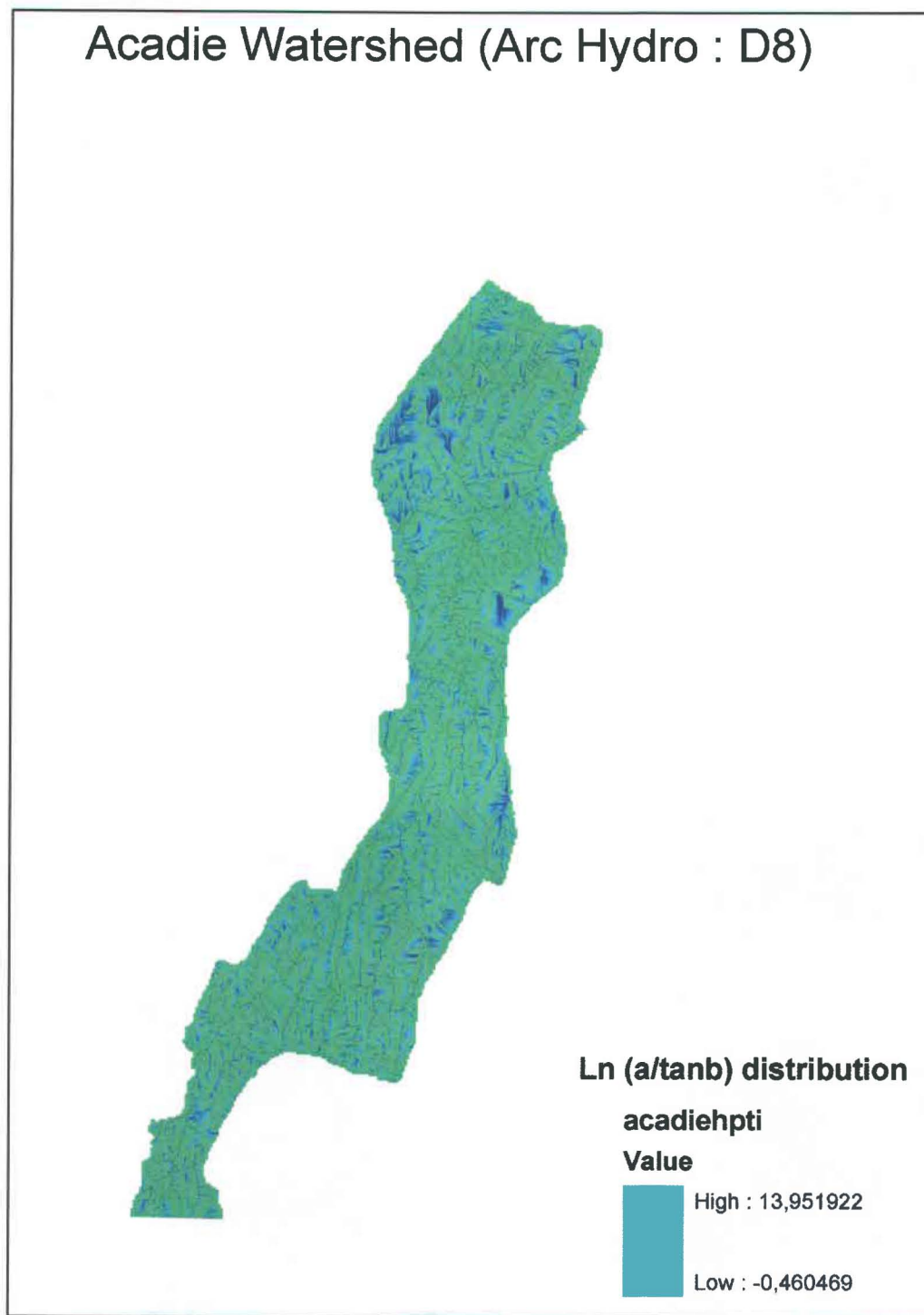


Figure A.17 : *TI* results for the Acadie river watershed using the D8 algorithm (Arc Hydro tool)

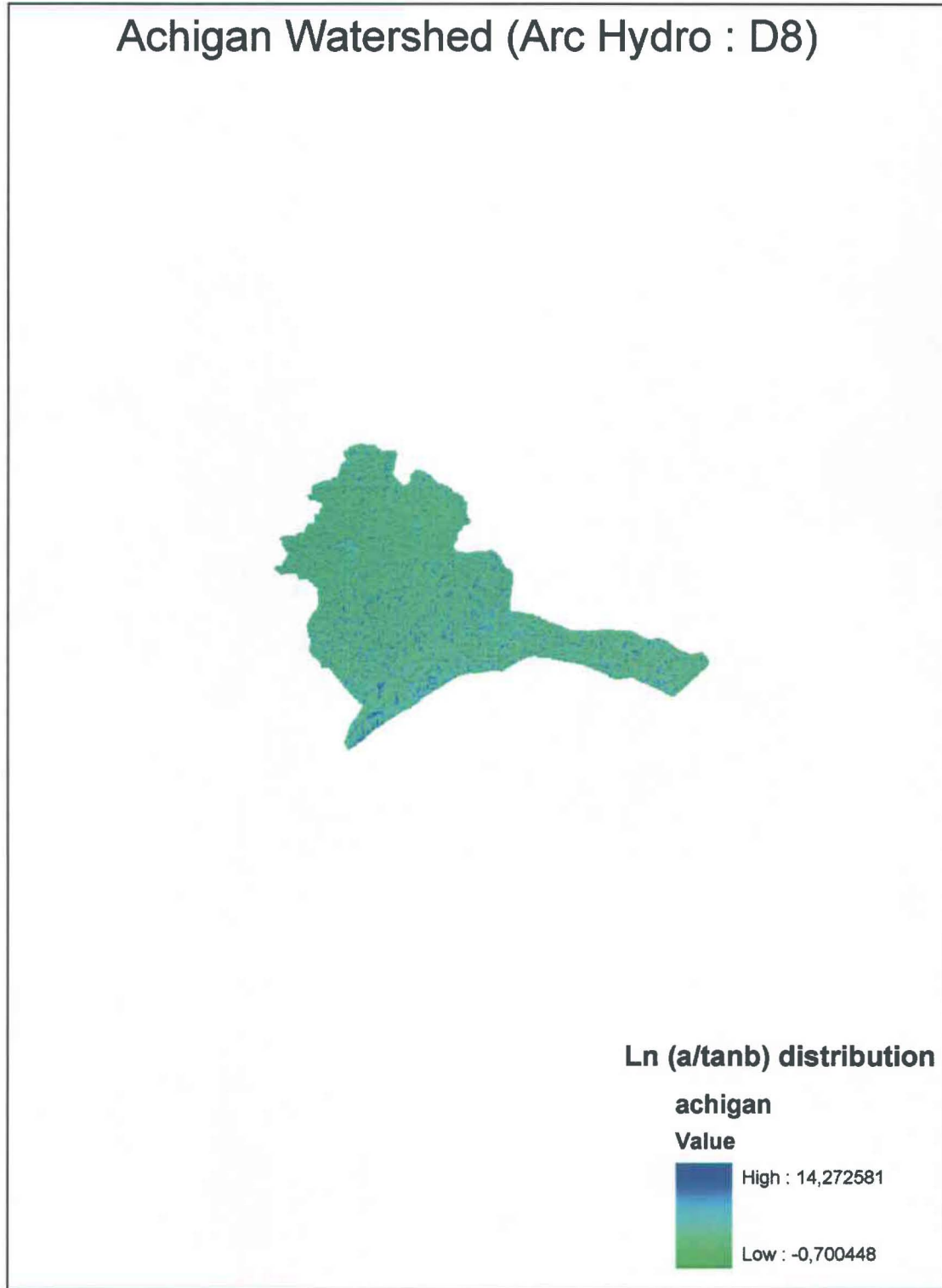


Figure A.18 : *TI* results for the Achigan river watershed using the D8 algorithm (Arc Hydro tool)

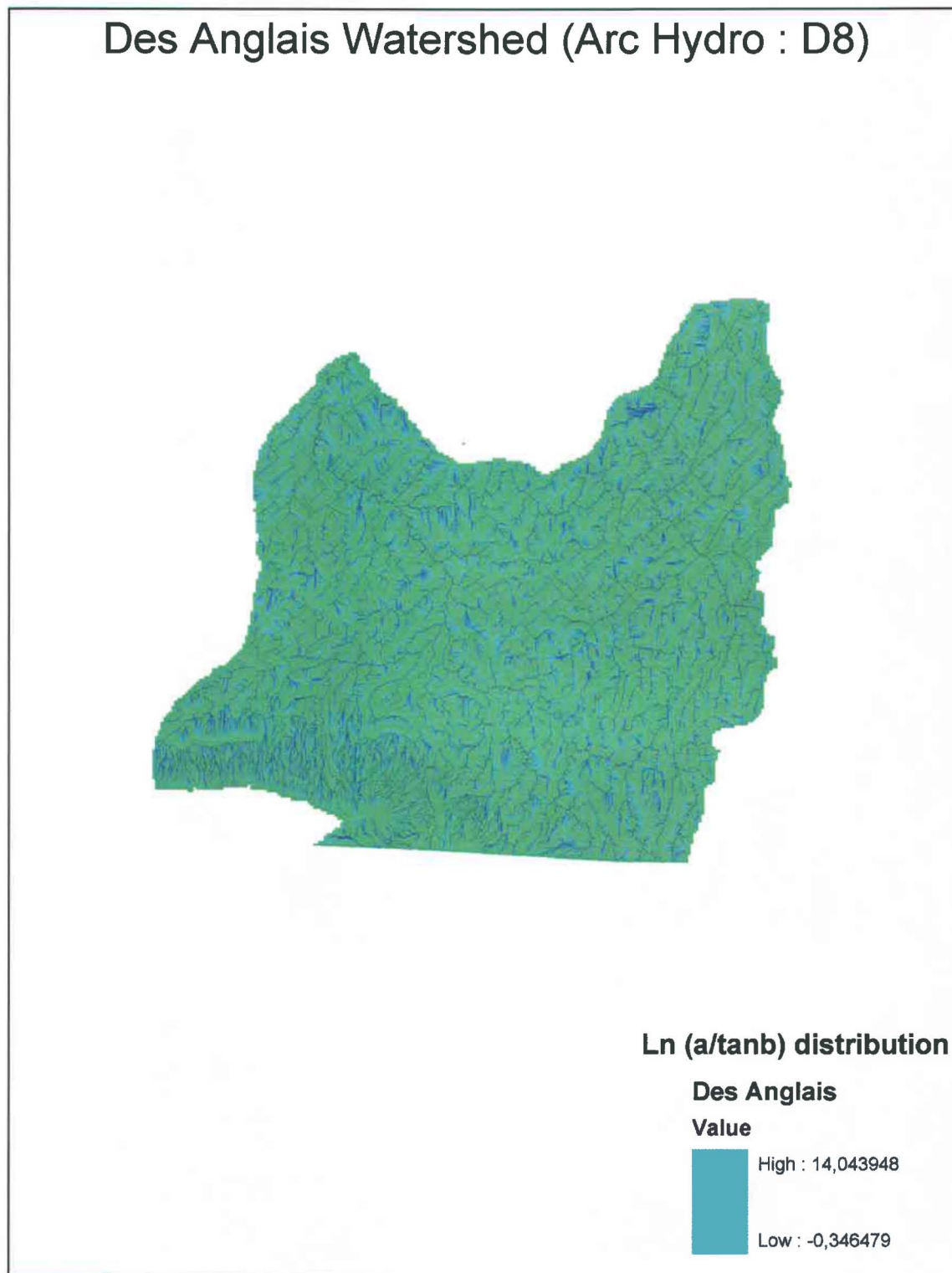


Figure A.19 : *TI* results for the Anglais river watershed using the D8 algorithm (Arc Hydro tool)

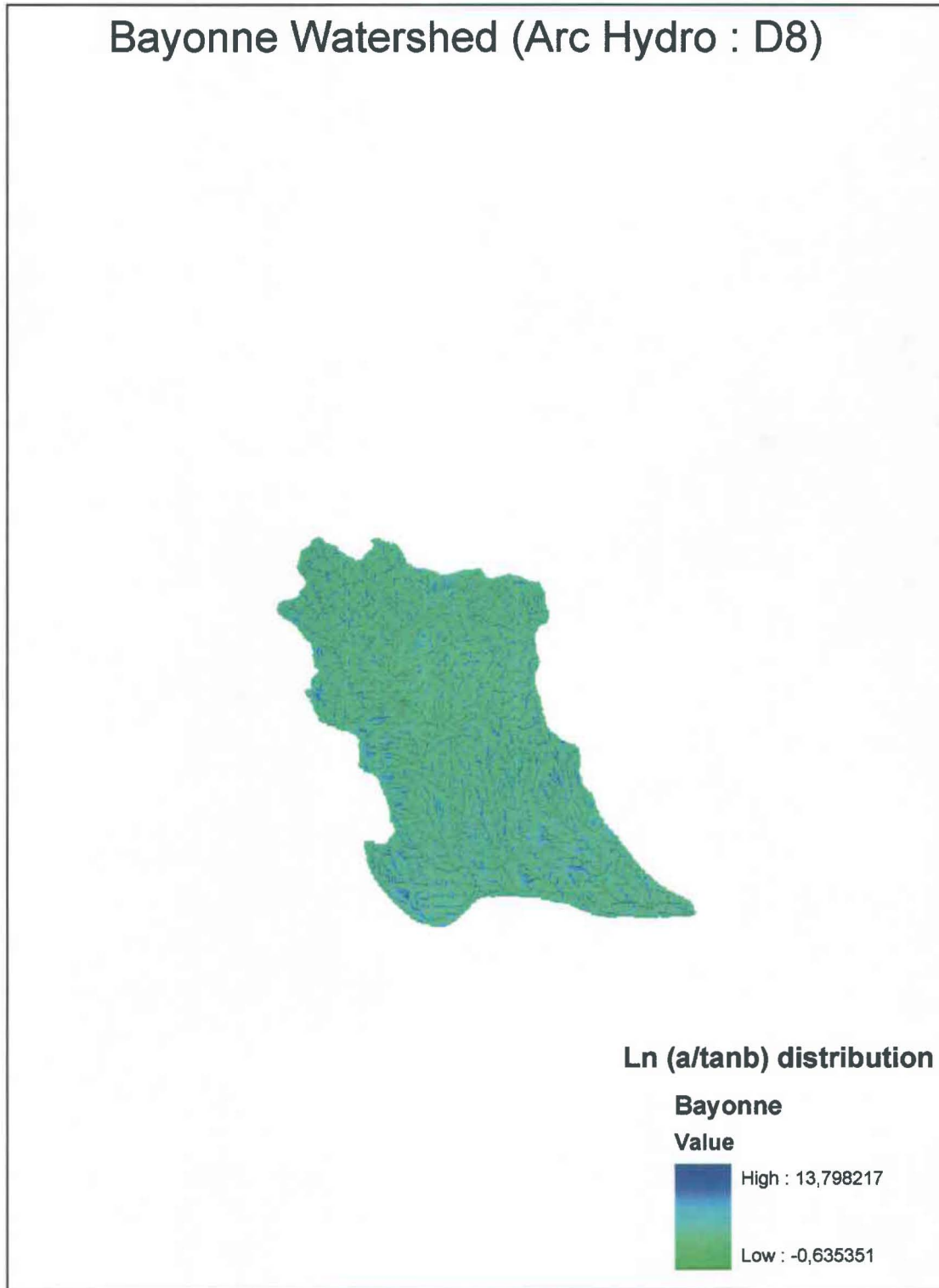


Figure A.20 : *TI* results for the Bayonne river watershed using the D8 algorithm (Arc Hydro tool)

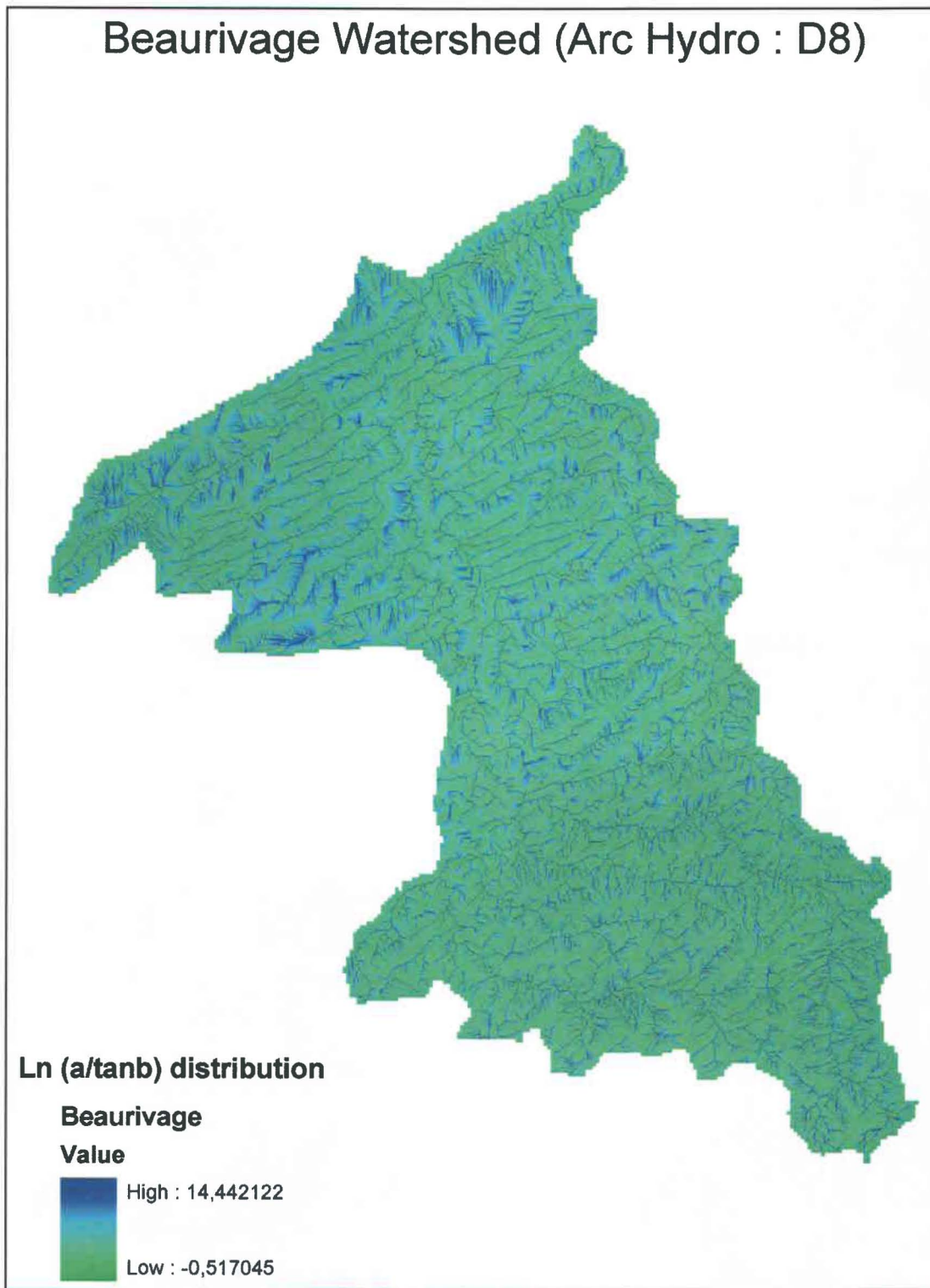


Figure A.21 : *TI* results for the Beaurivage river watershed using the D8 algorithm (Arc Hydro tool)



Figure A.22 : *TI* results for the Boyer river watershed using the D8 algorithm (Arc Hydro tool)

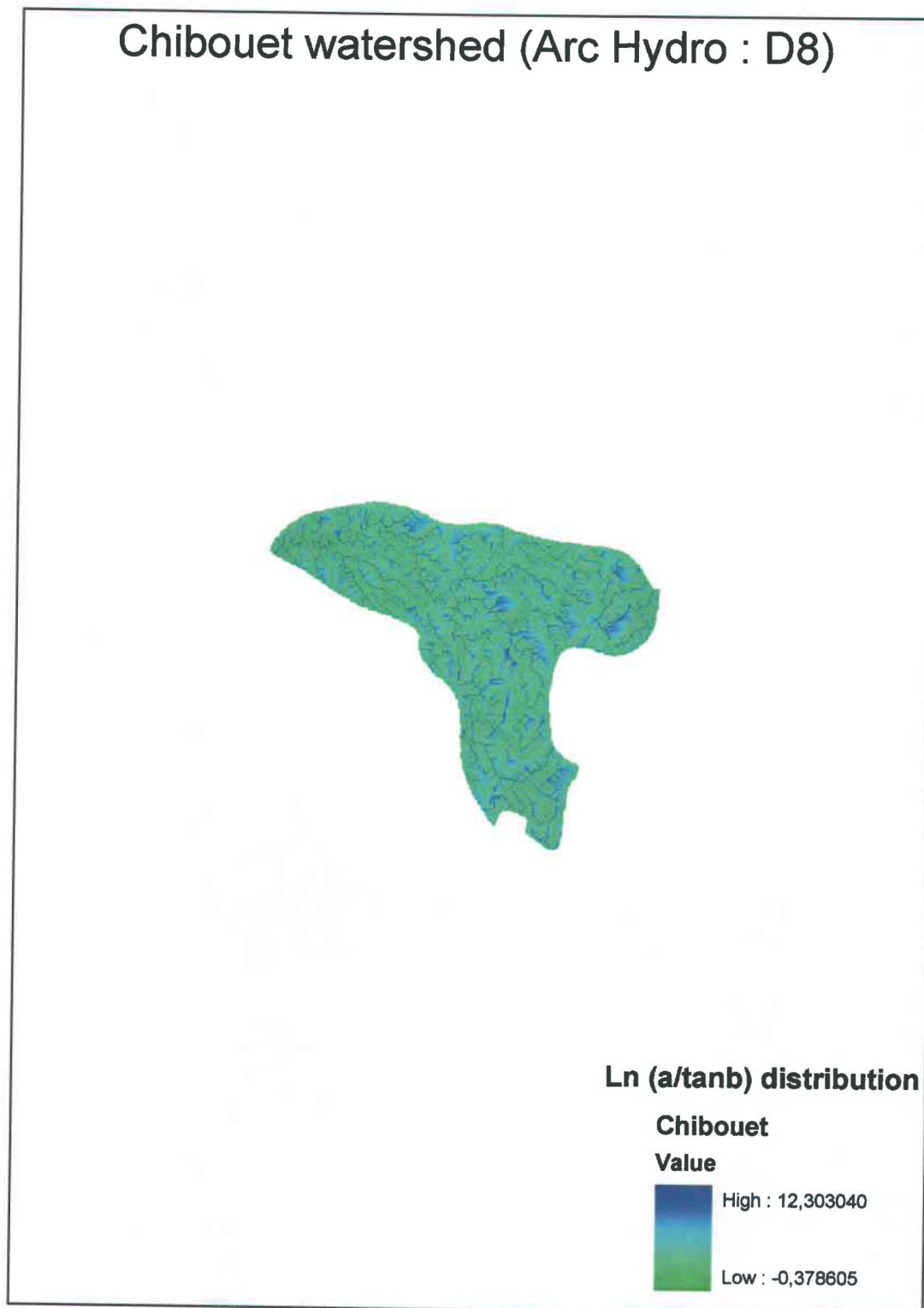


Figure A.23 : *TI* results for the Chibouet river watershed using the D8 algorithm (Arc Hydro tool)

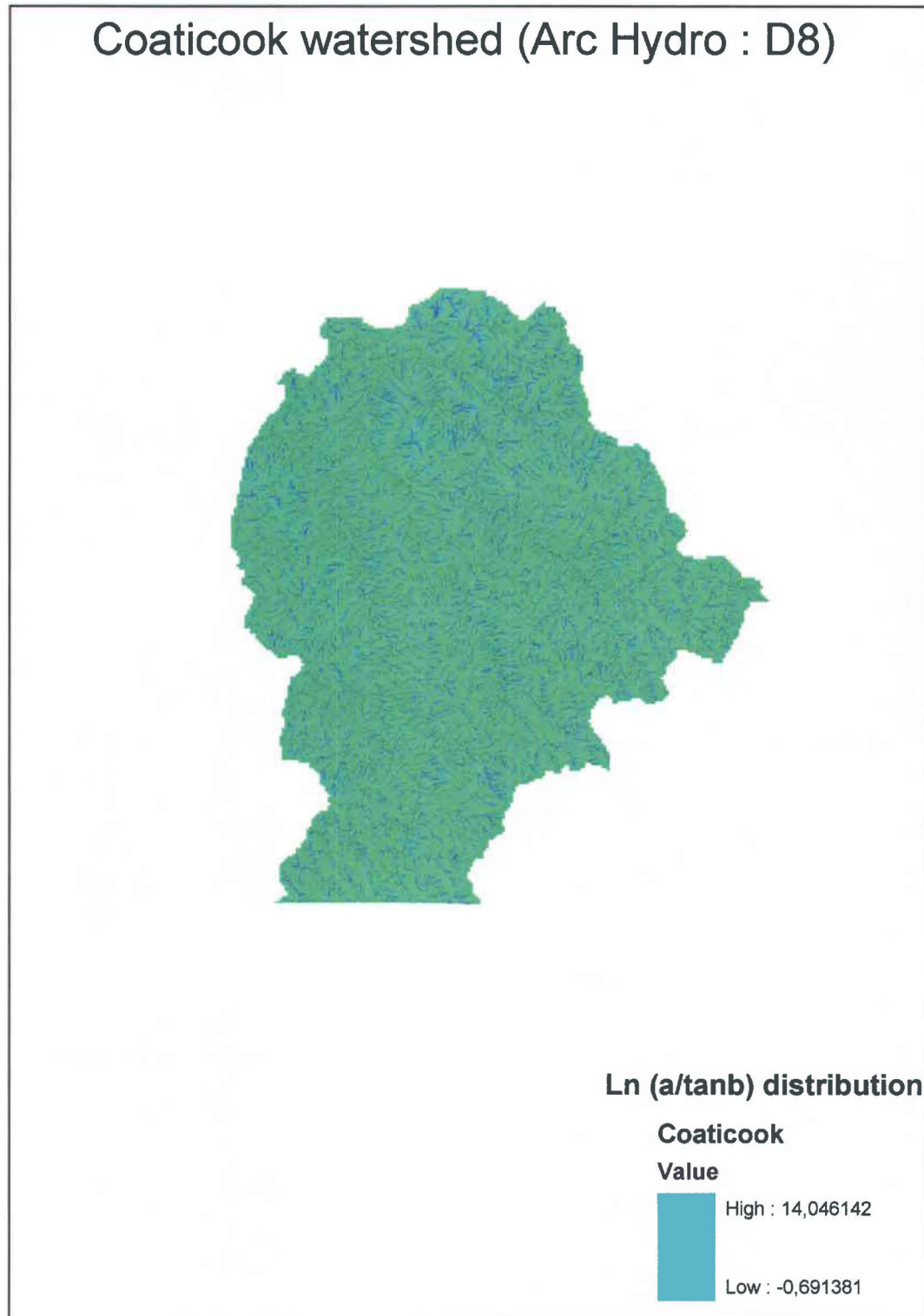


Figure A.24 : *TI* results for the Coaticook river watershed using the D8 algorithm (Arc Hydro tool)

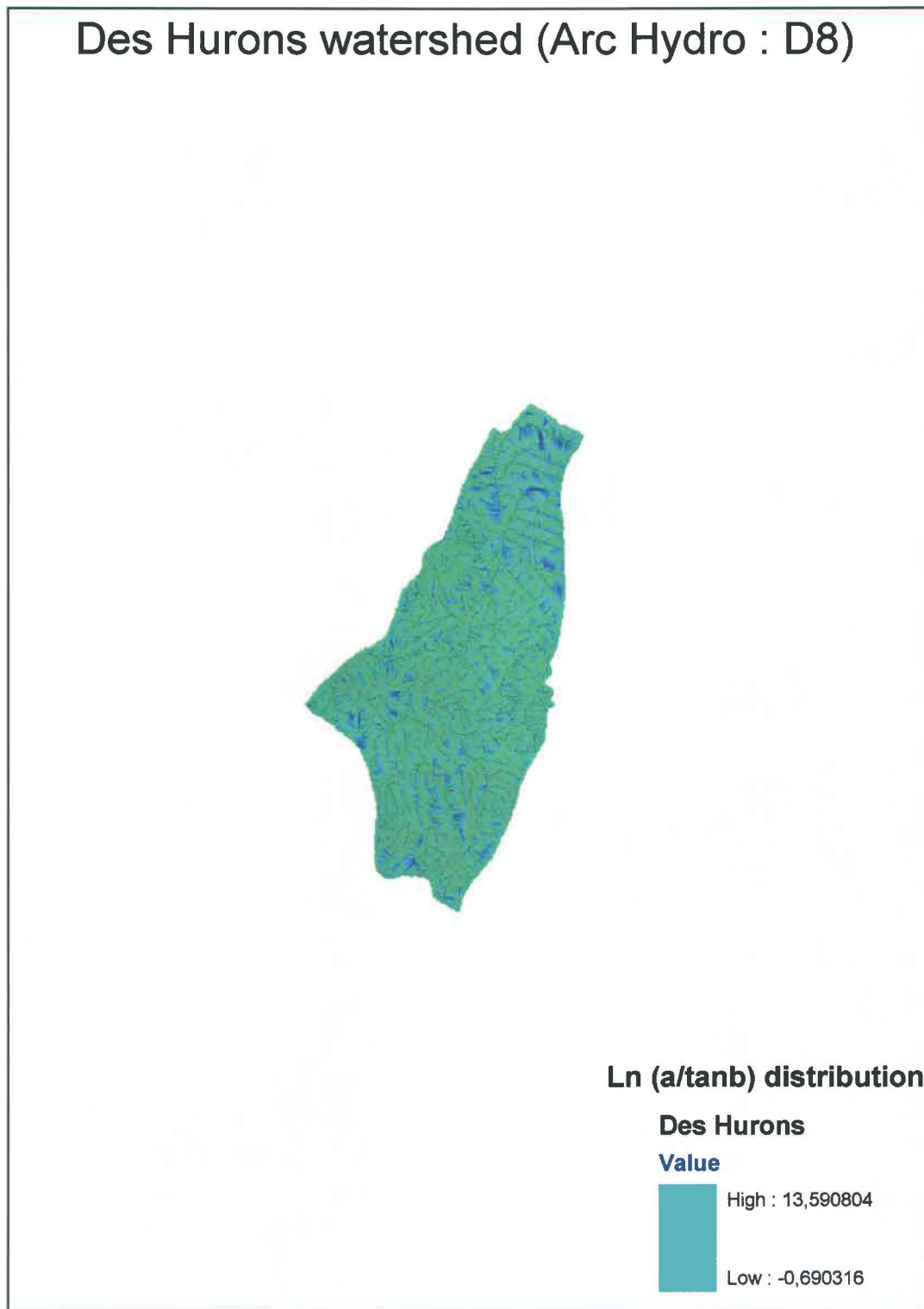


Figure A.25 : *TI* results for the Des Hurons river watershed using the D8 algorithm (Arc Hydro tool)

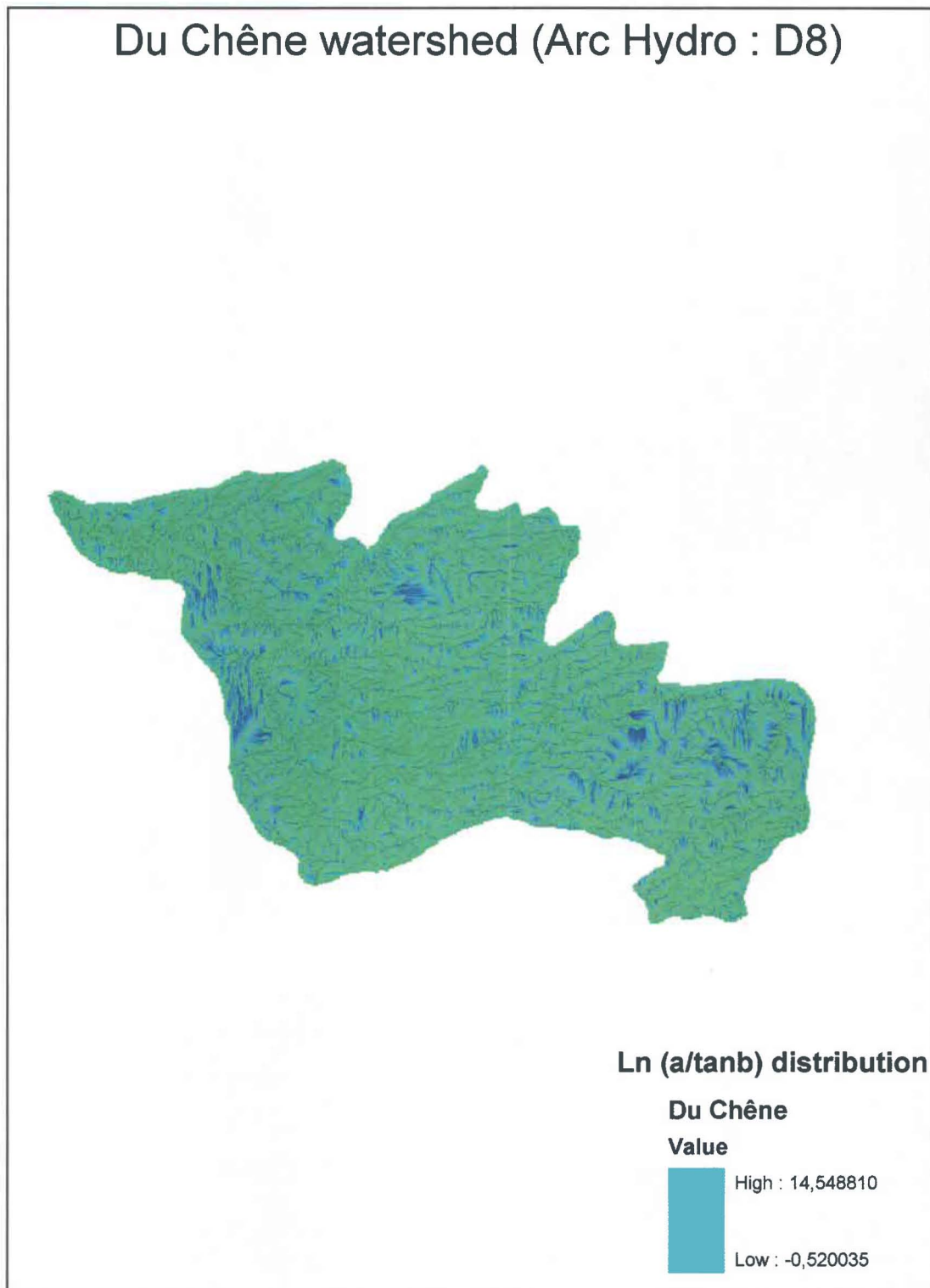


Figure A.26 : *TI* results for the Du Chêne river watershed using the D8 algorithm (Arc Hydro tool)

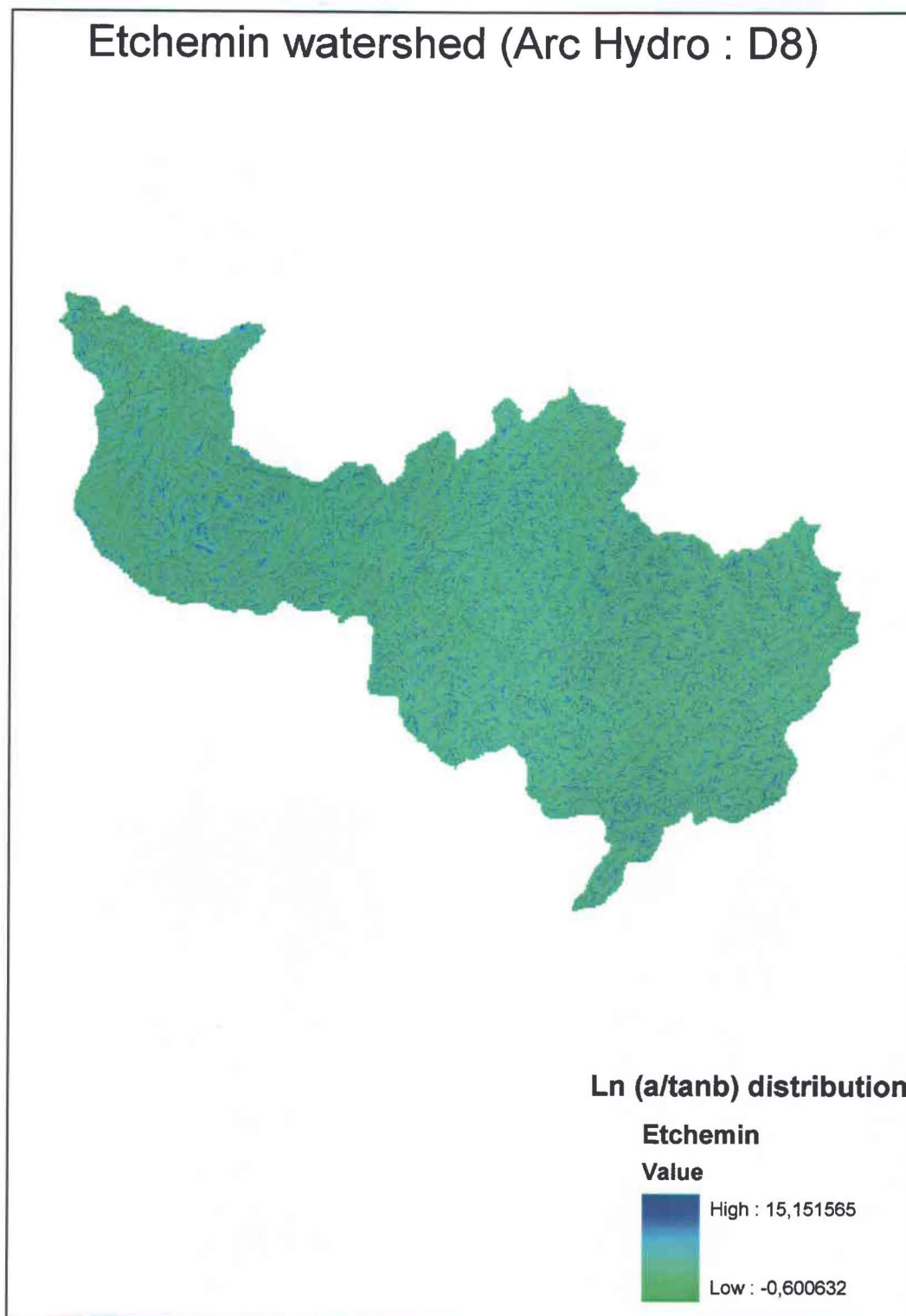


Figure A.27 : *TI* results for the Etchemin river watershed using the D8 algorithm (Arc Hydro tool)

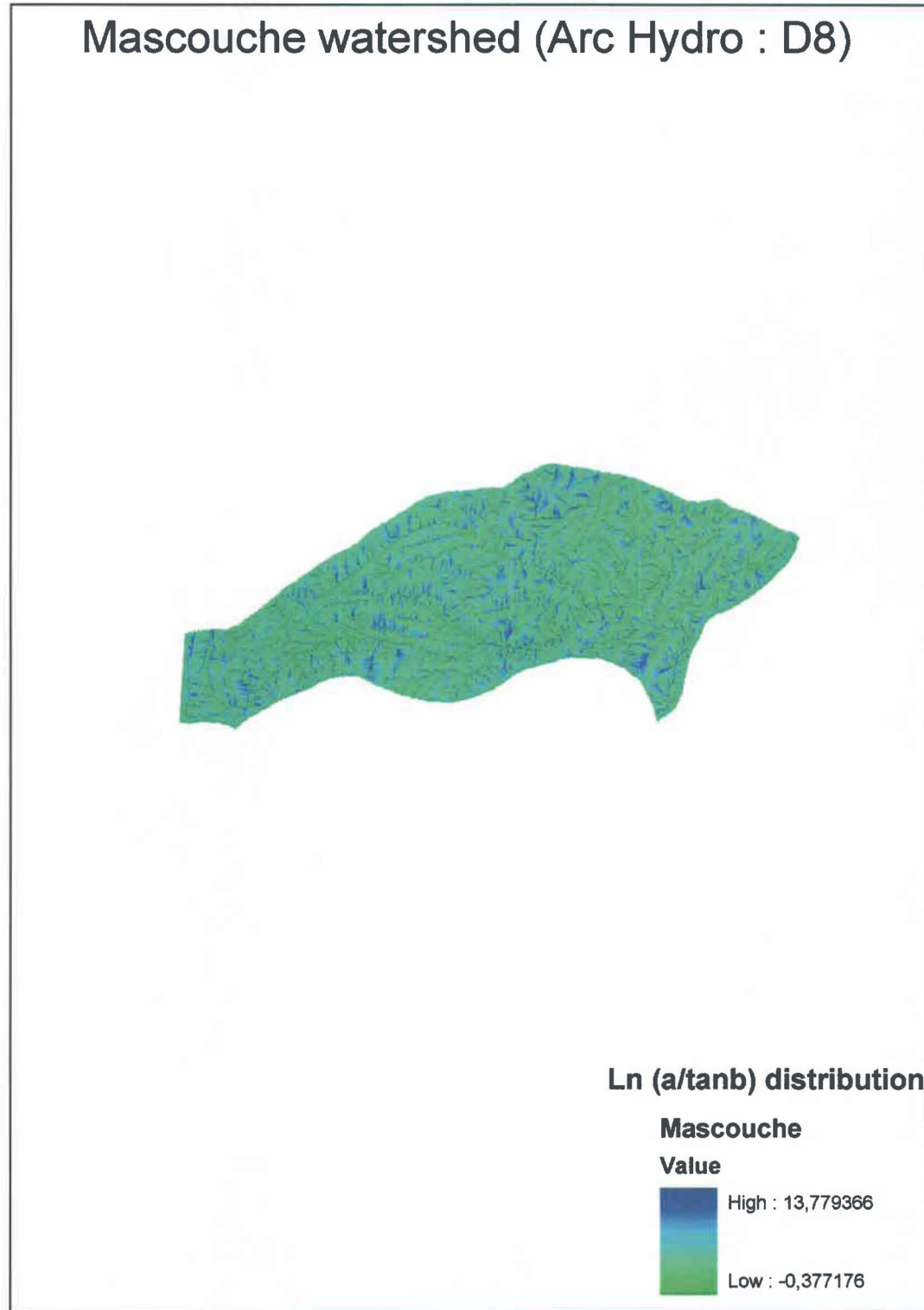


Figure A.28 : *TI* results for the Mascouche river watershed using the D8 algorithm (Arc Hydro tool)

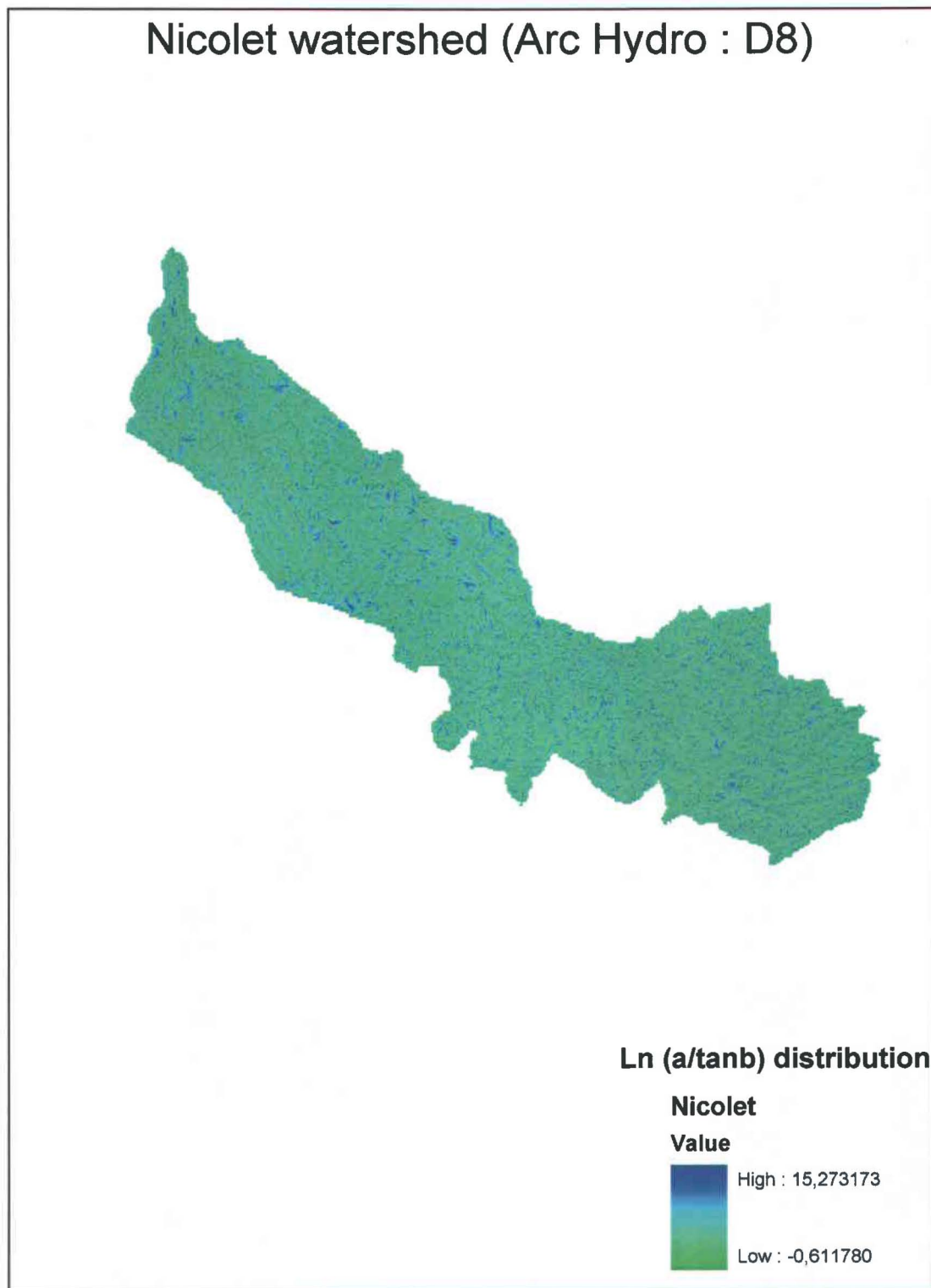


Figure A.29 : *TI* results for the Nicolet river watershed using the D8 algorithm (Arc Hydro tool)

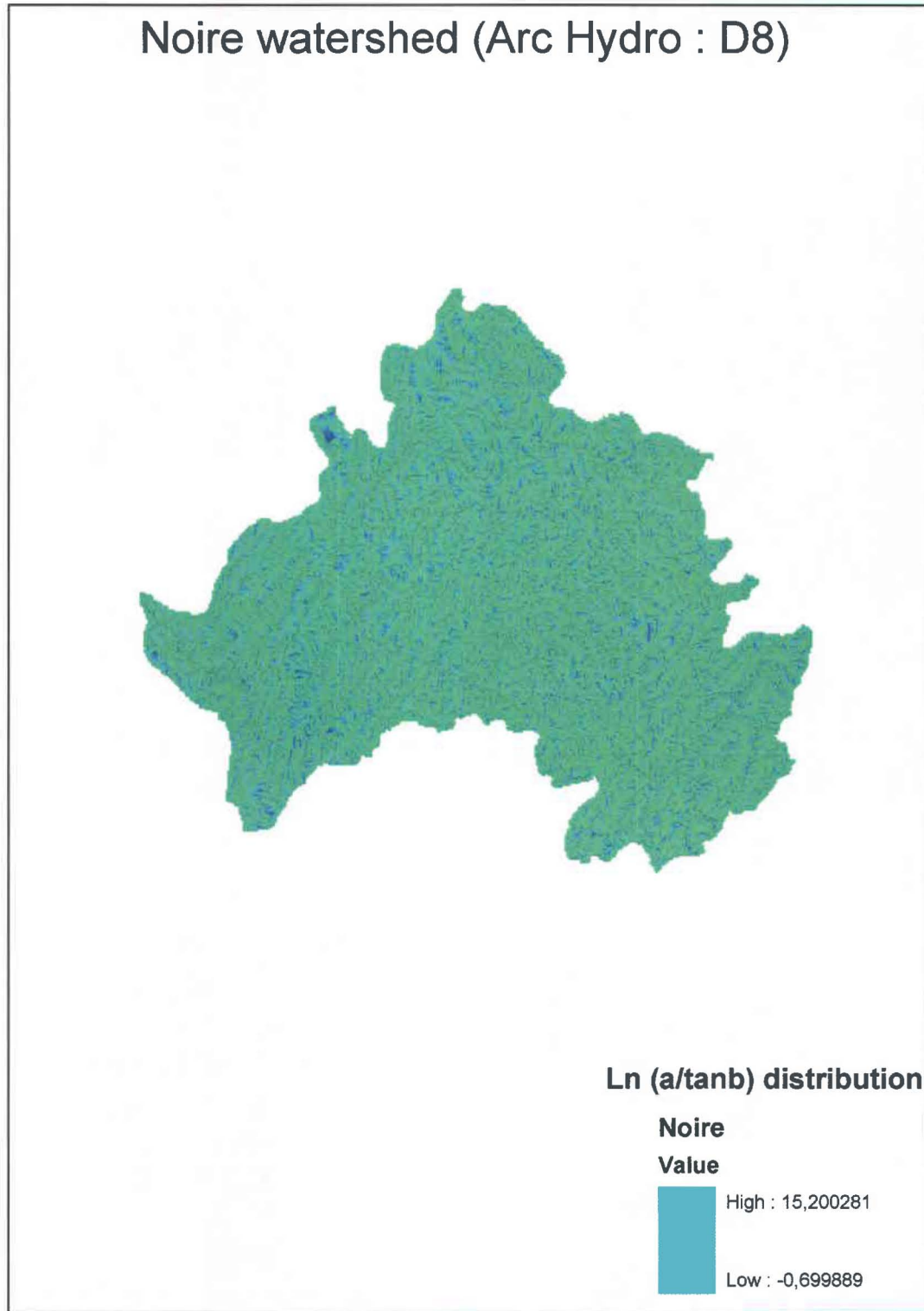


Figure A.30 : *TI* results for the Noire river watershed using the D8 algorithm (Arc Hydro tool)

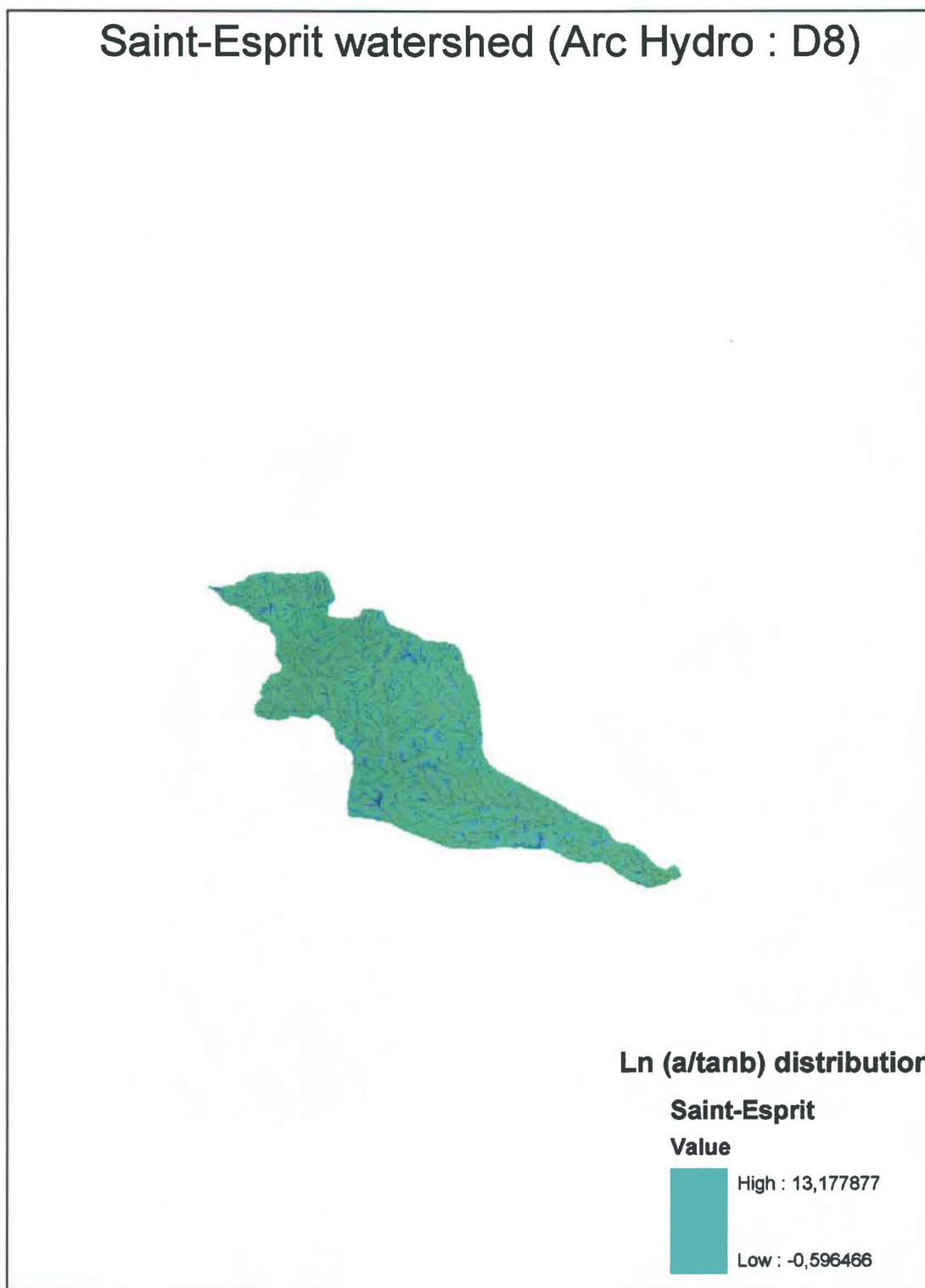


Figure A.31 : *TI* results for the Saint-Esprit river watershed using the D8 algorithm (Arc Hydro tool)



Figure A.32 : *TI* results for the Yamaska river watershed using the D8 algorithm (Arc Hydro tool)

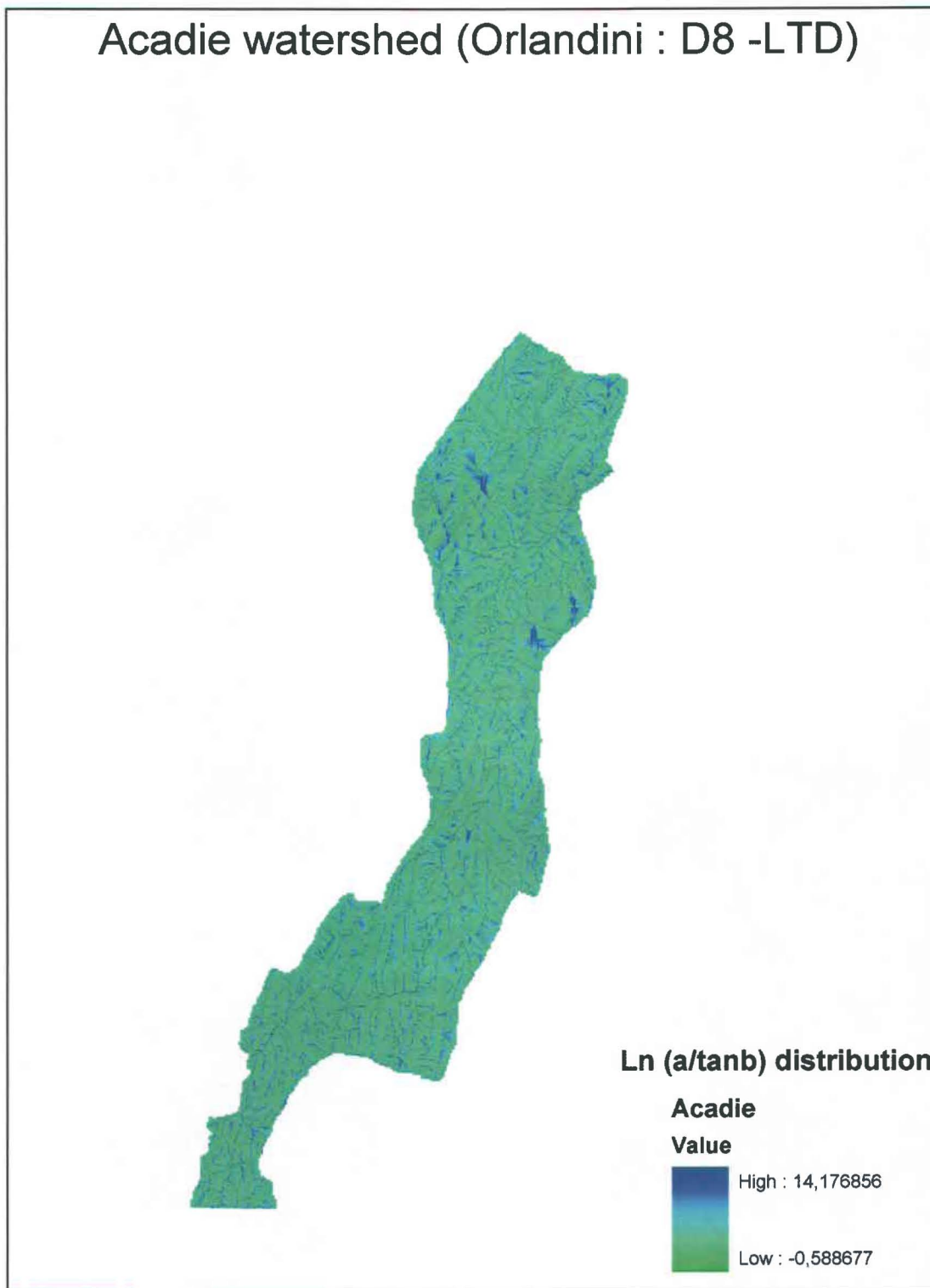


Figure A.33 : *TI* results for the Acadie river watershed using the D8-LTD algorithm

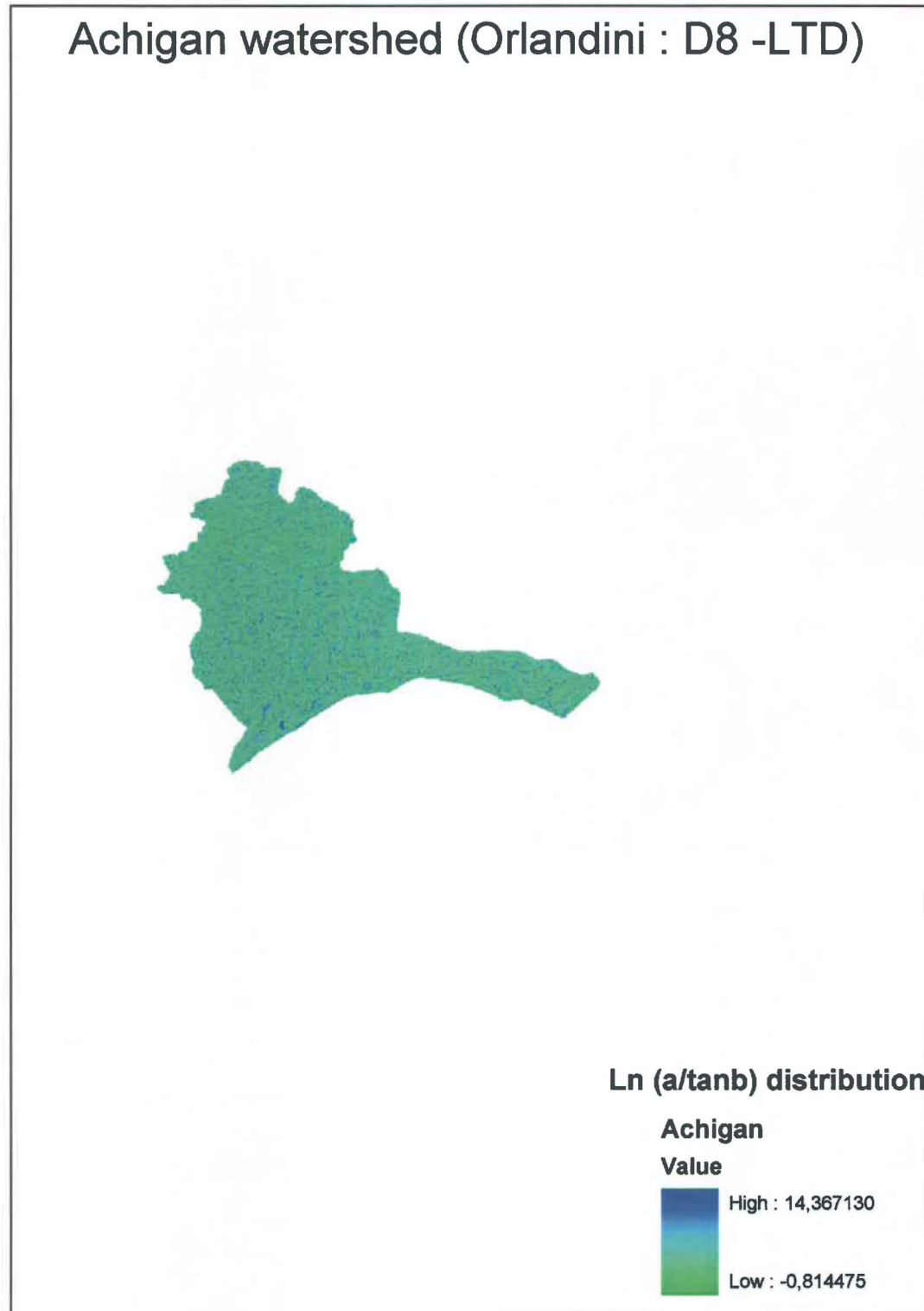


Figure A.34 : *TI* results for the Achigan river watershed using the D8-LTD algorithm

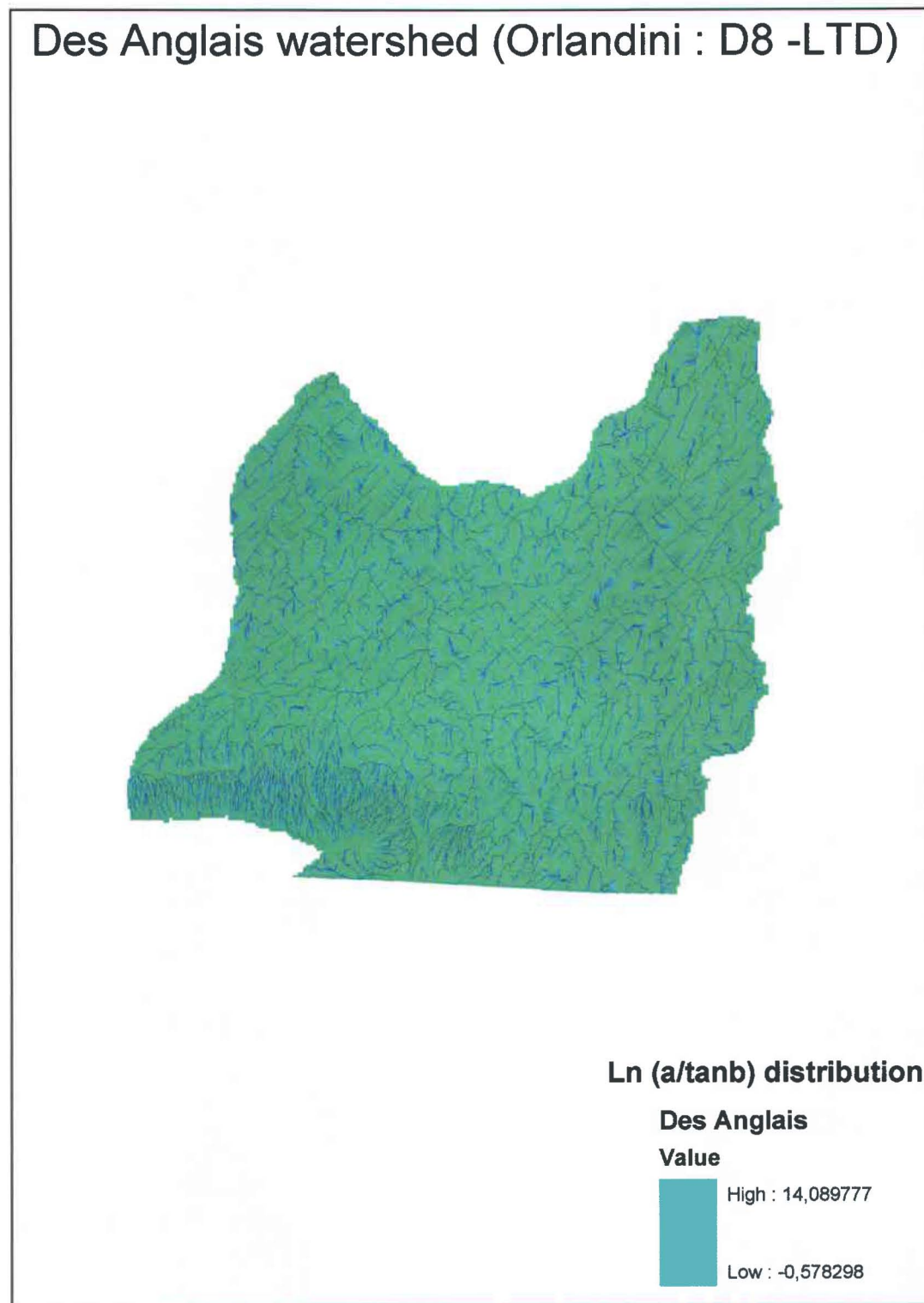


Figure A.35 : *TI* results for the Des Anglais river watershed using the D8-LTD algorithm



Figure A.36 : *TI* results for the Bayonne river watershed using the D8-LTD algorithm

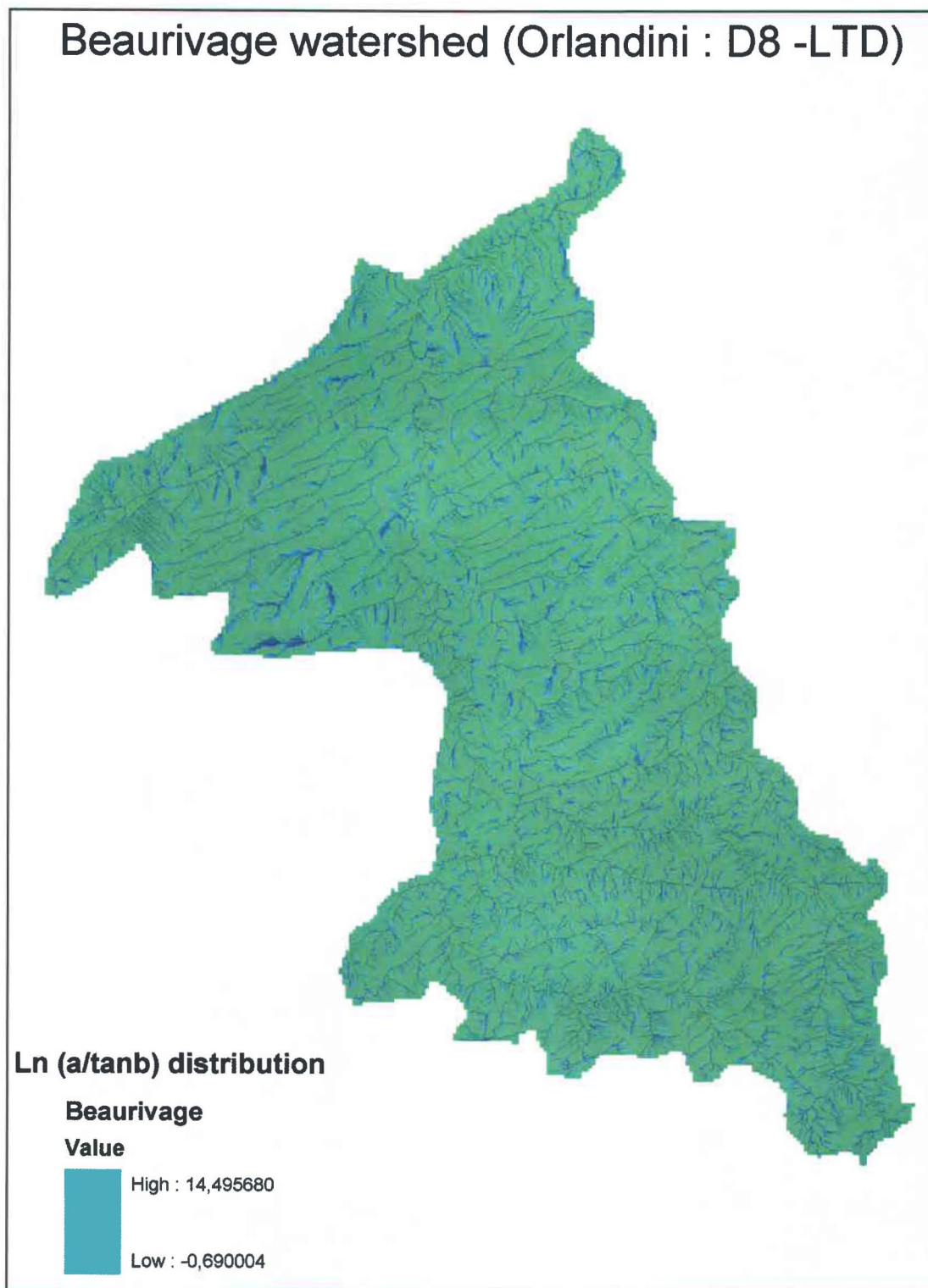


Figure A.37 : *TI* results for the Beaurivage river watershed using the D8-LTD algorithm

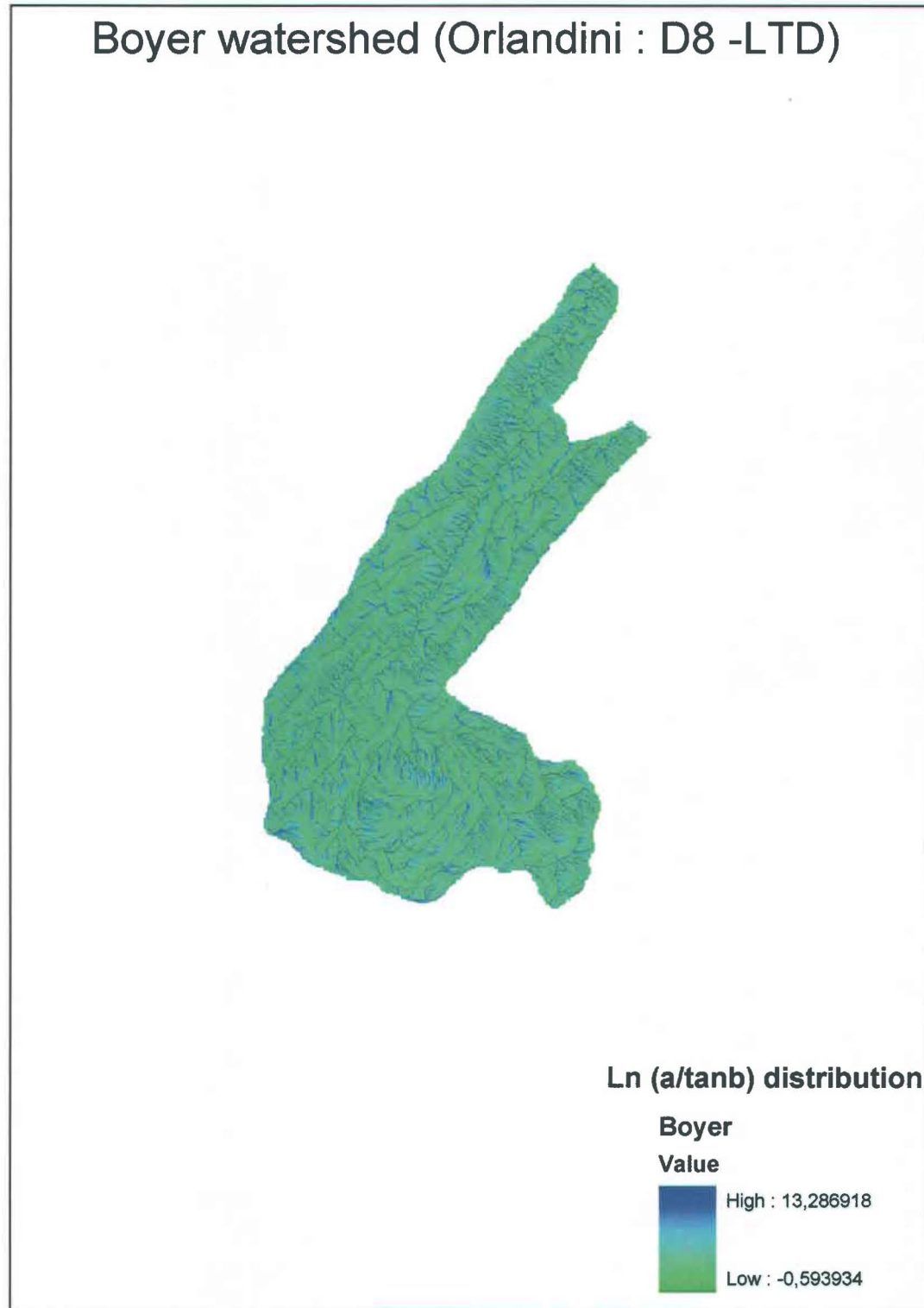


Figure A.38 : Tl results for the Boyer river watershed using the D8-LTD algorithm

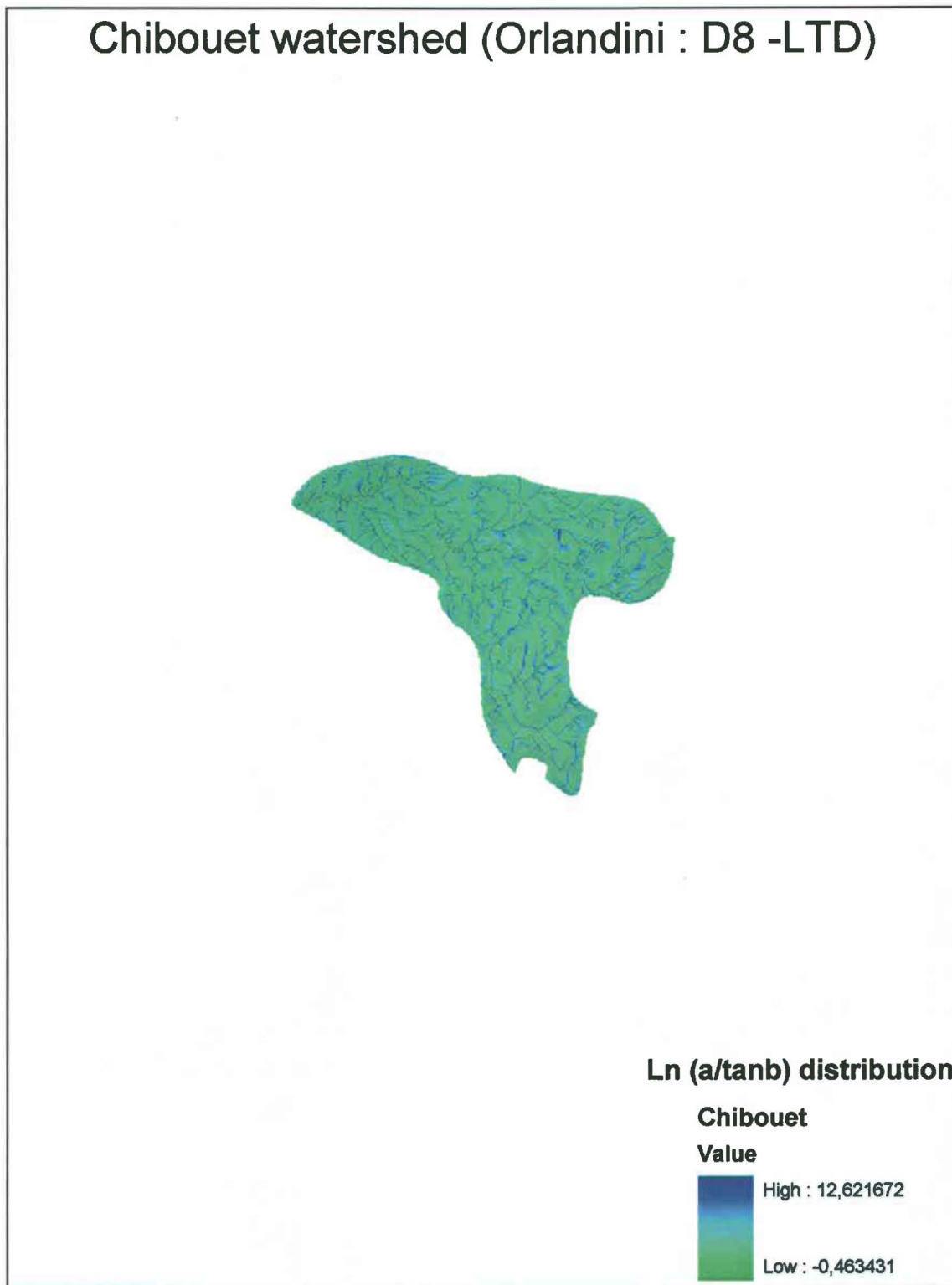


Figure A.39 : *TI* results for the Chibouet river watershed using the D8-LTD algorithm



Figure A.40 : *TI* results for the Coaticook river watershed using the D8-LTD algorithm

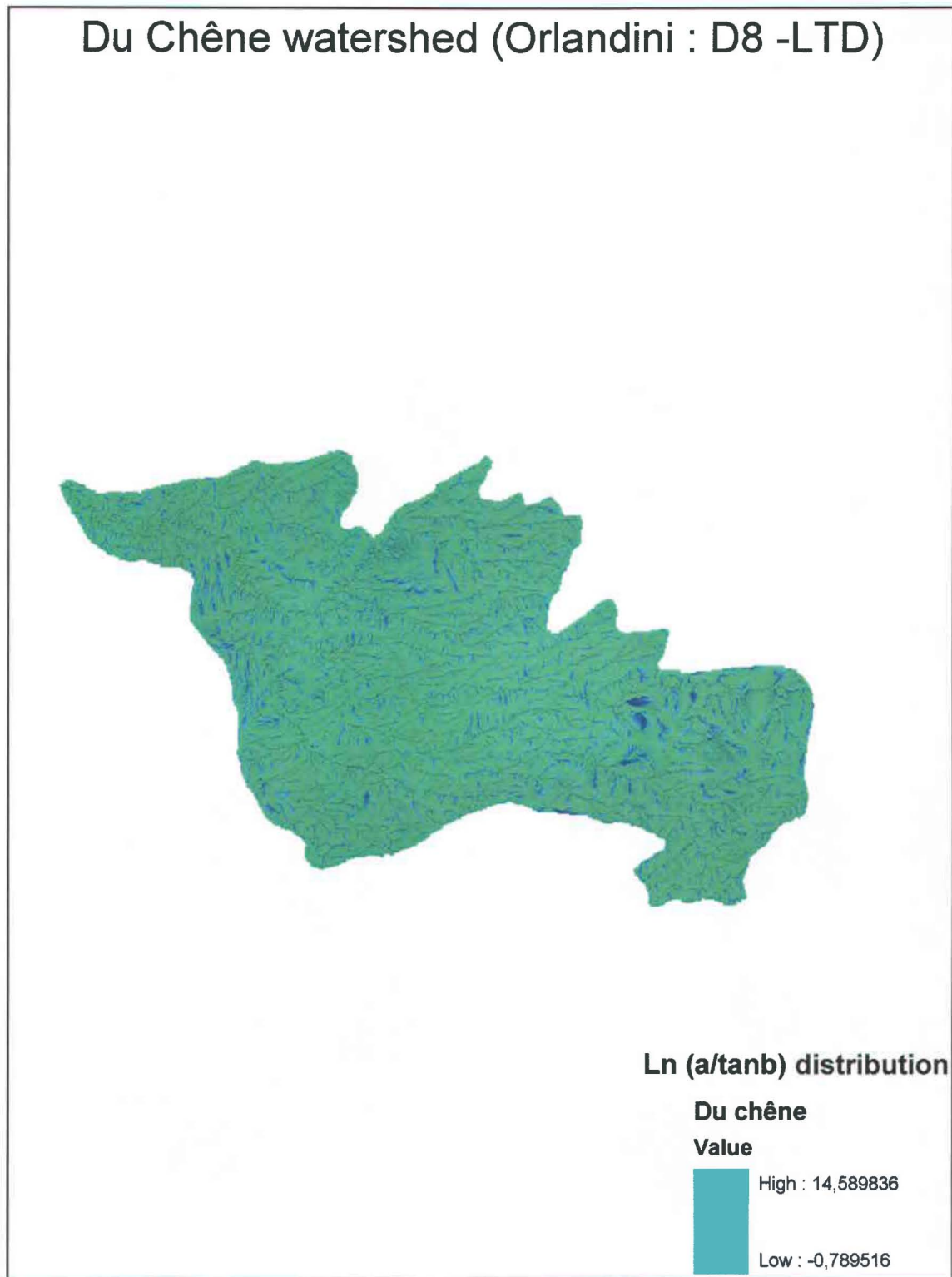


Figure A.41 : *TI* results for the Du Chêne river watershed using the D8-LTD algorithm

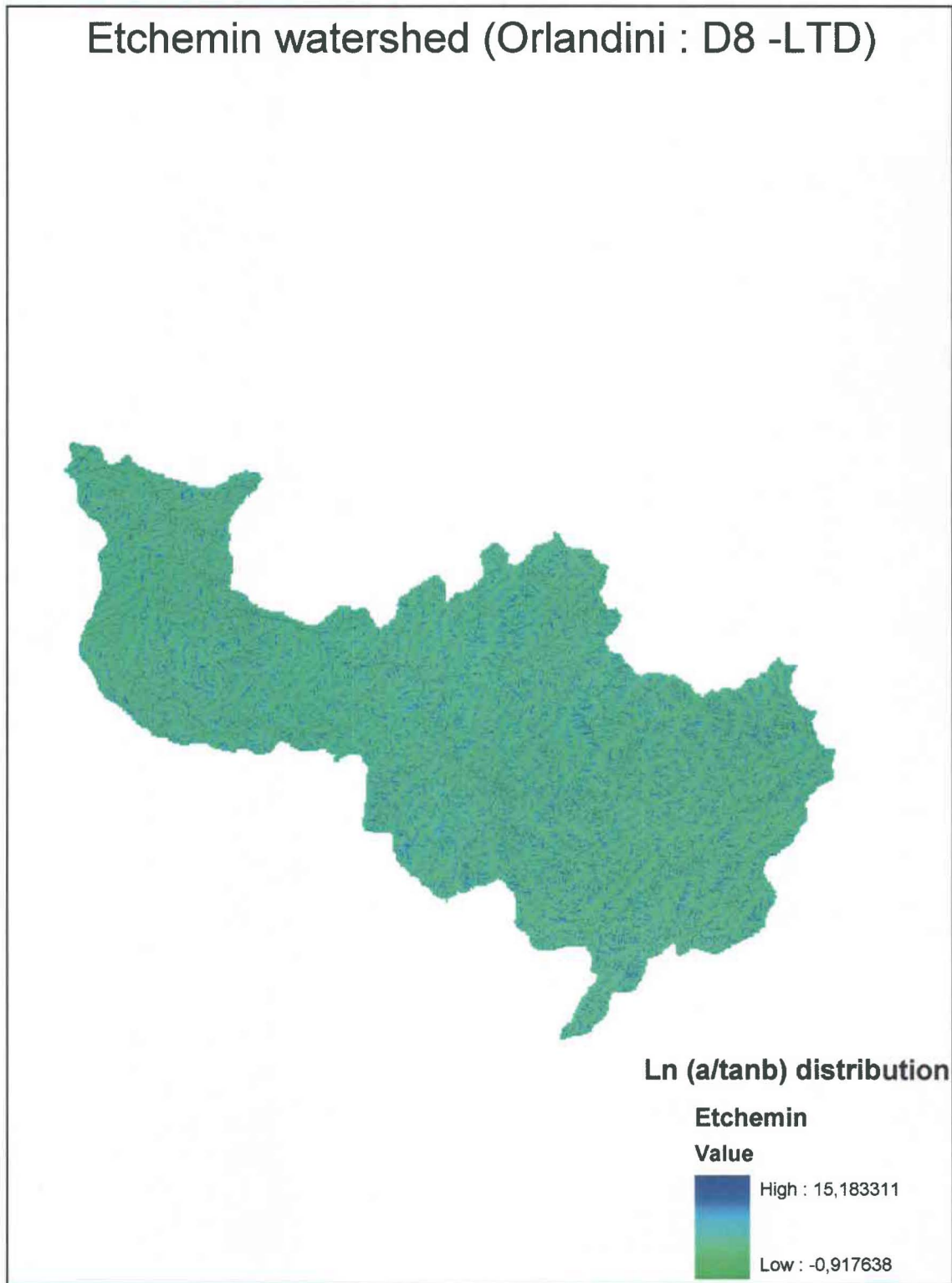


Figure A.42 : TI results for the Etchemin river watershed using the D8-LTD algorithm

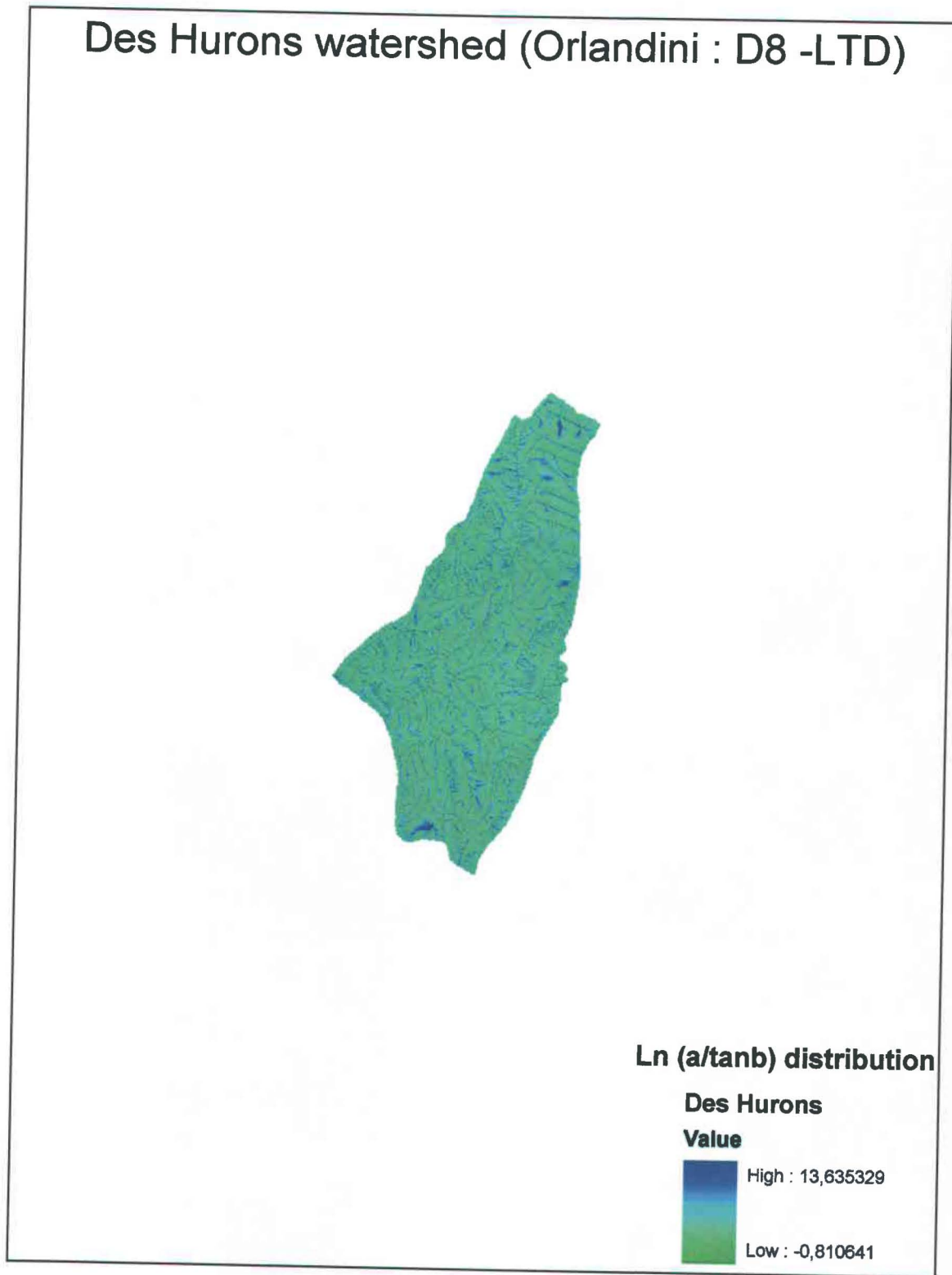


Figure A.43 : *TI* results for the Des Hurons river watershed using the D8-LTD algorithm



Figure A.44 : *TI* results for the Mascouche river watershed using the D8-LTD algorithm

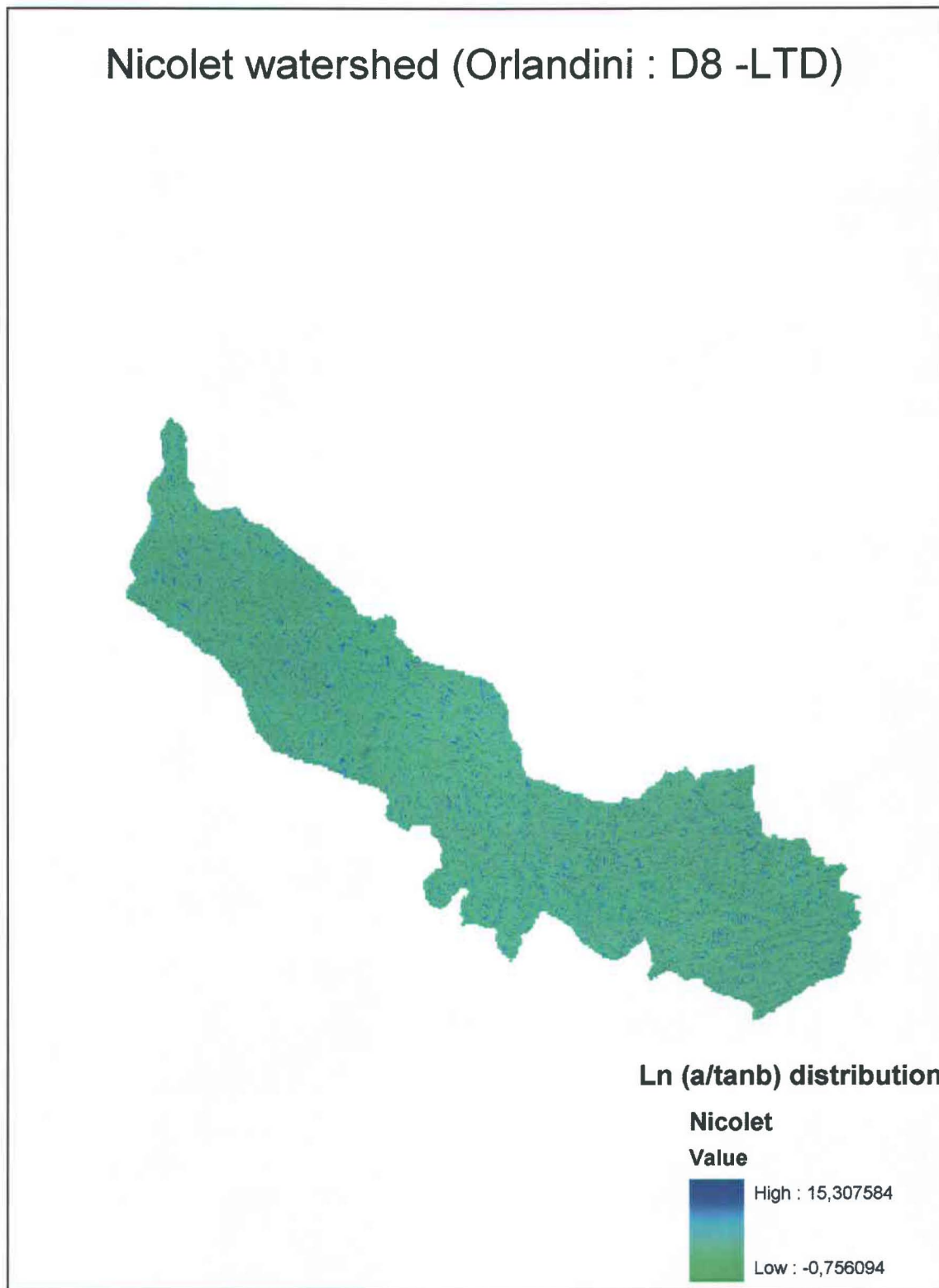


Figure A.45 : *TI* results for the Nicolet river watershed using the D8-LTD algorithm

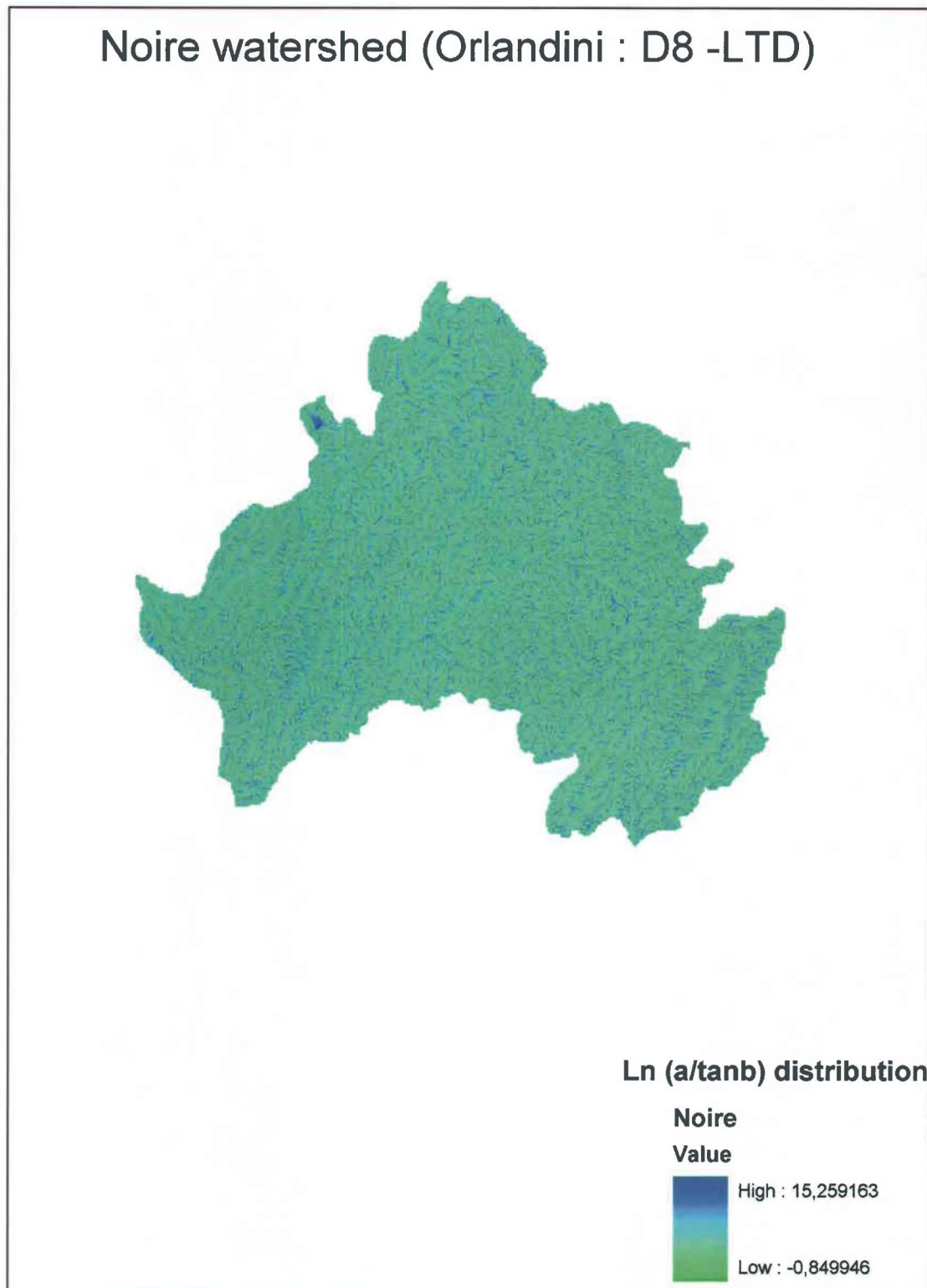


Figure A.46 : *TI* results for the Noire river watershed using the D8-LTD algorithm



Figure A.47 : *TI* results for the Saint-Esprit river watershed using the D8-LTD algorithm



Figure A.48 : *TI* results for the Yamaska river watershed using the D8-LTD algorithm

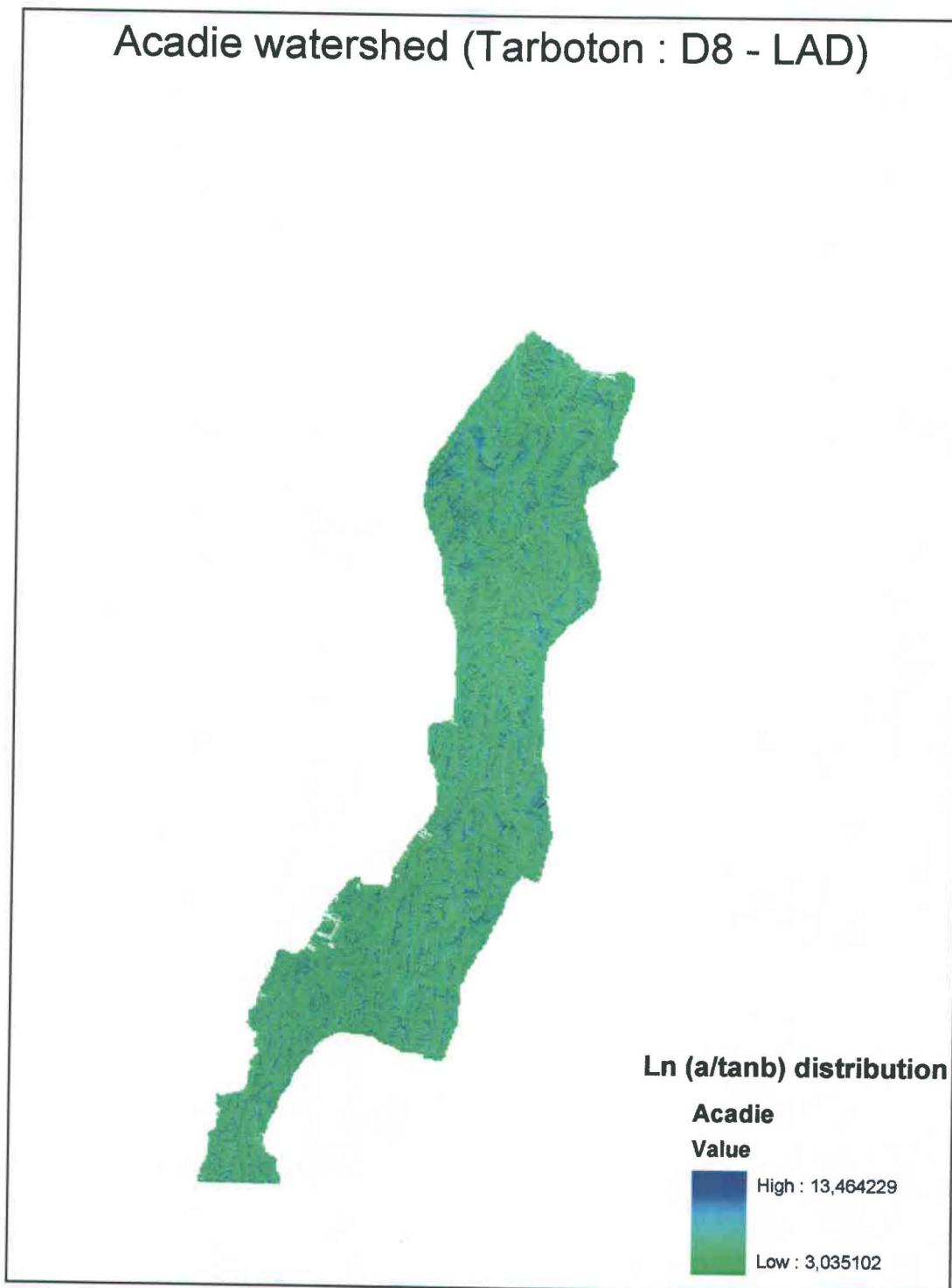


Figure A.49 : *TI* results for the Acadie river watershed using the D8-LAD algorithm (TauDEM)

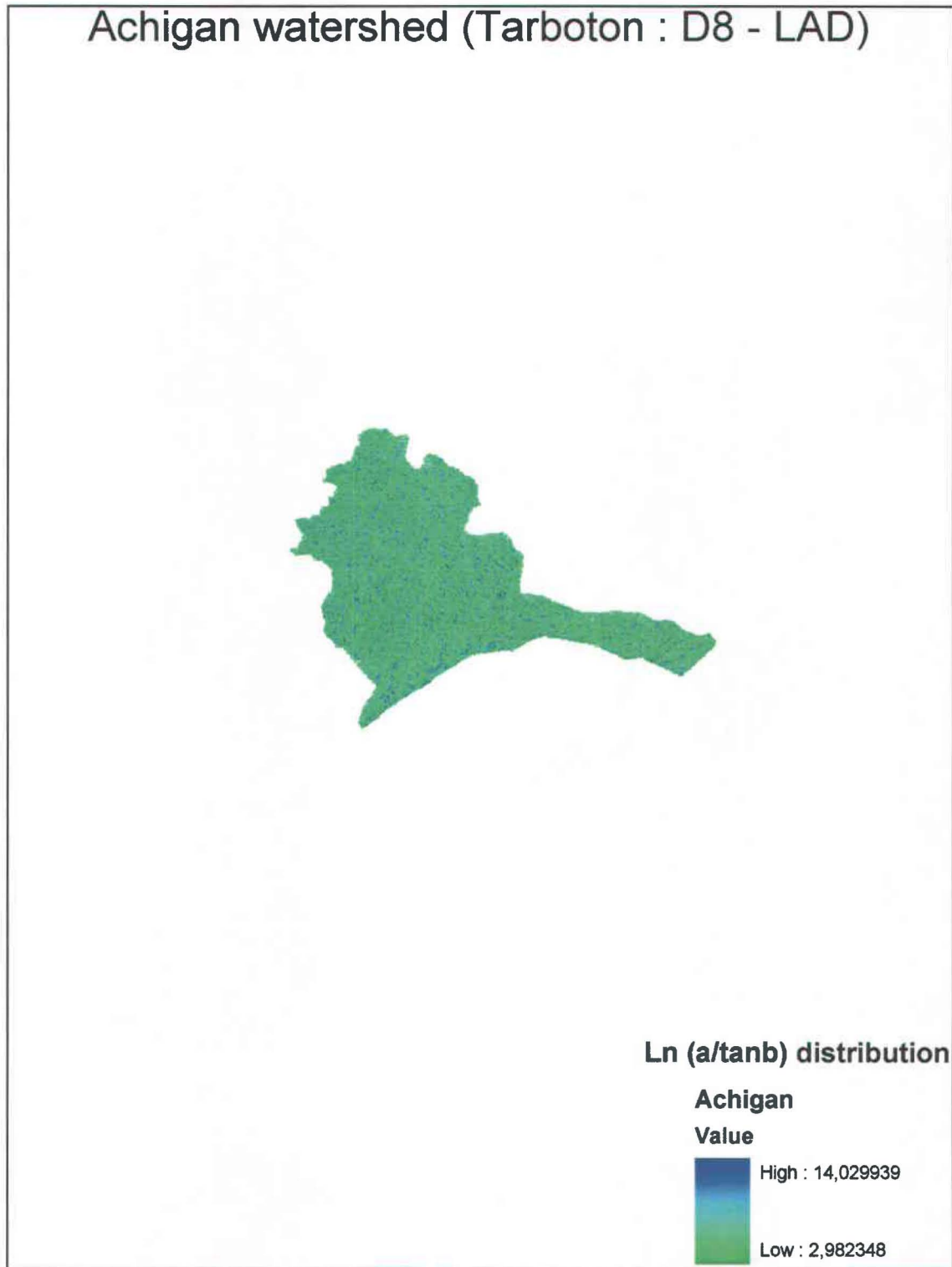


Figure A.50 : *TI* results for the Achigan river watershed using the D8-LAD algorithm (TauDEM)

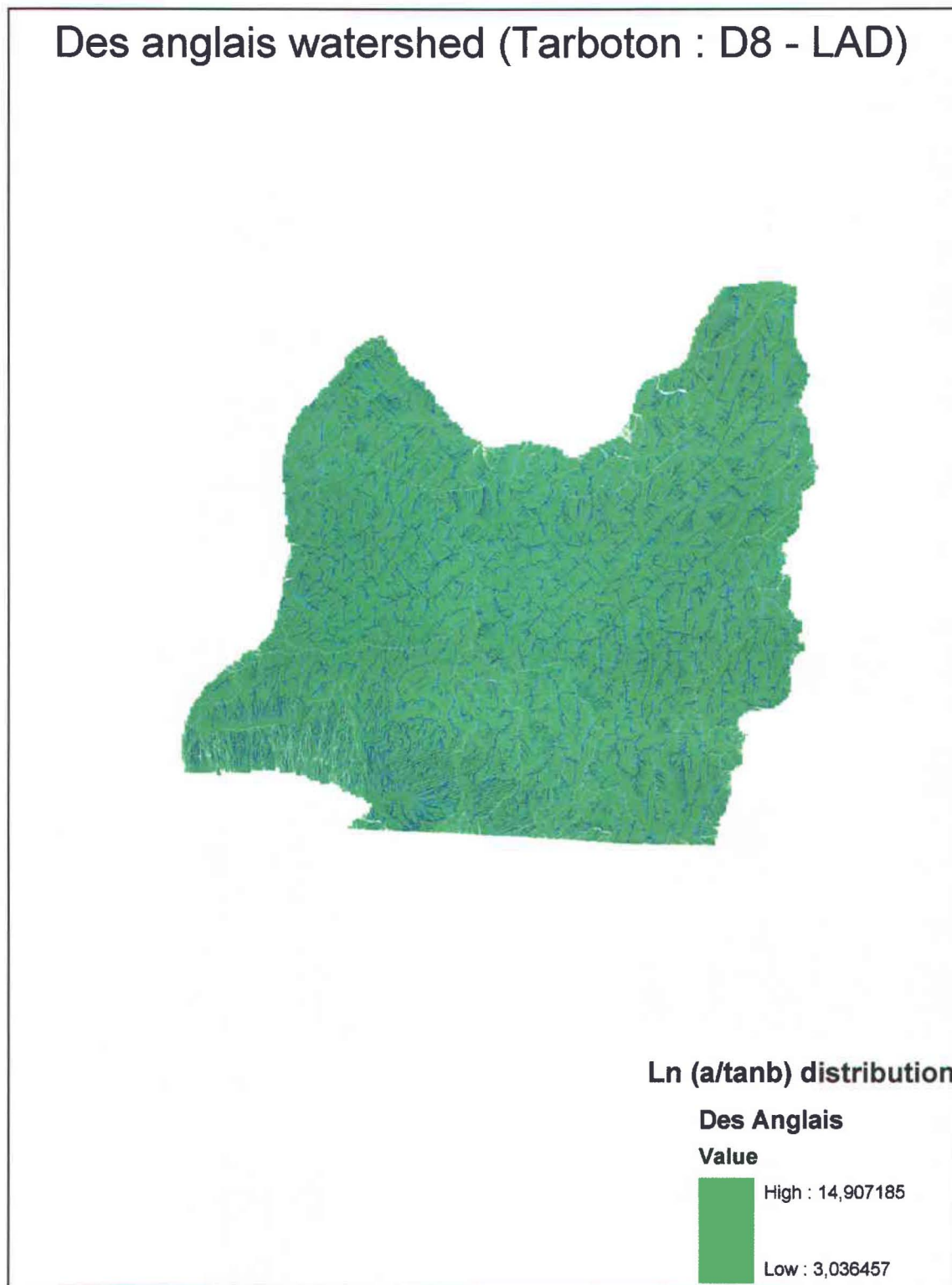


Figure A.51 : *TI* results for the Des Anglais river watershed using the D8-LAD algorithm (TauDEM)



Figure A.52 : *TI* results for the Bayonne river watershed using the D8-LAD algorithm (TauDEM)

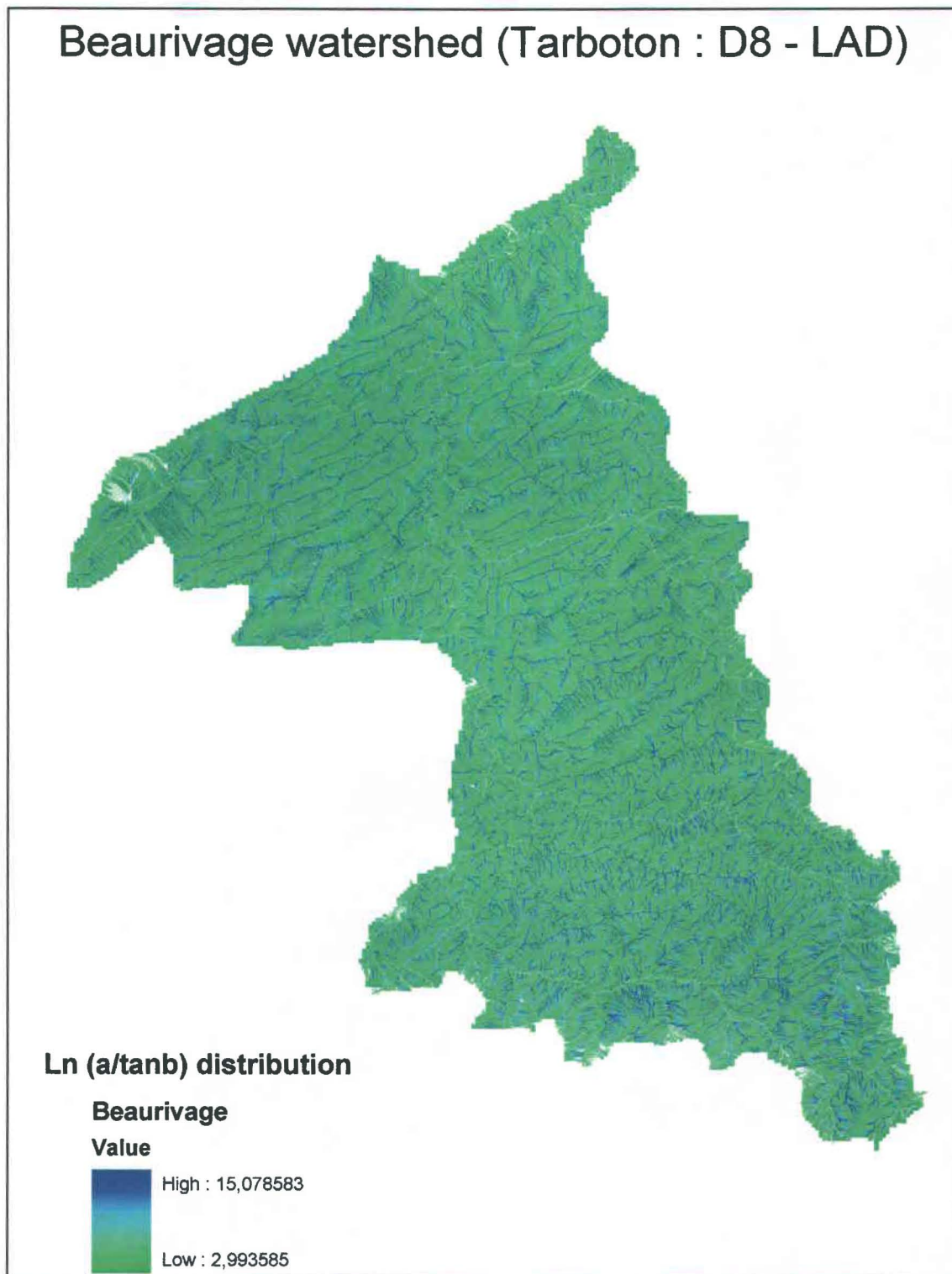


Figure A.53 : *TI* results for the Beaurivage river watershed using the D8-LAD algorithm (TauDEM)



Figure A.54 : *TI* results for the Boyer river watershed using the D8-LAD algorithm (TauDEM)

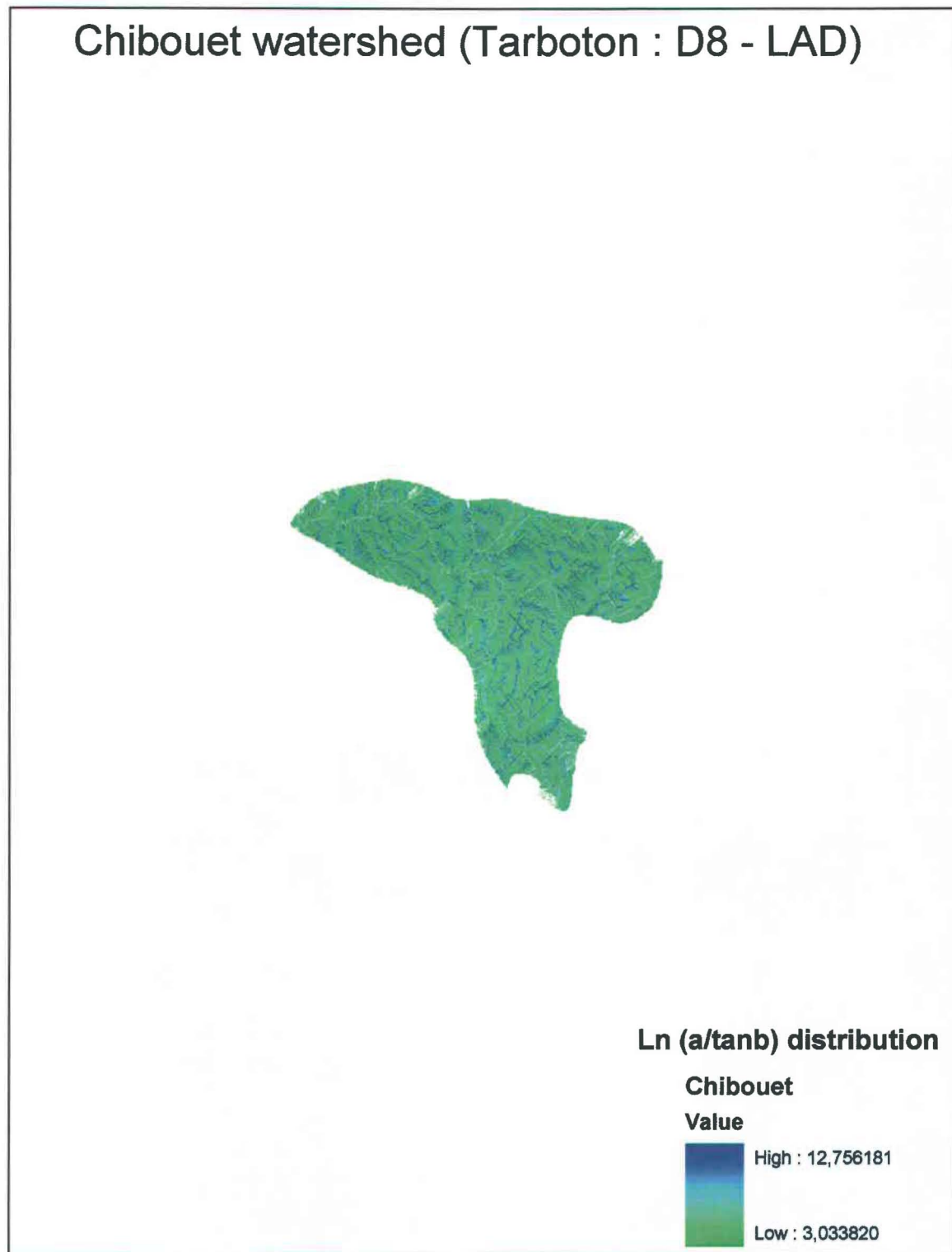


Figure A.55 : *TI* results for the Chibouet river watershed using the D8-LAD algorithm (TauDEM)

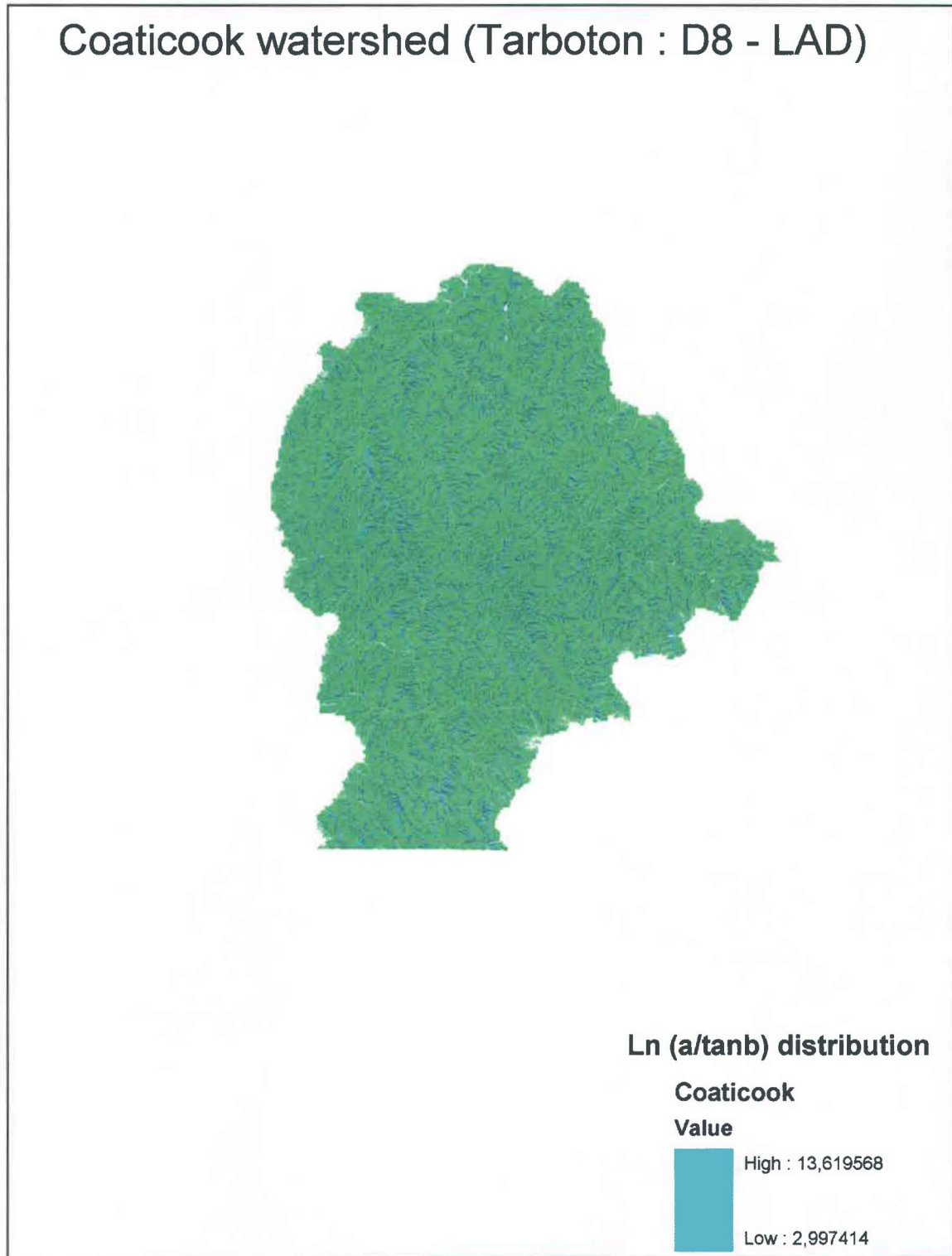


Figure A.56 : *TI* results for the Coaticook river watershed using the D8-LAD algorithm (TauDEM)

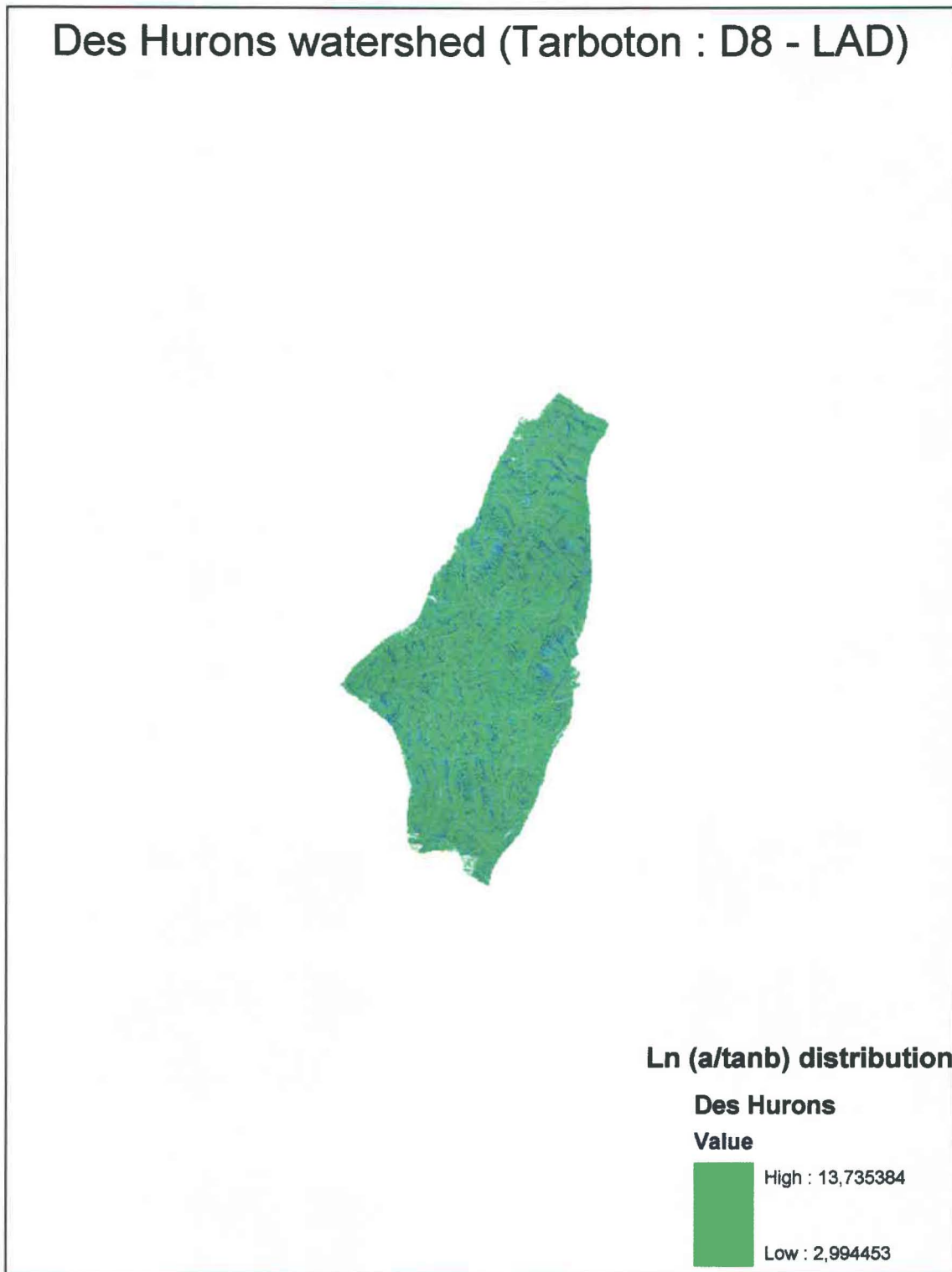


Figure A.57 : *TI* results for the Des Hurons river watershed using the D8-LAD algorithm (TauDEM)

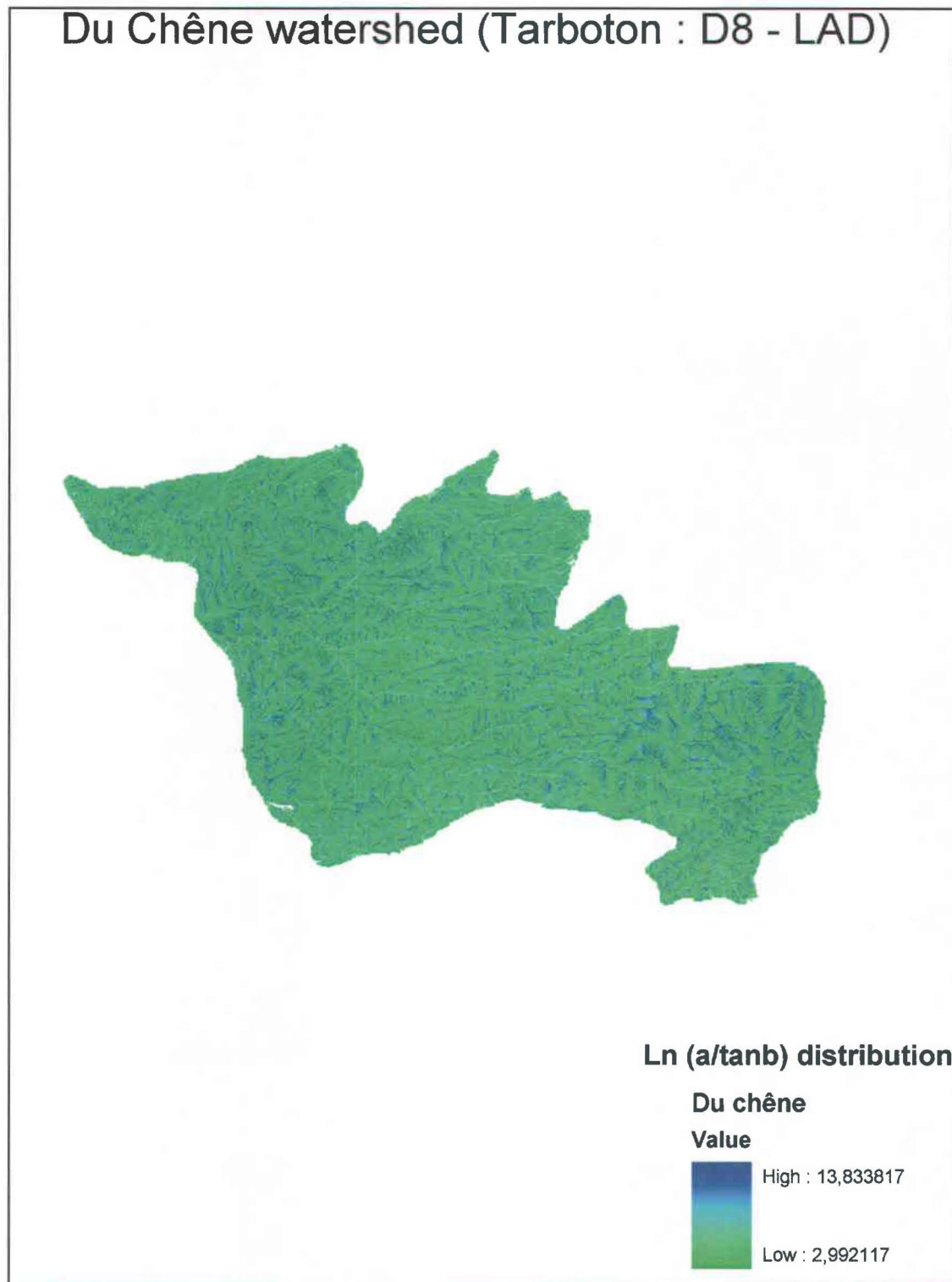


Figure A.58 : *TI* results for the Du Chêne river watershed using the D8-LAD algorithm (TauDEM)

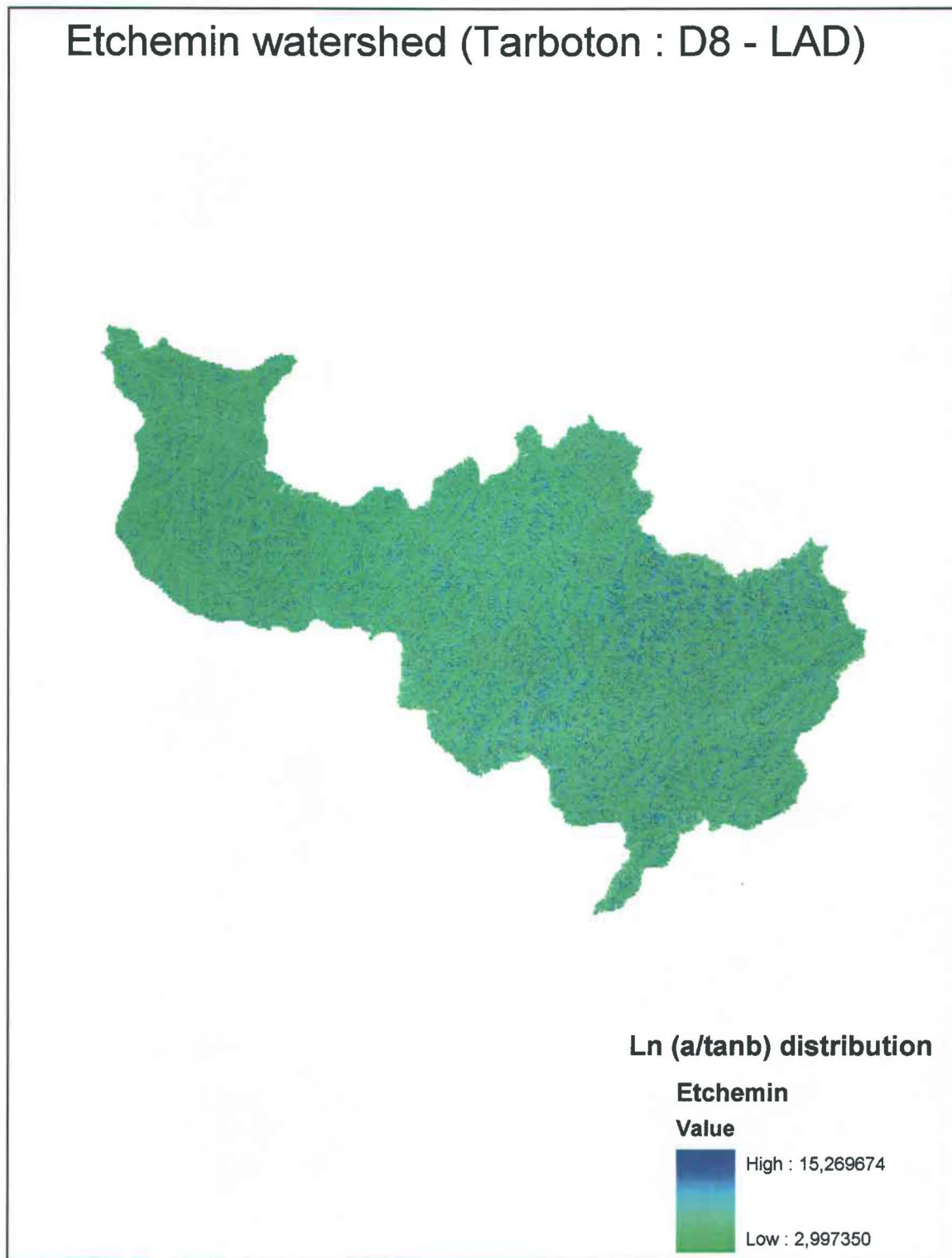


Figure A.59 : *TI* results for the Etchemin river watershed using the D8-LAD algorithm (TauDEM)

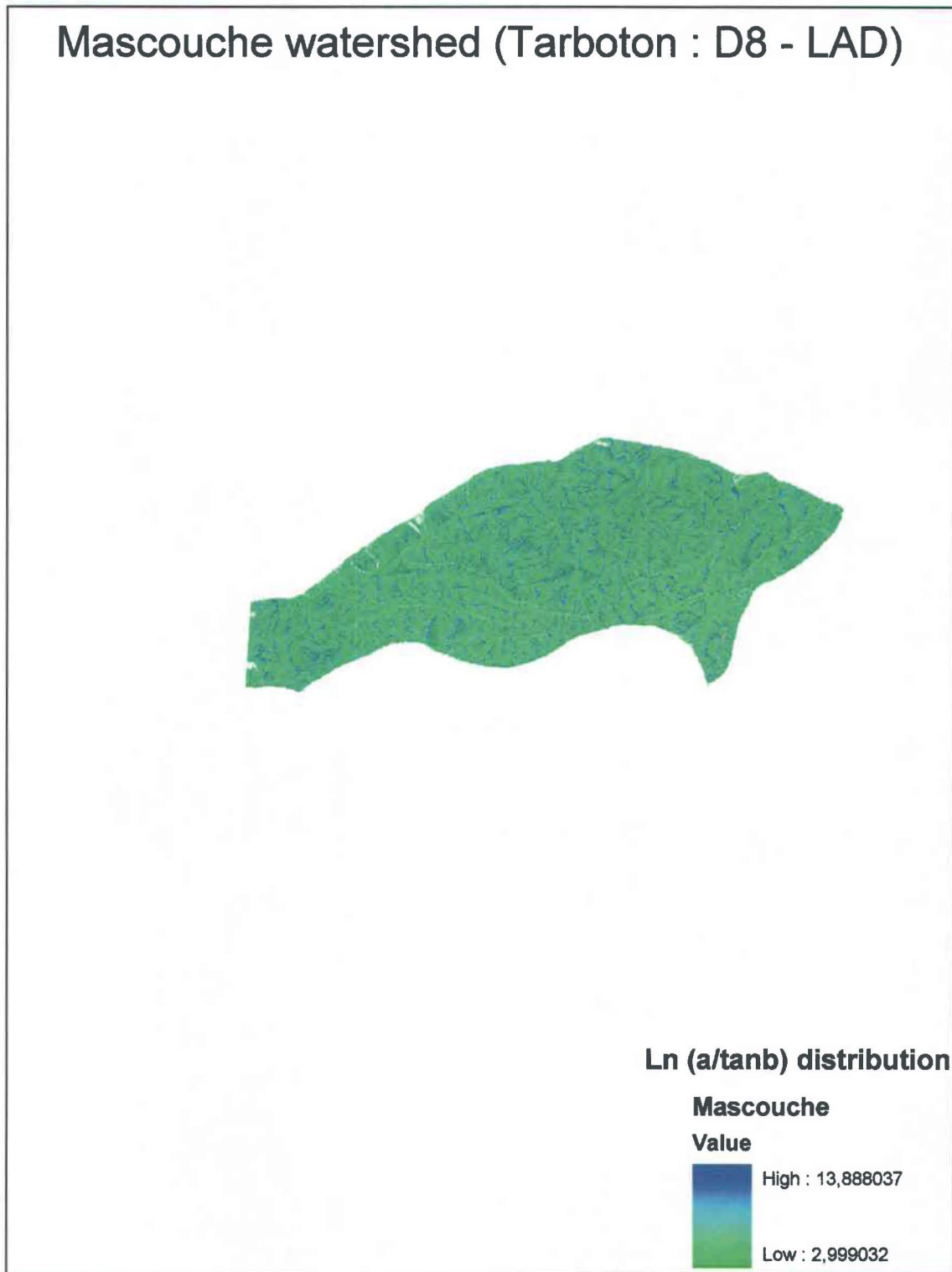


Figure A.60 : *TI* results for the Mascouche river watershed using the D8-LAD algorithm (TauDEM)

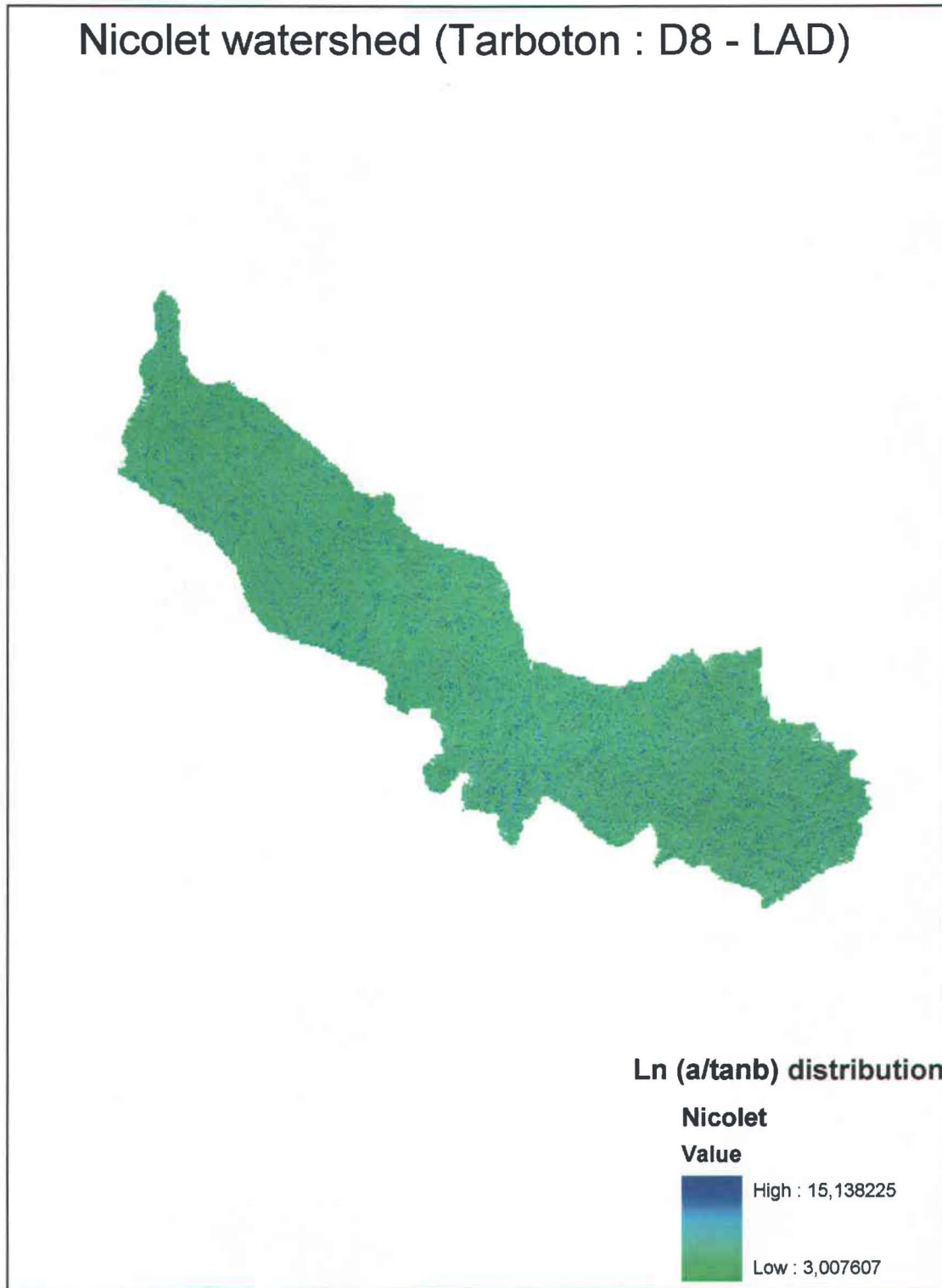


Figure A.61 : *TI* results for the Nicolet river watershed using the D8-LAD algorithm (TauDEM)



Figure A.62 : *TI* results for the Noire river watershed using the D8-LAD algorithm (TauDEM)

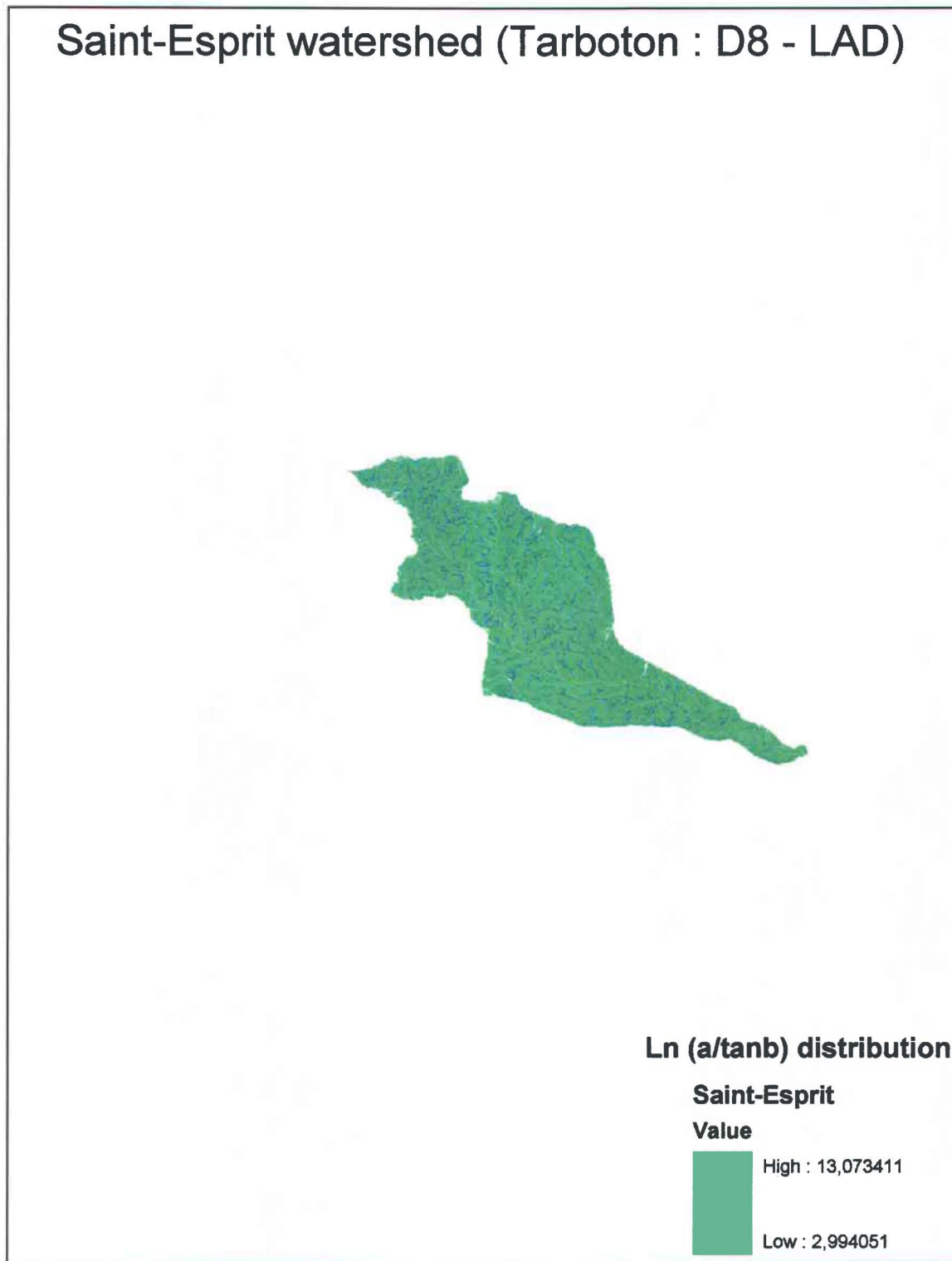


Figure A.63 : *TI* results for the Saint-Esprit river watershed using the D8-LAD algorithm (TauDEM)

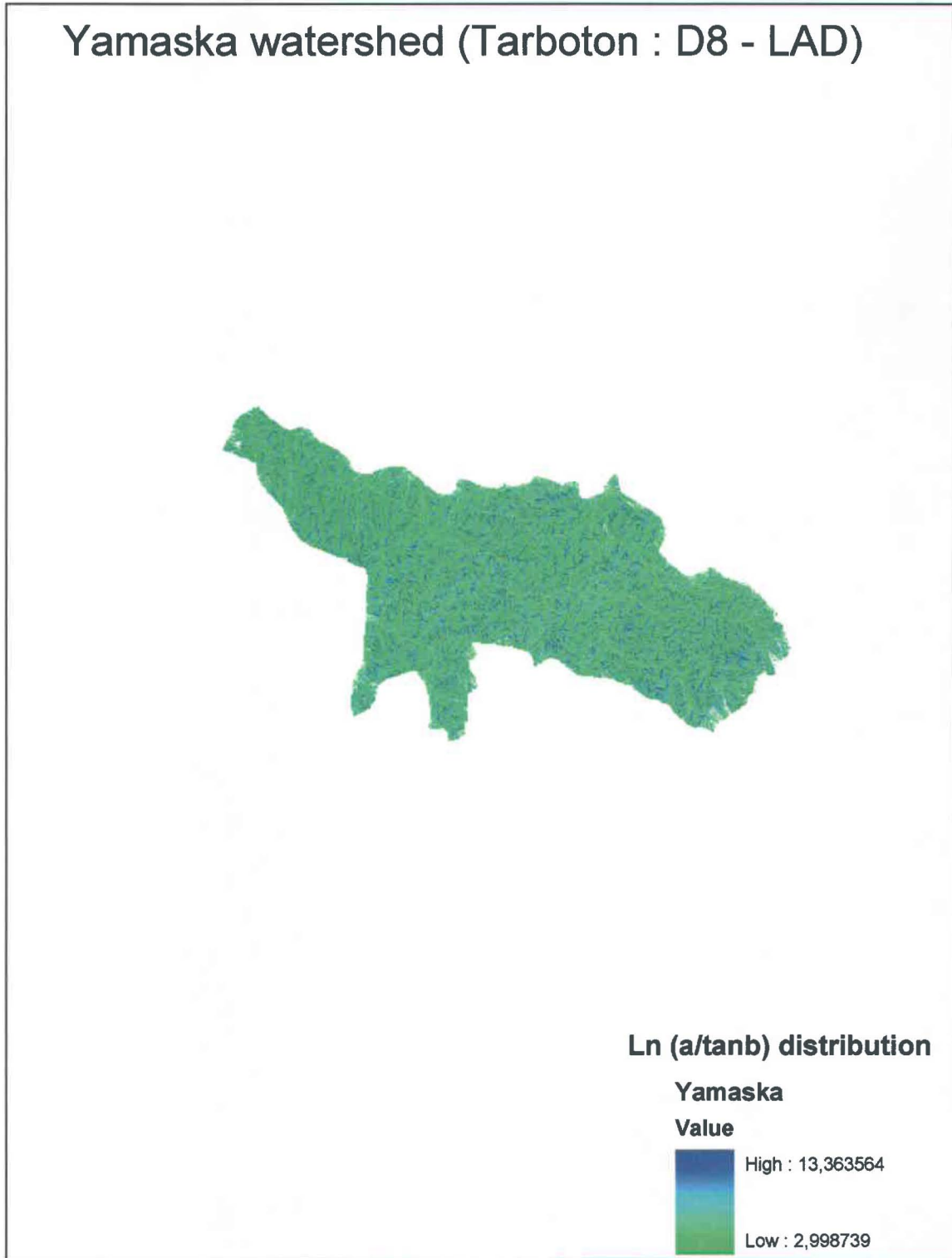


Figure A.64 : *TI* results for the Yamaska river watershed using the D8-LAD algorithm (TauDEM)